Interorgan Crosstalk between the Heart and Adipose Tissue during Heart Failure Establishment

Inaugural thesis presented to the Faculty of Mathematics and Natural Sciences of Heinrich Heine University Düsseldorf for the degree of Doctor of Natural Sciences by

Vici Oenarto

Düsseldorf, December 2019

from the Institute of Cardiovascular Physiology
Heinrich Heine University, Düsseldorf

Printed by permission of
The Faculty of Mathematics and Natural Sciences of
Heinrich Heine University, Düsseldorf

Examiners:
1. Prof. Dr. Axel Gödecke
2. Prof. Dr. Jens Fischer

Date of the oral examination:

Table of Contents

Abstract

The development of heart failure is often accompanied with cardiac lipid accumulation and inflammation which have been linked to a progressive decline in cardiac function. However, whether cardiac lipid accumulation leads to immune cell-mediated cardiac inflammation is not fully known. Thus, the aim of this work was to study the interaction of heart failure, cardiac lipid deposition and inflammation in a mouse model of pressure overloaded heart. In addition, changes in adipose tissue under chronic cardiac stress conditions should be analyzed.

Cardiomyocyte-specific knock-out of p38 MAPKα (iCMp38KO) was generated in adult mice by tamoxifen injection. Adipose tissue lipolysis was pharmacologically inhibited by atglistatin (anti-lipolytic compound, 0.4 mg/g food), starting from two days prior to pressure overload induction. Pressure overload was induced by angiotensin II (AngII) infusion (1.5 mg/kg/day) for 48 hours via mini-osmotic pumps which were implanted subcutaneously. Echocardiographic analysis of cardiac function was performed using Vevo 2100 imaging system. Hearts were harvested and analyzed for immune cell contents via FACS and histological staining. Transcriptional analysis of heart and adipose tissue was performed by Agilent 8x60K Mouse Array and RT-PCR.

iCMp38KO developed pressure overload-induced heart failure after 48h of AngII administration, with a low ejection fraction (20.5 ± 4.9%) compared to the AngII-treated controls (52.8 ± 7.3%). Pressure overload stress in the AngII-treated iCMp38KO induced lipolysis as indicated by the three-fold increase in circulating glycerol (0.22 ± 0.04 mM) from control level (0.07 ± 0.04 mM). Atglistatin, a small molecule inhibitor of adipose triglyceride lipase (ATGL) was used to inhibit adipose lipolysis. Stress-induced glycerol release in the atglistatin-treated iCMp38KO was lowered by 2-fold. Lipid accumulation was higher in the pressure overloaded iCMp38KO heart (9.96 ± 4.98 $pixel^2$) in contrast to the control heart (0.20 ± 0.09 $pixel^2$). Atglistatin significantly reduced lipid accumulation in iCMp38KO heart by 8-fold. FACS analysis of the cardiac immune cell showed a higher number of neutrophils in iCMp38KO heart (1471 ± 140 cells/mg tissue) compared to the control heart (323 ± 189 cells/mg tissue). Atglistatin treatment led to a reduction in the number of cardiac neutrophils in the iCMp38KO (1059 ± 97 cells/mg tissue). The number of infiltrating macrophages, T cells and B cells tended to be lower in the cardiac tissue of atglistatin-treated iCMp38KO. Left ventricular ejection fraction of the KO was significantly improved to 26.9 ± 5.1% (unpaired Student's t-test, $p < 0.01$) with atglistatin treatment, possibly due to significant improvement in fractional shortening. Transcriptional analysis of perigonadal white adipose tissue revealed alterations consistent with an induction of browning, immune cell migration and proliferation, and tissue inflammation in atglistatin-treated iCMp38KO, suggesting an additional role of ATGL which is not restricted to lipolysis.

This study demonstrates that inhibition of adipose tissue lipolysis is a novel approach to reduce cardiac lipid accumulation and to modulate cardiac infiltration of immune cells. Therefore, the iCMp38KO model of pressure overload-induced HF offers the opportunity to study the impact of lipolysis on HF and to evaluate novel therapeutic approach.

1

Introduction

1.1. Metabolic risks and consequences of cardiovascular disease

Cardiovascular disease (CVD) is the leading cause of death, accounting for 45% of mortality in Europe (Wilkins et al 2017) and 31% of mortality globally (World Health Organization 2016). Amongst the major determinants of CVD, metabolic risk factors such as hyperlipidemia, hyperglycemia, physical inactivity, and dietary risks, are associated with a high percentage of CVD-related mortality. Despite the numerous established treatment options aimed to target these metabolic factors, the mortality due to CVD has still been increasing over the past 25 years. This emphasizes the need for a better understanding of the disease pathophysiology and the metabolic complications to improve clinical management and therefore outcome.

Metabolic syndrome encompasses a number of metabolic factors which increase the risks of not only metabolic diseases such as type 2 diabetes mellitus (T2DM), but also CVD, including coronary heart disease (CHD), myocardial infarction (MI) and stroke (Alberti et al 2009). Metabolic syndrome centers on alterations in the function of adipose tissue driven by energy imbalance. Altered adipose tissue lipolysis and endocrine function, and therefore the release of lipolytic products and adipokines, contribute to the manifestation of the main features which constitute metabolic syndrome. Circulating free fatty acid (FFA) supplied by adipose tissue lipolysis is a potential mediator of organ crosstalk. For example in skeletal muscle, elevated FA uptake can lead to intracellular lipid deposit which can activate protein kinase C (PKC). This kinase can directly inactivate insulin receptor substrate-1 (IRS-1) resulting in a decrease in insulin signaling and the downstream glucose uptake (Samuel et al 2010). In the liver, FFA has been shown to increase gluconeogenesis (Williamson et al 1966). Furthermore, insulin resistance in the adipose tissue itself results in an impaired

inhibition of lipolysis and an increase in FFA release into the circulation (Morigny et al 2016). Overall, excess circulating FFA leads to hyperglycemia, hyperinsulinemia and the reduction in insulin action in the normally sensitive tissues.

Positive energy balance as a result of physical inactivity and imbalanced diets lead to visceral adiposity. Visceral adiposity is marked by adipocyte hypertrophy and hyperplasia, adipose tissue hypoxia, and the overproduction of proinflammatory cytokines such as tumor necrosis factor alpha (TNFα), interleukin 6 (IL6), and adipokines such as leptin. These factors mediate local and systemic inflammation. FFA released as a result of adipose tissue lipolysis lead to triacylglycerol (TAG) accumulation in the liver, overproduction of very low density lipoprotein (VLDL) and impaired low density lipoprotein (LDL) clearance, and consequently, hypertriglyceridemia (Lewis & Steiner 1996).

On the other hand, as depicted in Figure 1.1, chronic CVD in turn could lead to systemic metabolic alterations, highlighting the potential crosstalk between metabolic and cardiac dysfunctions. Chronic exposure to cardiac stress is accompanied by a chronic activation of adrenergic signaling. The cardiovascular consequences of this include a persistent increase in peripheral vascular resistance and tachycardia, eventually resulting in the inability of the heart to maintain sufficient supply of oxygen to the whole body (i.e. heart failure (HF)). Moreover, adrenergic signaling is known to induce adipose tissue lipolysis via the activation of β-adrenergic receptors (Himms-Hagen 1970), which in white adipose tissue (WAT) leads to the mobilization of the lipolytic products glycerol and FFA. Excessive lipolysis consequently leads to systemic insulin resistance and inflammation, creating further stress to the cardiovascular system.

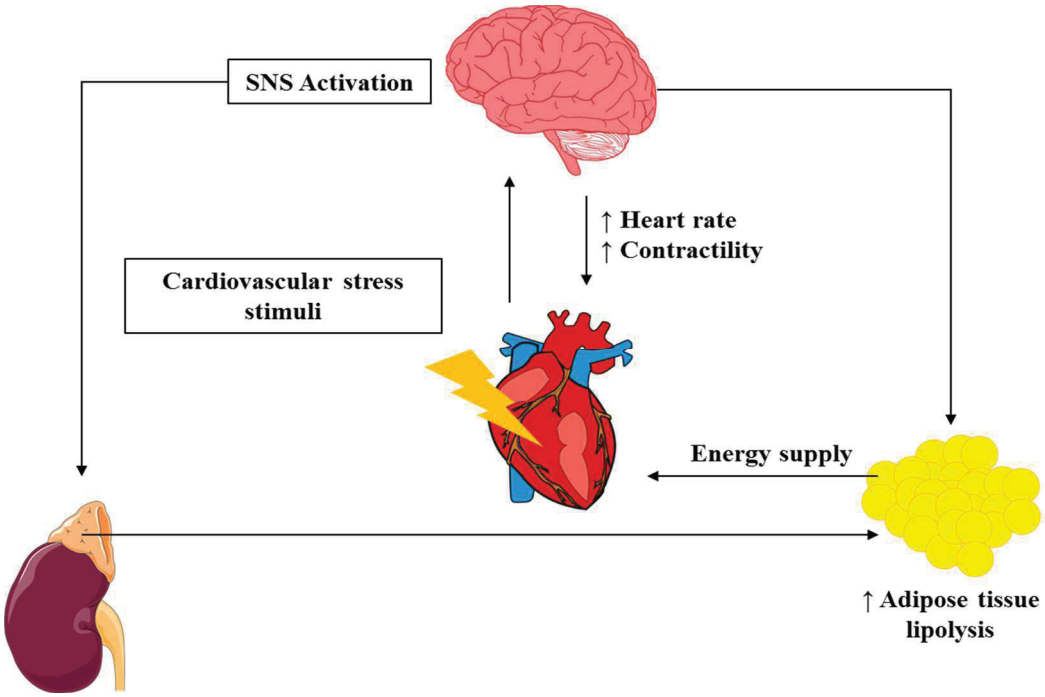

Figure 1.1: Schematics of cardiac stress-stimulated lipolysis. Cardiac stress activates the sympathetic nervous system (SNS), which in turn signals to the heart via adrenergic innervation to compensate by increasing heart rate and contractile force. SNS stimulates the adrenal glands to release stress hormones such as catecholamines. Catecholamines induce adipose tissue lipolysis in order to supply other organs including the heart with the release of stored energy substrate (lipid).

1.2. Cardiac fatty acid metabolism under normal vs stress conditions

To perform its normal functions, the heart requires a high amount of energy in the form of adenosine triphosphate (ATP). Over 95% of ATP in the heart is produced via the mitochondrial oxidative phosphorylation (Ingwall 2002, Doenst et al 2013). Under normal conditions, 60 to 90% of the produced ATP is derived from fatty acid (FA), and the remaining 10 to 40% is supplied by glucose and lactate (Doenst et al 2013). Cardiac metabolic flexibility is a term which describes the ability of the heart to utilize various energy substrates to ensure sufficient and constant production of ATP and maintain cardiac performance, as the energy requirement changes.

There are two sources of circulating FA which can be consumed by cardiomyocytes: albumin-bound FA released from WAT as a result of lipolysis, and chylomicron- or VLDL-bound TAG which is further hydrolyzed intravascularly by lipoprotein lipase (LPL) released from vascular endothelial cells and cardiomyocytes (Korn 1955a, b).

FA uptake requires the transport via plasma membrane transporters. Amongst the FA transporters expressed in the heart, CD36 appears to be the main transporter, since the loss of CD36 results in 50% reduction in FA uptake (van der Vusse et al 2000), even in the presence of other FA transport protein (FATP) family members. There are two identified signaling pathways which regulate CD36 translocation into the sarcolemma; insulin-mediated FA uptake and contraction-mediated FA uptake. The insulin-activated phosphatidylinositol-3-kinase (PI3K)-Akt/protein kinase B (PKB) pathway has been shown to stimulate the translocation of CD36 to the sarcolemma (Luiken et al 2001). As the energy demand of the heart increases due to increased workload, the intracellular concentration of adenosine monophosphate (AMP) increases, thereby increasing the activity of AMPK. AMPK activation also increases the translocation of CD36 to the sarcolemma (Luiken et al 2003), and therefore FA uptake.

Figure 1.2 summarizes the fate of FA upon entry into cardiomyocytes. Upon entry, FA is converted to long-chain fatty acyl CoA in the cytosol by the enzyme acyl-CoA synthetase long-chain (ACSL). 10 to 30% of long-chain fatty acyl-CoA undergo esterification into triacylglycerol (TAG) as the critical energy reserve (described in section 1.3.1, page 6). The remaining 70 to 90% are transported into the mitochondria, facilitated by mitochondrial membrane proteins: carnitine palmitoyltransferase 1 (CPT-1), with CPT-1β as the predominant isoform in cardiomyocytes, carnitine acyltranslocase (CACT), and carnitine palmitoyltranferase 2 (CPT-2). Once inside the mitochondria, long-chain fatty acyl-CoA undergoes β-oxidation, supplying electrons for the production of energy in the form of ATP by the complexes of the electron transport chain.

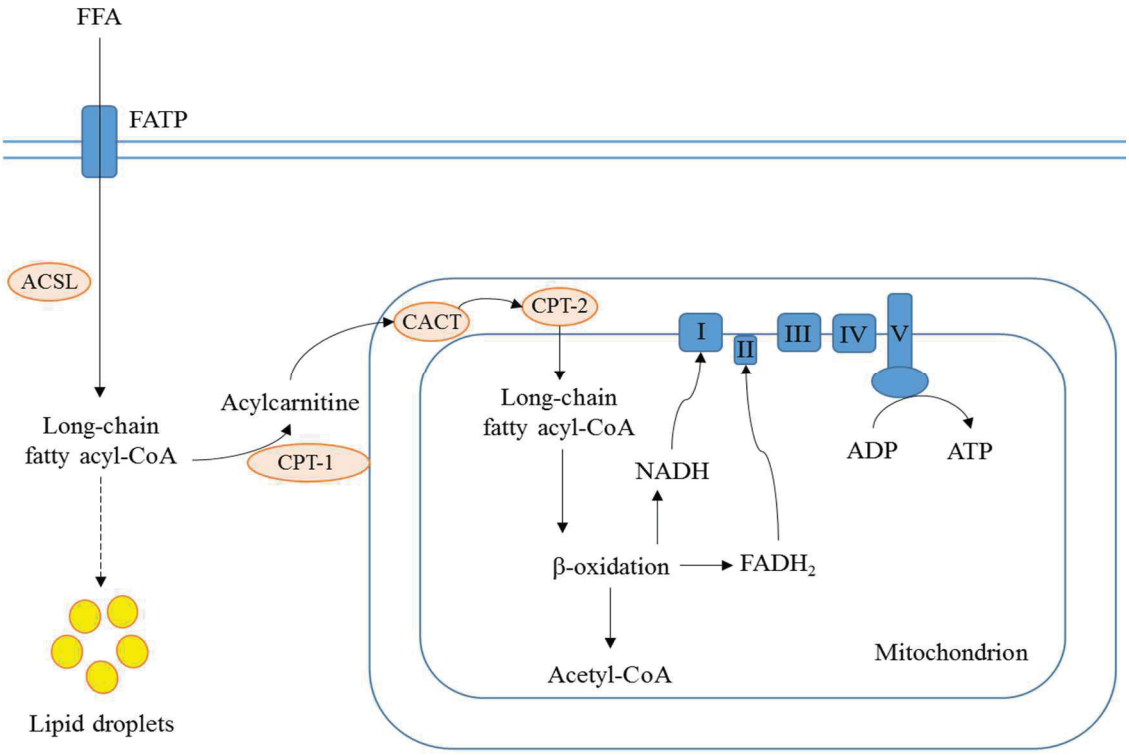

Figure 1.2: Fate of FA in cardiomyocyte upon uptake. FFA taken up from the circulation are either stored in lipid droplets or utilized for ATP production. Abbreviations: free fatty acid (FFA), FA transport protein (FATP), acyl-CoA synthetase long-chain (ACSL), carnitine palmitoyltransferase 1 (CPT-1), carnitine acyltranslocase (CACT), carnitine palmitoyltransferase 2 (CPT-2), nicotinamide adenine dinucleotide hydrogen (NADH), flavin adenine dinucleotide dihydrogen ($FADH_2$), adenosine diphosphate (ADP), adenosine triphosphate (ATP).

Under pathological conditions such as left ventricular dilation and increased peripheral resistance, the heart requires an even higher amount of ATP to maintain a sufficient performance. As cardiac impairment progresses to a later-stage HF, the increase in workload along with hypoxia due to hypertrophy trigger a metabolic switch in the cardiomyocytes to increase the utilization of glucose instead of the normally preferred substrate, FA. In the case of low oxygen supply, glucose is preferred as it requires less oxygen to produce ATP (6 mol oxygen per mol glucose) compared to FA (23 mol oxygen per mol FA) (Stanley & Chandler 2002). In clinical as well as experimental models of HF, the electron transport chain (ETC) was found to be impaired (Buchwald et al 1990, Marin-Garcia et al 2001). In line with this, the enzymes of FA metabolism were found to be downregulated, leading to an apparent decrease in FA oxidation. Additionally, the mitochondria displayed disrupted membranes, and reduced capacities for respiration and oxidative phosphorylation.

1.3. Intramyocardial lipid accumulation and lipotoxicity in CVD

As described earlier, in healthy hearts the majority of FA which is taken up by cardiomyocytes is oxidized to produce ATP, and the remainder is stored as TAG-rich lipid droplets in the cytosol as a temporary energy reserve. However, during the progression of HF, FA oxidation is reduced and consequently, intramyocardial TAG content is altered. This alteration of cardiomyocyte TAG homeostasis has been associated with the impaired cardiac function in T2DM, metabolic syndrome, aging,

and CVD. Furthermore, intramyocardial lipid accumulation was reported in patients with non-ischemic HF and associated with left-ventricular dilation and contractile dysfunction (Sharma et al 2004). The regulation of TAG turnover, i.e. the balance between TAG synthesis and hydrolysis, in cardiomyocytes is therefore important for the maintenance of sufficient cardiac function, particularly under pathological conditions.

1.3.1. TAG synthesis – the formation of intramyocardial lipid storage

Lipid droplets are organelles which contain a neutral lipid core, i.e. TAG, cholesterol esters and retinyl esters encapsulated by cell type-specific scaffolding proteins and a phospholipid monolayer (Guo et al 2009). Due to the high energy need, cardiomyocytes oxidize the majority of FA and therefore contain relatively small lipid droplets. The most important lipid droplet coating protein in cardiomyocytes is perilipin-5 (Wolins et al 2006, Yamaguchi et al 2006). Perilipin-5 tightly regulates TAG homeostasis in cardiomyocytes through its interaction with lipases and the ability to facilitate FA oxidation by increasing the access of neutral lipids to the mitochondria. In the absence of lipolysis stimulation, perilipin-5 protects against excessive TAG hydrolysis. Uncontrolled lipolysis could overload FA oxidation by the mitochondria leading to reactive oxygen species (ROS) formation, cellular apoptosis, and consequently impaired cardiac function. On the other hand, perlipin-5 has the ability to recruit mitochondria to the surface of lipid droplets, providing access to FA oxidation and ATP production (Dalen et al 2007, Granneman 2011, Wang et al 2011). Thus, perlipin-5 plays a crucial role in the balance of cardiomyocyte TAG content and FA oxidation.

The molecular mechanism of TAG synthesis is summarized in Figure 1.3. The esterification of FA to produce TAG occurs in a sequential manner, with each step regulated by a specific enzyme (Kennedy & Weiss 1956). TAG synthesis is initiated by the esterification of glycerol-3-phosphate (G3P) with one FA molecule to produce lysophosphatidic acid (LPA) by the action of glycerol-3-phosphate acyltransferase (GPAT). Another FA molecule is transferred onto LPA by lysophosphatidic acid acyltransferase (AGPAT), producing phosphatidic acid (PA). PA is then dephosphorylated by lipin, with lipin-1 as the predominant isoform in the heart, resulting in diacylglycerol (DAG) formation. Finally, DAG can be further esterified into TAG by the action of DAG acyltransferase (DGAT, isoforms 1 and 2). A reduced formation of TAG may redirect excess FA to other pathways such as ceramide synthesis, and may therefore enhance accumulation of lipids with lipotoxic properties.

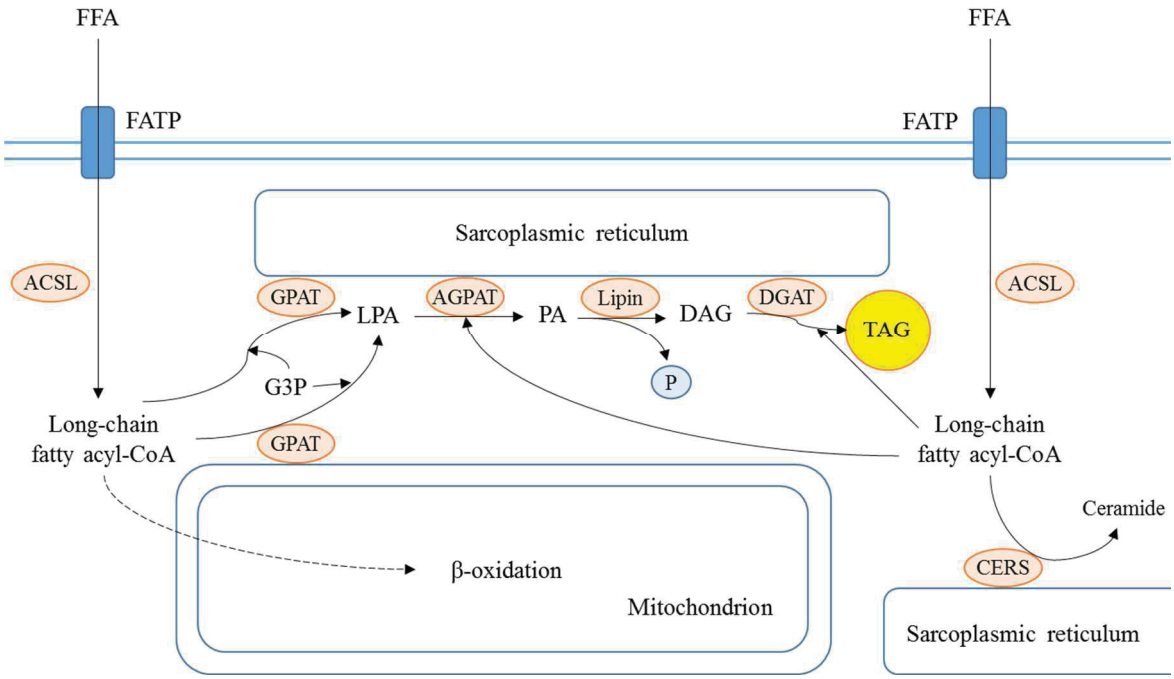

Figure 1.3: Summary of the sequential formation of TAG. TAG synthesis is tightly regulated by enzymes. Abbreviations: glycerol-3-phosphate acyltransferase (GPAT), glycerol triphosphate (G3P), lysophosphatidic acid (LPA), lysophosphatidic acid acyltransferase (AGPAT), phosphatidic acid (PA), phosphate (P), diacylglycerol (DAG), DAG acyltransferase (DGAT), triacylglycerol (TAG), ceramide synthase (CERS).

1.3.2. Definition and potential mechanisms of cardiac lipotoxicity

Cardiac lipotoxicity is defined as excess accumulation of lipids such as DAG, ceramides, and long-chain fatty acyl-CoA in the heart, causing apoptosis and consequently a decline in cardiac function (Chokshi et al 2012, Galloway et al 1987, McGavock et al 2007, Sharma et al 2004, Szczepaniak et al 2003). A number of factors have been proposed to contribute to lipotoxic cardiomyopathy, which include excess FA uptake, insulin resistance and cardiac inflammation.

Dysregulated uptake of FA by CD36 has been linked to a number of lipotoxic cardiomyopathies. Uncontrolled CD36 translocation contributes to lipid accumulation in diabetic hearts and is associated with left ventricular hypertrophy and cardiac contractile dysfunction (Luiken et al 2003). In this case, the excess FA uptake is attributed to (i) high circulating FA, (ii) hyperinsulinemia, which causes permanent localization of CD36 in the sarcolemma, and (iii) hyperglycemia, which increases the mRNA expression of CD36. Excess FA uptake leads to excessive FA oxidation which causes mitochondrial stress and overproduction of ROS, as well as excessive storage and accumulation of toxic lipids (Listenberger et al 2001, Ostrander et al 2001).

Initially, excessive FA uptake leads to excess mitochondrial FA oxidation and overproduction of ROS. ROS mediates damage to the mitochondria as well as to the endoplasmic reticulum, activating apoptotic signaling. Eventually, FA uptake overcomes FA oxidation due to mitochondrial dysfunction or damage, and alters glucose utilization. These alterations increase the reliance on a less ATP-efficient energy production. Toxic lipids may also accumulate in the cytosol and activate

apoptotic signaling, as well as impair insulin signaling. Ceramides can activate the apoptotic pathway and block Akt signaling, leading to a decrease in glucose uptake (Aoki et al 2002). In combination, these factors could contribute to cardiac dysfunction due to an imbalanced intramyocardial lipid pool.

1.3.3. Experimental and clinical evidence of intramyocardial lipid accumulation and cardiomyopathy

A number of animal models have been developed to study cardiac lipid accumulation and lipotoxicity. For instance, cardiac overexpression of PPAR-α led to increased FA uptake, oxidation and lipid content, as well as decreased glucose uptake and oxidation (Finck et al 2001). These factors were associated with cardiac hypertrophy, left-ventricular dilation and decreased fractional shortening. The global homozygous KO of adipose triglyceride lipase (ATGL) also led to an increase in intramyocardial lipid accumulation (Haemmerle et al 2006). This was linked to cardiac dysfunction characterized by increased heart weight, cardiac fibrosis, left-ventricular dilation, increased wall-thickness, and consequently pulmonary as well as peripheral congestion.

Moreover, cardiac lipotoxicity (clinically termed cardiac steatosis) has been reported in patients with CVD and metabolic complications. Sharma and colleagues (Sharma et al 2004) described cardiac steatosis and its consequences in cardiac metabolism in patients with non-ischemic HF. Non-ischemic HF patients tended to accumulate lipid in the heart, with the highest prevalence in diabetic and obese patients. Cardiac steatosis was associated with dysregulated expression of FA oxidation-related genes, increased myosin heavy chain-β (MHC-β) mRNA expression, increased TNFα mRNA expression and contractile dysfunction. High circulating FA appear to increase FA uptake, exceeding the FA oxidizing capacity. The mechanism of lipid-induced increase in TNFα has yet to be elucidated, however, its consequences have been determined. TNFα has been shown to impair insulin signaling and cardiac contractility, contributing to the decline in cardiac function during the disease progression. Moreover, TNFα was positively correlated with the disease severity. McGavock and colleagues (McGavock et al 2007) later confirmed that cardiac steatosis in CVD preceded the onset of diabetes mellitus and left-ventricular dysfunction.

Left-ventricular mass has also been linearly correlated with cardiac lipid content (Szczepaniak et al 2003). Chokshi and colleagues (Chokshi et al 2012) identified that accumulated lipids in pressure-overloaded hearts included to a large extent the toxic lipid metabolites DAGs and ceramides. Interestingly, cardiac TAGs, long-chain fatty acyl-CoA and CPT-1 were reduced. This suggests that the cytosolic lipid pool consists of toxic lipid species which mediate an impaired insulin signaling and decreased glucose uptake, attributed to the inhibition of Akt by increased PKC activity in failing hearts. Noteworthy, mechanical unloading by left-ventricular assist device implantation decreased intramyocardial lipid accumulation and improved insulin signaling. CVD patients with metabolic syndrome exhibit intramyocardial lipid accumulation which inversely correlated with ejection fraction (EF).

1.4. Mechanism of stress-stimulated adipose tissue lipolysis

Non-adipose tissues such as the heart do not undergo *de novo* FA synthesis (Lopaschuk et al 2010, Van der Vusse et al 2000); the heart relies on exogenous FA uptake from the circulation as energy supply. Since the heart requires a high amount of energy to meet the normal cardiac demand, the regulation of FA uptake from the circulation is important to maintain a sufficient cardiac function. Therefore, adipose tissue lipolysis could be the major source of lipids accumulating in cardiomyocytes in non-ischemic HF.

Adipose tissue is a complex organ which serves as the master regulator of whole-body energy homeostasis. There are two classical types of adipose tissue; white adipose tissue (WAT) and brown adipose tissue (BAT). WAT is further subdivided into visceral and subcutaneous WAT. The major differences between these tissues are summarized in Table 1.

Properties	**Visceral WAT**	**Subcutaneous WAT**	**BAT**
Major location in rodents	Perigonadal, mesenteric, perirenal (retroperitoneal) regions	Inguinal regions	Interscapular region
Major location in adult humans	Around vital organs (e.g. heart), omental and mesenteric regions	Upper body subcutaneous, femoral regions	Supraclavicular and spinal regions
Morphology	Uniformly occupied by large unilocular adipocytes.	Heterogenous adipocytes consisting of large unilocular cells and smaller multilocular cells.	Uniformly occupied by small multilocular adipocytes, richly innervated and vascularized, and containing a high amount of mitochondria.
Function	Organ storage of chemical energy in the form of lipid droplets. Under the conditions of high energy demand, e.g. fasting or exercise, this stored energy is mobilized by lipolysis. In addition, visceral adipose tissue acts a cushion for vital organs which are often exposed to mechanical stress.		Upon induction, BAT dissipates chemical energy in the form of heat (non-shivering thermogenesis) via the activity of uncoupling protein 1 (UCP1).

Table 1: Summary of the major factors distinguishing the classical types of adipose tissue. Adipose tissues can be categorized according to depot location, tissue morphology and function in energy homeostasis.

In the 1980s to early 1990s, several groups identified a subpopulation of adipocytes within the classical WAT depots which express uncoupling protein 1 (UCP1) upon cold stimulation (Loncar et al 1988, Loncar 1991, Young et al 1984), which were later named beige adipocytes. The accumulation of beige adipocytes via *de novo*

adipogenesis (Klaus et al 1995, Lee et al 2012, Petrovic et al 2010) or transdifferentiation from pre-existing white adipocytes (Rosenwald et al 2013) under conditions of increased energy expenditure was termed “browning”. In addition to UCP1 expression, beige adipocytes are characterized by other brown adipocyte-like features such as high rates of metabolism, increased mitochondrial biogenesis and oxidative function. Browning has been a topic of interest since the discovery of functional BAT in humans (Cypess et al 2009, Nedergaard et al 2007) due to its capacity to regulate glucose and lipid metabolism. Additionally, browning can be induced by secreted factors from other organs, and thus could be a result of interorgan crosstalk (Bartelt & Heeren 2014).

There are several ways of adipose tissue-mediated interorgan crosstalk: altered nutritional state, neural changes and secreted factors (adipokines) acting in auto-/para-/endocrine manner. Under conditions of negative energy balance, lipolysis is induced to fuel other organs whilst sparing glucose for the central nervous system (CNS). Conversely, under situations with positive energy balance, adipose tissue responds by taking up the excess energy substrates, thus controlling plasma levels of FA. Adipose tissue is innervated by the sympathetic and parasympathetic nervous systems, which regulate adipogenesis and adipocyte hypertrophy, with the former promoting lipolysis and the latter promoting lipid synthesis.

Adipose tissue lipolysis is mainly activated via β-adrenergic stimulation (summarized in Figure 1.4). Briefly, catecholamines such as adrenaline and noradrenaline bind to β-adrenergic receptors ($\beta_{1/2/3}$) expressed on the plasma membrane of adipocytes, initiating a cascade of lipolytic signaling. The breakdown of stored TAG occurs sequentially, with each step catalyzed by an enzyme: adipose triglyceride lipase (ATGL) (Jenkins et al 2004, Villena et al 2004, Zimmermann et al 2004), hormone sensitive lipase (HSL) and monoglycerol lipase (MGL) (Vaughan et al 1964). ATGL exhibits preference towards TAG for its hydrolyzing activities, thereby initiating the first step of FA mobilization. Phosphorylation of ATGL by PKA increases its activity (Ahmadian et al 2011). The full lipolytic activity of ATGL requires binding to its coactivator protein, Comparative Gene Identification-58 (CGI-58) (Lass et al 2006). The coactivation of ATGL by CGI-58 is tightly regulated by perilipin to prevent uncontrolled lipolysis. In adipocytes, CGI-58 is bound to perilipin-1 under baseline conditions, preventing it from binding to ATGL. Upon β-adrenergic activation of PKA, the phosphorylation of perilipin-1 leads to the release of CGI-58, allowing access to ATGL. Additionally, endogenous inhibitors of ATGL have also been identified; long-chain fatty acyl CoA as a product of ATGL lipolysis in return provides a negative feedback regulation of ATGL activity, G0/G1 switch gene 2 (G0S2) and hypoxia-inducible gene 2 (HIG2) both inhibit ATGL activity by direct binding (Yang et al 2010).

Although HSL mainly hydrolyzes DAG to release monoacylglycerol (MAG) and FA (Haemmerle et al 2002), it expresses a broad spectrum of substrate specificity including TAG and other long-chain lipids (Fredrikson et al 1986). PKA phosphorylates HSL at multiple activating phosphorylation site (Anthonsen et al 1998). Insulin inhibits the transcriptional expression of HSL, as well as inhibiting its lipase activity by inhibition of PKA signaling. MGL catalyzes the final step of FA mobilization, which is the

hydrolysis of MAG to release glycerol and FA. Unlike HSL, MGL preferentially hydrolyzes all MAG stereoisomers, produced as a result of hydrolysis by other lipases.

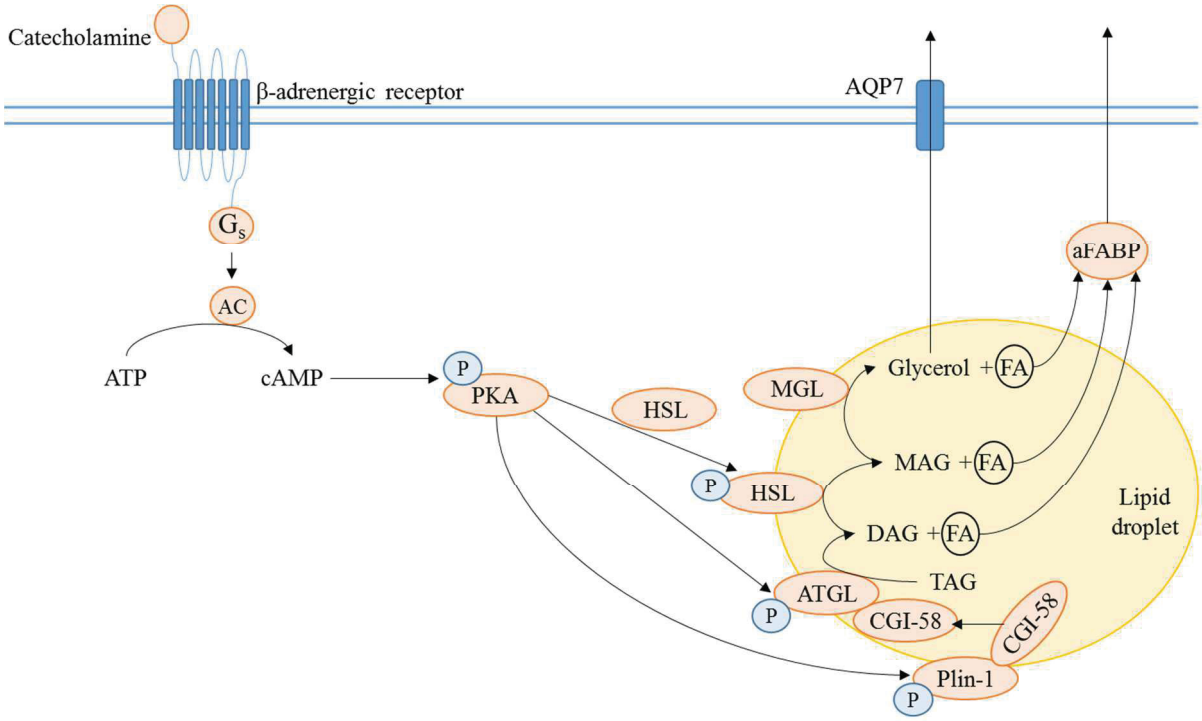

Figure 1.4: Signaling pathway of β-adrenergic-stimulated adipocyte lipolysis. Stress hormones such as catecholamine are able to activate β-adrenergic receptors expressed by adipocytes. Activation of β-adrenergic receptors initiates a signaling cascade resulting in enzymatic degradation of neutral lipid storage. Abbreviations: stimulatory G protein (G_s), adenosine triphosphate (ATP), cyclic adenosine monophosphate (cAMP), adenylyl cyclase (AC), phosphate (P), protein kinase A (PKA), adipose triglyceride lipase (ATGL), perlipin-1 (plin-1), Comparative Gene Identification 58 (CGI-58), triacylglycerol (TAG), diacylglycerol (DAG), fatty acid (FA), hormone sensitive lipase (HSL), monoacylglycerol (MAG), MAG lipase (MGL), aquaporin 7 (AQP7), adipose FA-binding protein (aFABP).

WAT lipolysis accounts for 94% of circulating FA in lean humans (Roden 2006), which are taken up by other organs, including the heart, as a substrate for ATP production. When lipolysis is stimulated, for example due to stress, circulating lipids which are available for intramyocardial lipid uptake become elevated, which may lead to excessive cardiac lipid accumulation and FA oxidation exceeding mitochondrial oxidative capacity.

1.5. The implication of intramyocardial lipid accumulation on cardiac inflammation

Systemic inflammation in patients with failing hearts is characterized by an increase in circulating proinflammatory markers such as TNFα, IL6 and interleukin 1 (IL1) family, as well as immune cell recruitment and activation in the heart. These factors lead to the activation of the nuclear factor kappa-light-chain-enhancer of activated B cell (NF-$_K$B) signaling pathway, further promoting the inflammatory state within the cardiac tissue. Lipids have been shown to activate toll-like receptors (TLRs), with TLR4 as the most highly expressed TLR isoform in the heart (Holland et al 2011, Yu & Feng 2018). Upon

activation of TLR, NF-$_K$B is activated, thus promoting the transcriptional expression of TNFα and IL6. In addition to the circulating lipids, TLRs can be activated by ROS and lipid peroxidation products released from damaged or injured cardiomyocytes. The activated TLRs in turn can also regulate cardiac lipid accumulation, lipid-induced insulin resistance and ceramide synthesis in a diabetic murine model, which was associated with impaired cardiac function (Dong et al 2012), thus linking lipid metabolism to cardiac inflammation under pathological conditions. TNFα provided the first link between cardiomyopathy and inflammation (Levine et al 1990) with sustained expression of TNFα resulting in left-ventricular dysfunction and adverse remodeling. Moreover, cardiac-specific overexpression of TNFα results in a dose-dependent decline in EF (Franco et al 1999). Additionally, TNFα induces protein degradation, including troponin I, resulting in reduced cardiac contractility (Adams et al 2006). Proinflammatory cytokines could enhance the inflammatory response also by acting on cardiac immune cell populations. For example, IL6 indirectly induces the infiltration of neutrophils and macrophages and therefore immune cell-associated tissue injury by stimulating the expression of intercellular adhesion molecule 1 (ICAM1) (Gwechenberger et al 1999). ICAM1 is strongly increased following transaortic constriction (TAC) and in HF patients, and is associated with the recruitment of other proinflammatory cells such as T cells (Salvador et al 2016) causing a decline in cardiac function. Overall, lipid-induced cardiac inflammation is attributed to NF-$_K$B-regulated proinflammatory cytokine release and a cytokine-mediated recruitment and activation of immune cells, therefore contributing to the decline in cardiac function.

Cardiac inflammation following a pathological insult occurs in distinct phases, which are dependent on the type of insult, i.e. ischemic injury-associated tissue necrosis or non-ischemic mechanical stress due to pressure overload. Ischemic injury following an infarction triggers an acute inflammatory response, driven by the rapid recruitment of neutrophils (Elgebaly et al 1989) and monocytes (Dewald et al 2005) to the site of injury. This inflammatory phase lasts for a week post-MI, after which the reparative phase is initiated by the disappearance of neutrophils and decreased proinflammatory cytokines and chemokines. Cardiac macrophages secrete transforming growth factor-β (TGF-β), which further suppresses inflammation and promotes fibrosis (Nahrendorf et al 2007).

In contrast, pressure overload without ischemia triggers a time-dependent inflammation in the heart, which occurs in four phases of heart failure development: acute decompensated phase, compensated phase, decompensated phase with HF establishment, and lastly congestive to end-stage HF (Brenes-Castro et al 2018).

Initially following a stimulation from a non-ischemic trigger such as mechanical stress, left-ventricular EF (LVEF) acutely declines without any sign of inflammation, marking the acute decompensation phase and the start of the progression to non-ischemic HF. After a period of three days, the heart compensates for the increase in peripheral resistance by hypertrophy, thus restoring LVEF. During this compensated phase, Ly6C^{hi} monocytes are recruited, contributing to the expansion of macrophage populations in the heart (Patel et al 2017). Neurohormonal mobilization of myeloid cells from the bone marrow and splenic reserves allow for the increase in circulating monocytes and consequently availability for recruitment (Leuschner et al 2010). AngII and oxidative

stress in the heart stimulates the local release of proinflammatory cytokines and chemokines, further promoting monocyte migration (Lindner et al 2014, Sriramula & Francis 2015). Recruited monocytes differentiate into proinflammatory macrophages which release proinflammatory cytokines, thereby promoting the recruitment and activation of T cells (Nevers et al 2015, Patel et al 2018). $CD4^+$ T cells in turn stimulate monocyte infiltration by increasing the expression of cysteine-cysteine chemokine ligand 2 (CCL2). Additionally, infiltrating B cells facilitate monocyte migration via the expression of CCL7 (Zouggari et al 2013). A peak in the dendritic cell (DC) population is also observed during this phase (Patel et al 2017). Altogether, macrophages, B cells and DCs act as antigen-presenting cells which co-stimulate T cells, thereby activating T cell-mediated inflammatory response (Laroumanie et al 2014, Kallikourdis et al 2017).

As the disease progresses, compensation is lost, leading to a decline in LVEF, fractional shortening (FS), and diastolic function, thereby marking the start of the decompensated phase and the establishment of HF. Monocyte recruitment, cardiac macrophage and DC populations progressively decline (Patel et al 2017), and eventually macrophages become dispensable in the progression of HF. In contrast, B and T cell populations remain high (Nevers et al 2015, Patel et al 2018, Zouggari et al 2013), and the expression of adhesion molecules such as ICAM-1 increases (Nevers et al 2015). Once HF is established and systolic function is significantly altered, the disease progresses to congestive to end-stage HF. This phase is marked by a further depression in cardiac function and a second peak in DC population (Patel et al 2017), suggesting co-stimulation of T-cells by DCs as a driver of cardiac inflammation at this phase of the disease timeline.

1.6. Cardiac specific deletion of p38 MAPK α: a model of pressure overload-induced HF with cardiac lipid accumulation

p38 MAPK α is a protein which regulates various cellular processes such as inflammation (Guan et al 1998, Hollenbach et al 2004), apoptosis (Ziegler-Heitbrock et al 1992), cellular maturation and proliferation (Iwasa et al 2003, Takenaka et al 1998). It is ubiquitously expressed, and is highly abundant in the heart. It is activated under stress conditions such as inflammation, heat shock, osmotic shock, oxidative stress and UV light exposure (Martin et al 2015).

p38 MAPK α has been shown to be activated in cardiac hypertrophy and remodeling during HF establishment (Bao et al 2007). However, whether its role is beneficial or detrimental is still controversial. For instance, mice lacking p38 MAPK α exposed to ischemia reperfusion developed a smaller infarction compared to wild-type mice (Otsu et al 2003). On the other hand, p38 MAPK α was reported to be cardioprotective in a TAC-induced HF model (Nishida et al 2004). Mice with cardiac-specific deletion of p38 MAPK α developed cardiac hypertrophy, dysfunction and dilation, one week after pressure overload induction by TAC. In contrast, wild-type mice developed cardiac hypertrophy without any significant alterations in function or left-ventricular dimensions.

Previous studies performed in our laboratory revealed a protective role of cardiac p38 MAPK α in AngII-induced pressure overload and HF establishment (Bottermann et al manuscript in preparation, Leitner 2017). In these studies, a cardiomyocyte-specific,

tamoxifen-inducible knock-out of p38 MAPK α (iCMp38KO) was generated by the Cre-lox P system. After exposure to 48 hours of AngII infusion, iCMp38KO showed impaired cardiac function characterized by left-ventricular dilation and reduced cardiac contractility, resulting in a marked reduction of cardiac output and EF. Histological analyses of the cardiac tissue revealed significant lipid accumulation and neutrophil infiltration, suggesting a potential mechanism of interaction between altered lipid homeostasis and inflammation in the heart. These results were reproduced in this study during the acquisition of baseline values, thus showing the reliability of this model as a rapid, inducible pressure overload-induced HF model (section 4.1). This model is also suitable for the study of cardiac lipid accumulation and inflammation during the establishment of pressure overload-induced HF. In addition, this model has also been used for the investigation of interorgan communication between the heart and skeletal muscle during HF progression (i.e. cardiac cachexia) (Leitner 2017).

For this thesis, cardiomyocyte-specific inhibition of p38 mitogen-activated protein kinase (MAPK) α was used for the study of cardiac lipid accumulation and the potential involvement of adipose tissue during the establishment of HF.

1.7. Project aims

Cardiac lipid accumulation has been shown experimentally and clinically in HF and is associated with the progressive decline in cardiac function. This leads to the question of the role of adipose tissue lipolysis as a source for cardiac lipid accumulation often seen in HF models. This highlights the importance to investigate the interorgan communication between the failing heart and adipose tissue. In addition, both cardiac metabolism and immune cell recruitment may affect cardiac performance, particularly under pathological conditions. Although the role of adipose tissue lipolysis under acute cardiac stress for instance following ischemic injury has been shown, little is known about heart – adipose tissue crosstalk under non-ischemic cardiac stress. Moreover, the exact interaction between cardiac lipid accumulation and immune cell infiltration in a non-ischemic HF model has not been fully established.

A number of hypotheses can be made according to the current literature: (1) adipose tissue undergoes lipolysis under stressed conditions, thus increasing circulating lipid available for uptake by other organs including the heart; (2) cardiac lipid uptake and impaired metabolism leads to intramyocardial lipid accumulation and lipotoxicity; (3) lipid accumulation leads to the recruitment of immune cells, which then mediate cardiac inflammation; (4) both cardiac lipid accumulation and immune cell-mediated inflammation contribute to further decline in cardiac function.

In this study, iCMp38KO mice were used in combination with AngII administration, to investigate lipolysis-mediated interorgan communication between the heart and adipose tissue. As mentioned in section 1.6, this model is a highly reproducible, accelerated advanced HF mouse model, showing a significantly impaired cardiac function after only 48 hours of AngII infusion. The iCMp38KO shows substantial cardiac lipid accumulation and neutrophil infiltration, thereby serving as a suitable HF model to test the proposed hypotheses.

- Firstly, the reproducibility of this model should be confirmed, by generating the knock-out and measuring cardiac function at baseline and 48 hours after AngII administration. Cardiac lipid accumulation and neutrophil infiltration should also be confirmed.

- Secondly, by blocking adipose tissue lipolysis and analyzing the effects on cardiac lipid accumulation and function, a mechanism of heart – adipose tissue crosstalk via lipolysis can be determined. Therefore, a lipolysis inhibitor and protocol suitable for the HF model must be established for the purpose of this study. This may be performed by testing pharmacological lipolysis inhibitors and measuring lipolysis markers such as plasma glycerol and FA.

- The interaction between cardiac lipid accumulation and immune cell infiltration can be determined by measuring immune cell populations in the heart following AngII-induced pressure overload in the iCMp38KO, and comparing to the control heart (with compensated cardiac function). Any changes in the immune cell profile due to adipose tissue lipolysis may indicate the role of cardiac lipid accumulation in immune cell recruitment and subsequent inflammation.

- Lastly, since communication may be bi-directional, the interorgan crosstalk between the heart and adipose tissue should be further characterized by screening for alteration in adipose tissue at the transcriptional level. This shall be performed on the iCMp38KO following pressure overload induction, to identify alteration associated with HF.

2

Materials

2.1. General Laboratory Equipment

Product name and model	Manufacturer
-20°C freezer Premium NoFrost	Liebherr, Germany
-80°C freezer	Thermo Fisher Scientific, Germany
100 µm cell filter	Greiner Bio-one, Germany
100 Sterican	B Braun, Germany
4°C refrigerator ProfiLine	Leiebherr, Germany
40 µm cell filter	Greiner Bio-one, Germany
96-Well Microtiter™ Microplates	Thermo Fisher Scientific, Germany
Adhesive sealing sheets	Thermo Fisher Scientific, Germany
Alzet micro-osmotic pump model 1003D	Durect, USA
BD FACSCantoII	BD Biosciences, Germany
Biometra OV3 incubator	Core Life Science, Inc., USA
Centrifuge 5402	Eppendorf, Germany
Coverslips 24 x 50 mm	Engelbrecht, Germany
Cryostat CM 1850	Leica, Germany
ELISA-reader SpectraCount BS10000	Packard, Germany
FACS tubes	Falcon, Germany
Fluorescent microscope Keyence BZ-9000	Keyence, Japan
Gilson Pipetman classic pipet	Fisher Scientific, UK
HistoBond Microscope slides	Marienfeld, Germany

Ice dispenser	Ziegra, Germany
StepOnePlus Real-Time PCR System	Applied Biosystems, USA
Thermomixer compact	Eppendorf, Germany
TissueRuptor	Qiagen, Germany
TissueRuptor Disposable Probes	Qiagen, Germany
VetEquip Inhalation Anesthesia System	VetEquip, USA
Vevo 2100 Imaging System	VisulaSonics Inc, Canada
Vortex Reax Top	Heidolph, Germany

2.2. General Chemicals

Product name (catalogue number)	**Manufacturer**
4OH-Tamoxifen (H6278)	Sigma-Aldrich, Germany
Angiotensin II (human) (A9525)	Sigma-Aldrich, Germany
Aquatex (108562)	Merck, Germany
Atglistatin (S7364)	Selleckchem, USA
Chloroform (102445)	Merck, Germany
Collagenase type I (LS004197)	Worthington, USA
DNAseI (10530400)	Roche Diagnostics, Germany
DAPI Fluoromount-G	SouthernBiotech, Germany
Entellan new (107961)	Merck, Germany
Ethylenediaminetetraacetic acid (E6758)	Sigma-Aldrich, Germany
Fc Block	BioLegend, Germany
Fettrot 7B (1A 272) (1A272)	Chroma Gesellschaft, Germany
Fixable viability dye	eBiosciences, Germany
GS-9667	Gilead Sciences, USA
Halt Protease & Phosphatase Inhibitor Single-Use Cocktail, EDTA-free (78443)	Thermo Fisher Scientific, Germany
HBSS (14025092)	Gibco Life Technologies, Germany
Isoflurane-Piramal (9714675)	Piramal Healthcare, UK
Isoprenaline hydrochloride (I5627)	Sigma-Aldrich, Germany
KP-Cryocompound	VWR, USA
Mayer's Hematoxylin (51275)	Sigma-Aldrich, Germany
Normal Goat Serum (S-1000)	Vector Laboratories, USA
Odessey blocking buffer (TBS) (927-40000)	LI-COR, USA
PageRuler Prestained Protein Ladder (26616)	Thermo Fisher Scientific, Germany
Paraformaldehyde (16005)	Sigma-Aldrich, Germany
Peanut oil (P2144)	Sigma-Aldrich, Germany
Qiazol Lysis Reagent (79306)	Qiagen, Germany
Saponin (6857.1)	Roth, Germany
Xylol (Isomere) (9713.1)	Roth, Germany

2.3. Cell Culture Materials

Material (catalogue number)	Manufacturer
6-Well Cell Culture Plate	Greiner Bio-One, Austria
Adenosine (A9251)	Sigma-Aldrich, USA
Albumin Fraktion V (8076)	Roth, Germany
Cell counting chamber	Laboroptik, Germany
Cell line 3T3-L1 (CL-173)	ATCC, USA
Cell scraper	VWR, USA
CO2 Incubator HERA cell vios 250i	Thermo Fisher Scientific, USA
Cryo Tube 20 (2 mL)	TPP, Switzerland
Dexamethasone (D8893)	Sigma-Aldrich, USA
Dimethyl Sulphoxide (DMSO) (D2438)	Sigma-Aldrich, USA
Dulbecco's Modified Eagle's Medium (DMEM) High Glucose 4500 mg/L	Sigma-Aldrich, USA
Epinephrine (E4250)	Sigma-Aldrich, USA
Fetal Bovine Serum	Biochrom AG, Germany
Glutamax (Gibco)	Thermo Fisher Scientific, USA
Insuman Rapid 40I.E./ml	Sanofi-Aventis, Germany
Isobutylmethylxanthine (IBMX) (I7018)	Sigma-Aldrich, USA
Kolliphor EL (C5135)	Sigma-Aldrich, USA
Laminar-Flow Bench Safe 2020	Thermo Fisher Scientific, USA
Liquid Nitrogen Tank	Air Liquide, France
Microscope ID 03	Zeiss, Germany
Penicillin/Streptomycin (Gibco)	Thermo Fisher Scientific, USA
Rosiglitazone (CAY71740)	Cayman Chemical, USA
Rotofix Centrifuge	Hettich, Germany
Serological pipette (2 mL, 5 mL, 10 mL, 25 mL)	Greiner Bio-One, Austria
Tissue Culture Dish 100 (10 cm)	TPP, Switzerland
Trypsin-EDTA	Sigma-Aldrich, USA
Water bath	GFL, Germany

2.4. Antibodies

Antibody (catalogue number)	Manufacturer
7AAD (420404)	BioLegend, Germany
Cy3-AffiniPure goat anti-rabbit IgG (111-165-144)	Jackson, USA
Fixable viability dye eFluor 780 (65-0865-14)	eBioscience
IR Dye 800CW Goat anti-rabbit (926-32211)	Odyssey, USA
Mouse anti-CCR2 (107613)	BioLegend, Germany

Mouse anti-CD115 (565249)	BD Biosciences, Germany
Mouse anti-CD11b (101235)	BioLegend, Germany
Mouse anti-CD19 (557399)	BD Biosciences, Germany
Mouse anti-CD3 (100312)	BioLegend, Germany
Mouse anti-CD45 (563891)	BD Biosciences, Germany
Mouse anti-CD64 (139309)	BioLegend, Germany
Mouse anti-Ly6C (150605)	BioLegend, Germany
Mouse anti-Ly6G (127654)	BioLegend, Germany
Mouse anti-MHCII (107627)	BioLegend, Germany
Rabbit anti-phospho HSL ser660	Cell Signaling, USA
Rabbit anti-UCP1 (10983)	Abcam, UK
Rat anti-Ly6G (551461)	BD Pharming, USA
Rhodamine Red-X-AffiniPure goat anti-rat IgG (112-295-167)	Jackson, USA
Wheat Germ Aglutinin (WGA) Alexa Fluor 488 conjugate (W11261)	Invitrogen, USA

2.5. Kits

Product Name (catalogue number)	**Manufacturer**
Free Fatty Acid, half micro test (11 383 175 001)	Roche, Germany
Glycerol Assay Kit (MAK117)	Sigma-Aldrich, USA
Maxima SYBR green/ROX qPCR master mix (K0221)	Thermo Fisher Scientific, USA
Pierce BCA Protein Assay kit (23225)	Thermo Fisher Scientific, USA
Quantitect Reverse Transcription kit (205311)	Qiagen, Germany
REVERT Total Protein Stain (926-11011)	LI-COR, USA
RNeasy Fibrous Tissue Mini Kit (74704)	Qiagen, Germany
RNeasy Lipid Tissue Mini Kit (74804)	Qiagen, Germany

2.6. RT-PCR Primers

Primer		**Sequence (5' - 3')**
Adipoq	Forward	CCACTTTCTCCTCATTTCTG
	Reverse	CTAGCTCTTCAGTTGTAGTAAC
Cidea	Forward	GTGTTAAGGAATCTGCTGAG
	Reverse	CTATAACAGAGAGCAGGGTC
Cox8b	Forward	ATCTCAGCCATAGTCGTTG
	Reverse	CTGCGGAGCTCTTTTTATAG
Csnk2b	Forward	GATCTTAGACCTGGAACCTG
	Reverse	CAACCCATAAAGCATCTCAG
Il1b	Forward	GGATGATGATAACCTGC

	Reverse	CATGGAGAATATCACTTGTTGG
Il6	Forward	AAGAAATGATGGATGCTACC
	Reverse	GAGTTTCTGTATCTCTCTGAAG
Lep	Forward	CTTTGGTCCTATCTGTCTTATG
	Reverse	TCTTGGACAAACTCAGAATG
Nudc	Forward	AGAACTCCAAGCTATCAGAC
	Reverse	CTTCAGGATTTCCTGTTTCTTC
Ppara	Forward	GATGTCACACAATGCAATTC
	Reverse	CAGTTTCCGAATCTTTCAGG
Pparg	Forward	AAAGACAACGGACAAATCAC
	Reverse	GGGATATTTTTGGCATACTCTG
Ppargc1a	Forward	TCCTCTTCAAGATCCTGTTAC
	Reverse	CACATACAAGGGAGAATTGC
Tnf	Forward	CTATGTCTCAGCCTCTTCTC
	Reverse	CATTTGGGAACTTCTCATCC
Ucp1	Forward	CTTTTTCAAAGGGTTTGTGG
	Reverse	CTTATGTGGTACAATCCACTG

3

Methods

3.1. Cardiac pressure-overload mouse model – iCMp38KO mice and AngII administration

To generate iCMp38KO mouse line, p38MAPKα$^{flox/flox}$ mice were crossed with heterozygous merCremer mice under the control of α-MHC promotor (Ventura et al 2004, Zhang et al 2006). Cardiomyocyte-specific KO of p38 MAPK α was induced via 10 consecutive days of 4OH-tamoxifen injection (i.p. 500 µg/day) at 6 - 8 weeks of age. After at least 4 weeks of recovery period, 12 – 14 week old mice were used for experiments. Cardiac pressure overload was stimulated with a continuous administration of AngII (1.5 mg/kg/day, AngII dissolved in phosphate buffered saline (PBS)) via subcutaneous implantation of micro-osmotic pump for 48 hours.

p38MAPKα$^{flox/flox}$ litter mates lacking Cre-recombinase were used as controls. For comparability, these mice also received tamoxifen and AngII.

3.2. Echocardiography

To assess cardiac function, echocardiographic analysis was performed using Vevo 2100 imaging system. Mice were placed into an anaesthetic chamber supplied with a flow of 4% isoflurane at 800 mL/min. After the mice had lost their reflexes, the anaesthesia was maintained using 2 – 2.5% isoflurane at 800 mL/min flow through a nose cone. Mice were laid onto a heated (40°C) plate in a supine position. Limbs were fixed to ECG electrodes to monitor heart as well as breathing rates. Body temperature was monitored using an anal temperature probe. Mice were kept at 37°C throughout the measurement. The chest area was shaved, and the residual hair was removed using hair removal cream. Warm sonication gel was then applied onto the shaved area to allow contact with the transducer (18-38 MHz). B- and M-mode of the long and short axes of the left

ventricles were captured and cardiac function parameters including end systolic volume (LVESV), end diastolic volume (LVEDV), stroke volume (SV), cardiac output (CO), fractional shortening (FS), and ejection fraction (EF) were measured using the Simpson method according to Heinen et al 2018.

3.3. 3T3-L1 cell culture

Growth medium:	Freezing medium:	Differention medium:	Starving medium:
89% DMEM	95% growth medium	89% DMEM	99% DMEM
12.5 mM glucose	5% DMSO	12.5 mM glucose	12.5 mM glucose
10% FBS		10% FBS	1% PS
1% PS		1% PS	4 mM L-glutamine
4 mM L-glutamine		4 mM L-glutamine	
		1 µM Dexamethasone	
		0.5 mM IBMX	
		1 µg/mL insulin	

Table 3.1: List of media and ingredients for the culture and differentiation of 3T3-L1 cell line.

3.3.1. Thawing and seeding of cells

Upon removal from storage (in liquid nitrogen at -196°C), cells were thawed rapidly at 37°C in a water bath. Cells were then removed from the cryo tube (approximately 1 x 10^5 cells/cryo tube), and transferred into a 15-mL falcon tube containing 9 mL pre-warmed growth medium. DMSO was removed via centrifugation at 700 rpm for 12 minutes at room temperature. The cell pellet was then re-suspended in the growing medium and seeded onto a 10-cm cell culture dish, and placed in a 37°C incubator supplied with 5% CO_2.

3.3.2. Cultivation

Cells were maintained below 80% confluency at 37°C with 5% CO_2 supply. Growth medium was replaced at every second day. When the cells reached 70 – 80% confluency, they were split to allow for efficient growth. Growth medium was removed, and cells were incubated with trypsin-EDTA at 37°C for 5 - 10 minutes to facilitate the detachment of the cells from the culture dish. Afterwards, fresh, pre-warmed growing medium was added to stop the activity of the trypsin-EDTA. Cell suspension was transferred into a falcon tube and centrifuged at 1000 rpm for 5 minutes at room temperature. The cell pellet was re-suspended in growth medium and seeded on 10-cm cell culture dishes for further passage, and 6-well cell culture plates for differentiation.

3.3.4. Freezing of cells for long term storage

Undifferentiated 3T3-L1 cells were trypsinized as per the splitting protocol. Upon centrifugation, the cell pellet was re-suspended in cold freezing medium, and approximately 1 x 10^5 cells were transferred into a cryo tube. Cells were frozen in -196°C liquid nitrogen for long term storage.

3.3.5. Differentiation protocol

After seeding of approximately 1 x 10^5 cells/well of 6-well cell culture plates, cells were cultured in growth medium until 100% confluency was achieved. Cells were then kept two days post-confluency in the same medium. Afterwards, the medium was replaced with the differentiation medium (differentiation day 0). On day 2, the medium was then replaced with growth medium. Full differentiation was achieved on day 7 – 8, after which, further experiments were performed.

3.3.6. *In vitro* lipolysis inhibition study

Fully differentiated 3T3-L1 adipocytes were starved for 2 hours in pre-warmed starvation medium following a quick rinse to remove residual serum-containing medium. After the starving period, medium was removed and replaced with fresh starvation medium containing 0.5% bovine serum albumin (BSA). Cells were pre-treated with lipolysis inhibitors (10 µM adenosine, 10 µM GS-9667 or 10 µM atglistatin, each was dissolved in DMSO) for 30 minutes. Lipolysis was stimulated by incubation of the cells with 1 µM epinephrine (dissolved in sterile water) for 45 minutes. Afterwards, media was collected from each well for the measurement of the released glycerol.

3.4. Cardiac tissue histological analysis

3.4.1. Freezing and cryosectioning

Fresh cardiac tissue was isolated and submerged in cold PBS to remove the residual blood. Only the ventricles were collected for histological analyses. Ventricles were submerged in KP-Cryocompound and frozen in -30°C to -40°C isopentane chilled in dry ice. Cryo-embedded tissue blocks were stored in -80°C. To obtain cryo-sections of the heart tissue, tissue blocks were warmed up to -22°C in a pre-cooled cryostat. 12 µM sections were obtained and placed onto microscope slides. The slides were air-dried for 30 minutes before storage in a microscope slide box containing desiccants. The slide boxes were kept at -20°C for long term storage. For usage, the slide boxes were warmed up to room temperature and condensation was dried using a hairdryer.

3.4.2. Sudan red staining

Solutions were prepared as follows:

Stock solution:	**Working solution:**	**Fixative solution (Baker's Formol):**
0.5 % Fettrot 7B dissolved in double-distilled water, incubate at room temperature for 24h	60% stock solution in 40% double-distilled water, filtered before use	1% calcium chloride
		37% formol
		Dissolved in double-distilled water

Table 3.2: List of solutions used in the Sudan red staining protocol.

Tissue sections were fixed using the fixative solution for 10 minutes. The fixative was washed off 3 x 10 minutes in distilled water. Sections ere incubated in 60% isopropanol in double-distilled water for 5 minutes. The sections were stained using the staining solution for 12 minutes with continuous shaking to avoid precipitation. The slides were

dipped two to three times in 60% isopropanol in double-distilled water. The sections were further washed for 3 x 5 minutes in distilled water. Coverslips were mounted using Aquatex mounting media and air-dried overnight. The stained sections were viewed under brightfield microscope set to 0.001 second exposure time at 4x magnification, and 0.008 second at 20x magnification. Images were analyzed using the ImageJ software. Briefly, background signal was subtracted based on the "rolling-ball" method and signal intensity of the staining was measured. The protocol is summarized below:

1. Open image using ImageJ program.
2. Adjust area of interest.
3. Select: Image → Type → RGB stack.
4. To subtract background, select: Process → Subtract Background. Set the rolling ball radius to 50 pixels.
5. To select signal measured, create a threshold by selecting: Image → Adjust → Threshold (0 - 220).
6. To quantify the signal, select: Analyze → Set Measurement, turn on "Limit to threshold" and "Area". Then select: Analyze → Measure.
7. The results will be displayed as area per pixel (i.e. pixel^2), meaning the area occupied by the signal within the set threshold.

3.4.3. Immunofluorescent staining

Tissue sections were fixed in 4% paraformaldehyde (PFA) dissolved in double-distilled water (pH 7.4) for 10 minutes. The fixative was washed off 3 x 10 minutes in PBS. The sections were blocked with the washing solution (2% saponin in PBS) containing 10% normal goat serum (NGS) for 1 hour at room temperature. Sections were incubated with the primary antibody diluted in PBS with 2% w/v saponin overnight at 4°C. The primary antibody was washed off 3 x 10 minutes with PBS with 2% w/v saponin. Sections were incubated with the secondary antibody diluted in PBS with 2% w/v saponin in a dark room at room temperature for 4 hours, with continuous shaking. Secondary antibody was washed off 3 x 10 minutes with PBS with 2% w/v saponin, and additionally for 10 minutes in PBS. Coverslips were mounted using DAPI Fluoromount-G and left to dry off in the dark at 4°C. Images were acquired using green, red and blue channels with the following set-up:

4x objective		20x objective		60x objective	
Channel	**Exposure time (seconds)**	**Channel**	**Exposure time (seconds)**	**Channel**	**Exposure time (seconds)**
Red	1	Red	1.5	Red	0.25
Green	0.5	Green	0.3	Green	0.03
Blue	2	Blue	3	Blue	0.7

Table 3.3: Set-up of the Keyence BZ-9000 microscope for image acquisition.

3.5. White adipose tissue histological analysis

3.5.1. Freezing and cryosectioning

White adipose tissue (WAT) was harvested from the perigonadal fatpad and fixed in cold 4% PFA (w/v double-distilled water, pH 7.4) for 1 to 2 hours at 4°C. The fixative solution was removed and replaced with 30% sucrose (w/v sterile PBS) and incubated

overnight at 4°C. Tissues were submerged in KP-Cryocompound and frozen at -20°C for 5 – 6 hours. Tissue blocks were transferred to -80°C for further freezing and long-term storage.

For cryosectioning, tissue blocks were warmed up to -35°C in a cryostat. 14 µM sections were cut and placed onto microscope slides. Sections were air-dried and placed in microscope slide boxes containing desiccants, and immediately stored at -20°C. For usage, the slide boxes were warmed up to room temperature and condensation was dried using a hairdryer.

3.5.2. Hematoxylin & Eosin staining

Sections were fixed in 4% PFA (w/v double-distilled water, pH 7.4) for 10 minutes. The fixative solution was rinsed briefly in distilled water, and was then left for 2 x 10 minutes in distilled water. Sections were stained with Mayer's hematoxylin for 5 minutes with continuous shaking. Sections were dipped two to three times in 0.1% HCl (v/v double-distilled water) and immediately washed for 12 minutes under running distilled water. Sections were further stained with Eosin G for 5 minutes. Sections were washed under running distilled water for 5 minutes. Sections were dehydrated in increasing concentration of ethanol and finally xylol. Coverslips were immediately mounted using Entellan new mounting medium and left to air-dry at room temperature overnight. Sections were imaged using a brightfield microscope set to 0.001 second exposure time at 4x magnification, 0.008 second at 20x magnification, and 0.08 second at 60x magnification.

3.5.3. Immunofluorescent staining

Sections were stained and imaged according to the protocol in section 3.4.3 (page 24).

3.6. Gene expression analysis

For RNA isolation, tissues were harvested and snap-frozen in liquid nitrogen, and stored at -80°C until further use. RNA was isolated using Qiagen Fibrous tissue RNeasy mini kit and Lipid tissue RNeasy mini kit according to the manufacturer's protocols.

3.6.1. RNA isolation from WAT

No more than 100 mg WAT was lysed and homogenized using a TissueRuptor (Qiagen) in the appropriate amount of Qiazol lysis buffer (1 mL per 100 mg tissue). The lipid phase was separated by incubating with chloroform and centrifuging at 4°C for 15 minutes at 12000 x g. The aqueous phase containing RNA was mixed at 1 : 1 volume with 70% ethanol in RNase-free water, and transferred into a RNA mini-spin column. In-column DNase digestion and a series of washing steps were performed. Finally, the RNA was eluted with 40 µL RNAse-free water, and the yield and purity were measured using Nanodrop ND-1000 spectrometer.

3.6.2. RNA isolation from cardiac tissue

Less than 30 mg tissue was lysed and homogenized using a TissueRuptor in the recommended amount of RLT buffer containing β-mercaptoethanol. Samples were treated with proteinase K and centrifuged. The supernatant containing RNA was obtained and mixed with 96% ethanol. The mixture was transferred into a RNA mini-

spin column. In-column DNase digestion and a series of washing steps were performed. Finally, the RNA was eluted with 50 µL RNAse-free water, and the yield and purity were measured using Nanodrop ND - 1000 spectrometer.

3.6.3. Reverse transcription

Reverse transcription into complementary DNA (cDNA) was performed using Quantitect Reverse Transcription Kit (Qiagen) according to the manufacturer's protocol. Briefly, RNA samples were treated with DNase, and reverse transcribed for 15 minutes at 42°C. The reverse transcriptase was inactivated by heating at 95°C for 3 minutes. Based on the RNA concentration measured by Nanodrop ND - 1000, 400 to 1000 ng in 20 µL was calculated for the reverse transcription reaction, to produce 20 ng/µL cDNA. Finally, cDNA samples were kept at -20°C for long-term storage.

3.6.4. Quantitative Real-Time PCR using SybrGreen

Transcripts expressions were detected by mixing the cDNA samples with the primer of interest and Maxima SYBR green/ROX qPCR master mix as follows:

Maxima SYBR green/ROX qPCR master mix	10 µL
Nuclease-free water	7.2 µL
cDNA (20 ng/µL)	1 µL
Primer (450 nM)	1.8 µL

Table 3.4: List of content per reaction well for transcript detection using SybrGreen.

Pre-designed primers of interest are listed in section 2.6 (page 19), and each transcript was analyzed in duplicates. The StepOnePlus Real-Time PCR System and Software were used for detection and analysis. For the detection, the software was set as follows:

Taq DNA polymerase was activated at 95° C for 10 minutes. The next step was 40 cycles of incubations at 95° C for 15 seconds and at 60°C for 60 seconds per cycle. The last step was the melting curve stage, where the efficiency of the reaction could be verified by firstly heating the reaction plate up to 95° C for 15 seconds, followed by cooling down to 60° C for 60 seconds, and finally heating back up to 95° C at a rate of 0.3° C/15 seconds.

3.6.5. Analysis using X_0 method

The X_0 method allows for the extrapolation of the starting expression of the transcript of interest. This method is based on the following equation (Livak & Schmittgen 2001):

$X_n = X_0 \bullet (1 + E)^n$, where:

X_n = the expression level of the transcript at n cycle

X_0 = the initial expression level of the transcript prior to its amplification

E = efficiency of amplification, i. e. E = 1 when the amplification is 100% per cycle

The efficiency was tested by analysis of the increase in fluorescence at the consecutive cycle. Cycle n was selected from the period in which the transcripts were amplified in a linear manner. Therefore, the X_0 could be extrapolated as such:

$X_0 = X_n / (2^n)$

X_n of the genes of interest were normalized to the X_n of the reference gene. The relative X_0 was calculated by normalizing to the X_0 of a control sample which was included in all reaction plates to allow for comparison between plates.

3.6.6. Microarray

Quality check and transcriptional profiles of isolated total RNA from WAT was performed in the laboratory of the Biologisch Medizinisches Forschungszentrum (BFMZ), Heinrich-Heine University, Düsseldorf, using Agilent 8x60K Mouse Array technology, which allows for the detection of 60,000 transcripts per chip.

RNA was isolated according to section 3.6.1 (page 25). Quality control was performed by the BFMZ, and only samples with higher integrity values (RQN: >8, Figure 3.1) were selected for microarray analysis. The samples were analyzed by Dr. Patrick Petzsch from the BFMZ.

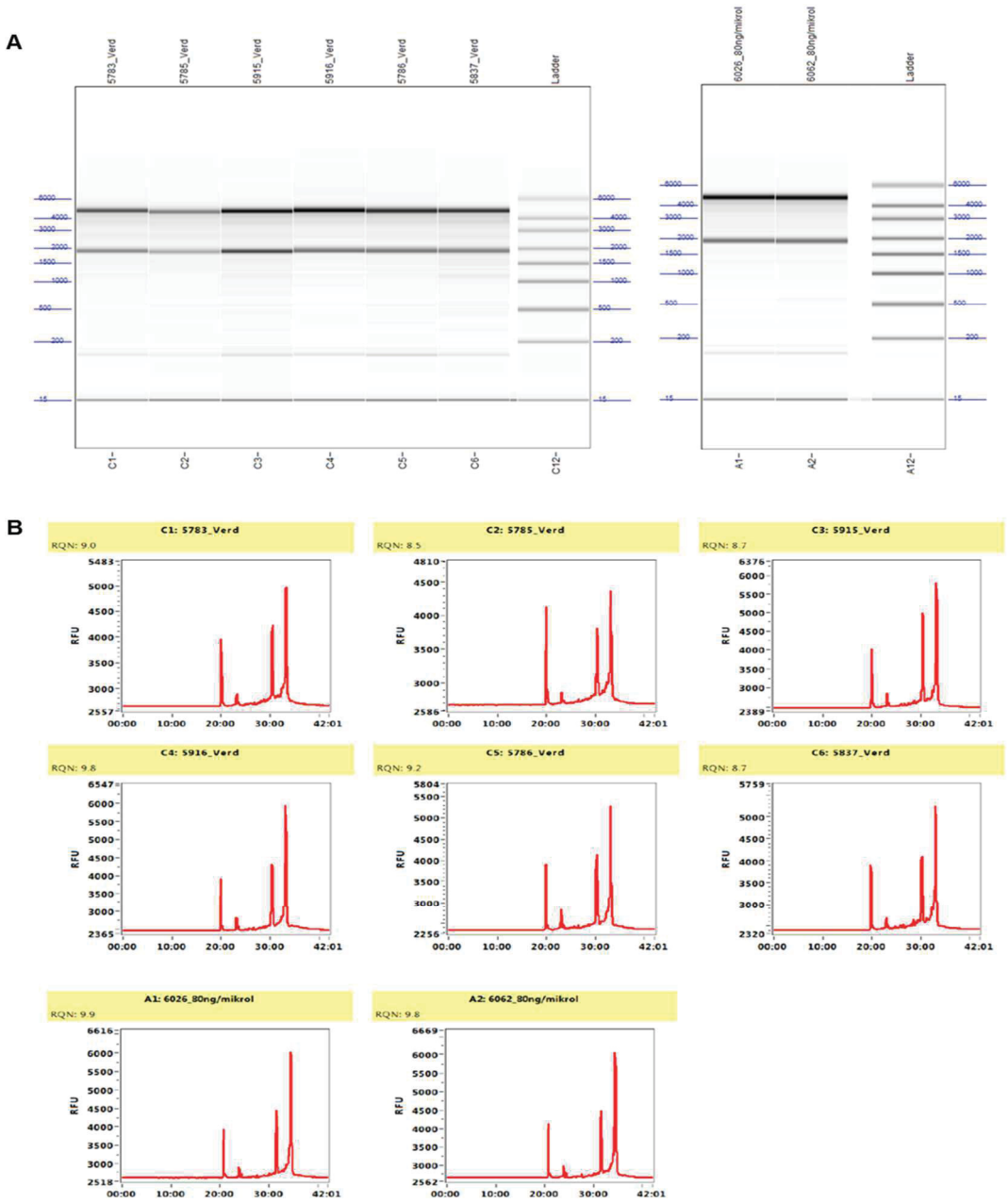

Figure 3.1: Quality control of total RNA samples isolated from WAT. RNA was separated by size using the RNA gel electrophoresis method (A). The amounts of 18S and 28S mRNA and RQN were then calculated based on fluorescence (B). © Copyright 2014 Advanced Analytical Technologies, Inc. All rights reserved.

3.7. Analysis of microarray data

Microarray data of heart and adipose tissue were analyzed based on p-value cut-off (0.05) and absolute fold-change (≥ 2). The prediction of altered canonical pathways and functions based on the microarray data of adipose tissue was performed using Ingenuity Pathway Analysis (IPA) software by Qiagen. Significant alterations was set according to log p-value (> 2) and absolute z-score (> 2).

3.8. *In vivo* pharmacological lipolysis inhibition

Two pharmacological inhibitors of lipolysis were tested *in vivo* to determine the suitability to our heart failure mouse model.

3.8.1. GS-9667

After an overnight fast, GS-9667 was administered via i. p. injection at a dose of 5 mg/kg. Control mice were injected with the vehicle (DMSO). Blood was sampled via tail bleeding at minutes 0, 10, 30, 60 and 120, for the measurement of plasma FFA and glycerol (section 3.9).

3.8.2. Atglistatin

Atglistatin was administered via food at a dose of 0.4 mg/g CHOW food throughout the course of the experiment. Briefly, food was crushed using mortar and pestle, and mixed with the appropriate amount of atglistatin powder. The powdered mixture was formed into a pellet using water, which was then dried overnight.

To determine the antilipolytic efficacy of atglistatin *in vivo,* a positive control experiment was performed on C57BL/6 mice. After 4 to 5 hours of starvation, baseline blood was sampled from the facial vein. Isoproterenol (ISO) was injected i. p. at a dose of 10 mg/kg to stimulate lipolysis. 15 minutes after injection, blood was collected from the heart for further analysis (section 3.9).

Atglistatin treatment on our heart failure model was commenced two days prior to AngII micro-osmotic pump implantation, and continued 48 hours after. Mice were starved for 4 to 5 hours prior to sacrifice.

3.9. Plasma and cell culture media FFA and glycerol measurements

Lipolytic activity was measured by the released amounts of the final products of lipolysis which are FFA and glycerol in the plasma. Plasma samples were obtained by centrifuging the blood samples at 4°C for 15 minutes, at a speed of 1500 x g. The measurements of FFA and glycerol were performed using commercial kits and according to the manufacturers' protocols (Roche and Sigma-Aldrich respectively).

For the measurement of FFA, plasma samples and kit reagents were brought to room temperature at least 10 minutes prior to the assay. 5 µL from each of the samples and standards (palmitic acid) were pipetted in duplicates into a clear, 96-well flat bottom microplate. 100 µL of Reaction mix A, containing acyl-CoA synthetase and ATP, was added and mixed into each well. 5 µL of N-ethyl-maleinimide was added and mixed into each well to remove excess co-enzyme A before the start of the assay reaction. The plate was read at 577 nm to obtain baseline absorbance. The detection reaction was commenced by adding and mixing 5 µL of Reaction mix B, containing acyl-CoA-oxidase, to each well, and incubated at room temperature for 15 minutes. Finally, the plate was read at 577 nm and the amount of FFA in the sample was determined from the absorbance of the standards.

For the measurement of glycerol, 10 µL of plasma samples and standards (glycerol) was pipetted into each well of a clear, 96-well flat bottom microplate. 100 µL of the Master

Reaction Mix was added into each well and incubated for 20 minutes at room temperature. The plate was read at 577 nm. The amount of glycerol in the sample was calculated from the absorbance of the standards.

3.10. Fluorescence-activated cell sorting (FACS) Analysis

3.10.1. FACS analysis of blood samples

For FACS analysis of blood, 100 µL of blood sample was drawn from the heart. Red blood cells were removed using red blood cells lysis buffer (155 mM ammonium chloride, 10 mM potassium hydrogen carbonate, 0.1 mM EDTA). Samples were centrifuged for 10 minutes at 4°C at a speed of 1400 rpm. The pellet was re-suspended in FACS buffer (0.5% BSA and 2 mM EDTA in PBS). The samples were then incubated with Fc Block for 10 minutes at 4°C. Antibodies (in FACS buffer) were added to the samples and incubated at 4°C for 15 minutes. Samples were then centrifuged for 10 minutes at 4°C with the speed of 1400 rpm and the pellets were re-suspended in FACS buffer and measured on BD FACSCanto II. Data analysis was performed by Dr. Rianne Nederlof using BD FACSDiva software v 8.0.2.

For the detection of:	Antibodies
Neutrophils	Anti-CD11b$^+$, anti-Ly6G$^+$, anti-CD45$^+$
Monocytes	Anti-CD11b$^+$, anti-Ly6G$^-$, anti-CD45$^+$, anti-CD115$^+$
T lymphocytes	Anti-CD45$^+$, anti-CD3$^+$, anti-CD19$^-$
B lymphocytes	Anti-CD45$^+$, anti-CD3$^-$, anti-CD19$^+$

Table 3.5: List of immune cells detected in blood by FACS and the antibodies used for the selection.

3.10.2. FACS analysis of heart tissue samples

Hearts were harvested and blood was removed by PBS/heparin perfusion. Atria and valves were removed and the remaining tissue (i.e. ventricles) was minced using a tissue chopper. Tissue was digested in collagenase type I (450 U/mL) and DNAseI (60 U/mL) dissolved in HBSS for 45 minutes at 37°C, with two to three triturations. After 45 minutes, a final trituration was performed and sample was centrifuged at 4°C for 10 minutes with the speed of 300 x g. The pellet was re-suspended in FACS buffer and filtered through 100 µm and 40 µm cell filters. Cardiomyocytes were pelleted and removed by centrifugation at 50 x g, 4°C. The remaining supernatant was centrifuged at 4°C for 10 minutes with the speed of 300 x g and the pellet was re-suspended in PBS and incubated with Fc Block and Fixable viability dye. Sample was then washed and stained with antibodies (in FACS buffer). Cells were washed and measured on BD FACSCanto II. Data analysis was performed by Dr. Rianne Nederlof using BD FACSDiva software v 8.0.2.

For the detection of:	Antibodies
Neutrophils	Anti-CD11b^{+}, anti-Ly6G^{+}
Monocytes	Anti-CD11b^{+}, anti-Ly6G^{-}, anti-CD45^{+}, anti-CD115^{+}
Macrophages	Anti-CD11b^{+}, anti-Ly6G^{-}, anti-CD64^{+}, anti-MHCII^{+}
T lymphocytes	Anti-CD45^{+}, anti-CD3^{+}, anti-CD19^{-}
B lymphocytes	Anti-CD45^{+}, anti-CD3^{-}, anti-CD19^{+}

Table 3.6: List of immune cells detected in heart tissue by FACS and the antibodies used for the selection.

3.11. Statistics

All data are shown as mean ± standard deviation. Statistical analyses were performed using Graph Pad Prism 5. For the comparison between two groups, unpaired, two-tailed Student's t-test was used. For the comparison between two time-points, paired, two-tailed Student's t-test was performed. For the comparison of multiple groups at one time-point, one-way ANOVA with Tukey's post-test was performed. For the comparison of multiple groups at different time-points, two-way ANOVA with Bonferroni's post-test was performed. For all statistical significance: * $p < 0.05$, ** $p < 0.01$, and *** $p < 0.001$.

4

Results

4.1. Heart failure mouse model: inducible cardiomyocyte specific p38 MAPK α knock-out with pressure overload

As described in section 1.6, our laboratory previously established a mouse model of pressure overload-induced heart failure (HF) for the investigation of interorgan communication during HF progression (Bottermann et al manuscript in preparation, Leitner 2017). The inducible, cardiomyocyte-specific knock-out of p38 MAPK α (iCMp38KO) model represents a highly reproducible HF model, based on the rapid induction of pressure overload using AngII as a vasocontrictor to increase blood pressure and therefore cardiac workload (Figure 4.1). Due to the loss of p38 MAPK α, the heart is not able to compensate in function, causing the observed HF phenotype with left ventricular dilation. As controls, litter mates with floxed p38 MAPK α alleles but lacking Cre-recombinase were used. These controls (Ctrl) received the same treatment as the iCMp38KO, including tamoxifen for 10 consecutive days and AngII infusion for 48 hours (Figure 4.1).

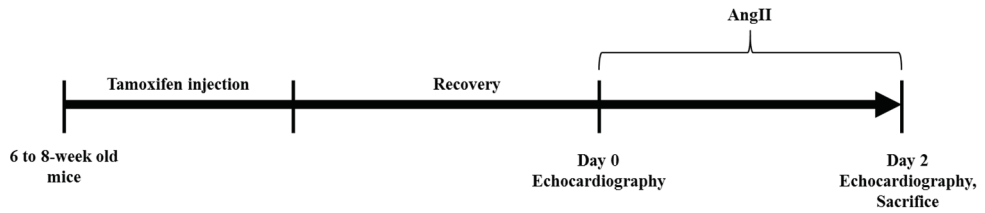

Figure 4.1: Protocol of HF induction in iCMp38KO mouse model. Tamoxifen (i.p. 500 µg/day) was injected for 10 consecutive days. Echocardiography was performed at baseline, after the recovery period (approximately four weeks), and following 48h of AngII administration. AngII was infused continuously for 48h via a mini-osmotic pump (1.5 mg/kg/day) which was implanted subcutaneously. Afterwards, mice were sacrificed to obtain plasma and tissues for subsequent analyses.

In the first set of experiments, cardiac parameters of this model were measured according to the previously described method, to verify the reproducibility of pressure overload-induced HF in this model. Echocardiography was performed at baseline and 48 hours following AngII administration. At baseline, both the Ctrl and iCMp38KO showed comparable cardiac function parameters which include the left ventricular end systolic volume (Figure 4.2A, Ctrl 30.1 ± 3.8 µL, iCMp38KO 30.1 ± 5.8 µL), left ventricular end diastolic volume (Figure 4.2B, Ctrl 79.9 ± 11.1 µL, iCMp38KO 78.3 ± 6.9 µL), fractional shortening (Figure 4.2C, Ctrl 15.2 ± 4.1%, iCMp38KO 15.9 ± 2.3%), stroke volume (Figure 4.2D, Ctrl 49.8 ± 8.2 µL, iCMp38KO 50.3 ± 6.9 µL), cardiac output (Figure 4.2E, Ctrl 28.3 ± 4.2 mL/min, iCMp38KO 29.9 ± 3.8 mL/min) and ejection fraction (Figure 4.2F, Ctrl 62.2 ± 3.0%, iCMp38KO 63.7 ± 4.0%).

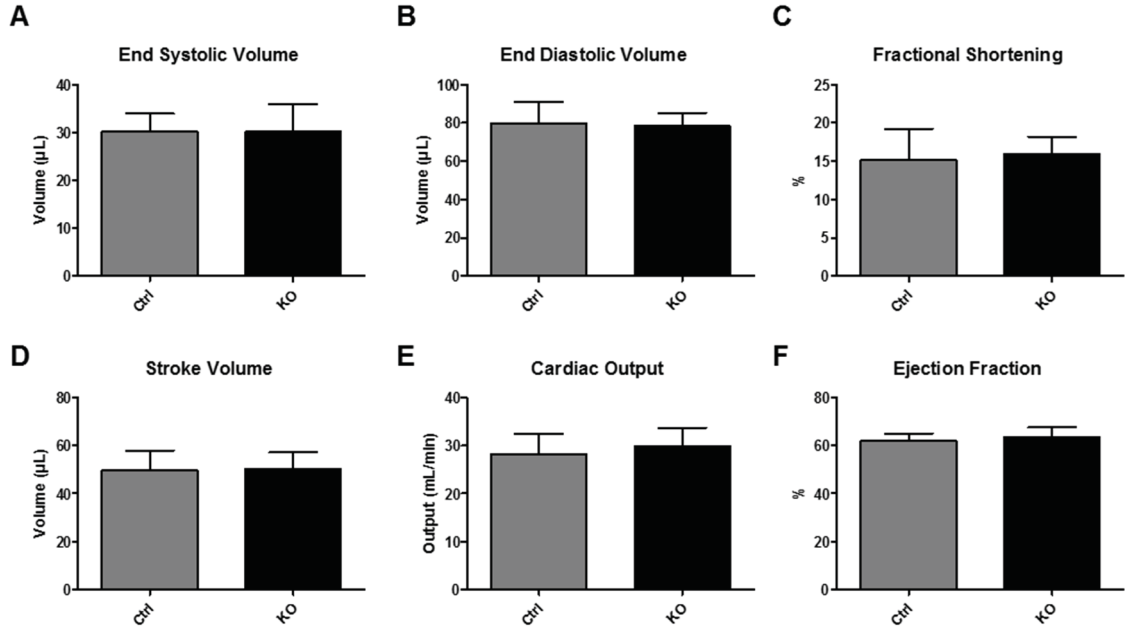

Figure 4.2: Echocardiography analyses of the Ctrl and iCMp38KO at baseline. Functional parameters which were calculated include: end systolic volume (A), end diastolic volume (B), fractional shortening (C), stroke volume (D), cardiac output (E) and ejection fraction (F). Data are presented as mean ± SD, n = 12 - 14.

After 48 hours of continuous administration of AngII via osmotic mini-pump, the iCMp38KO mice developed pressure overload-induced cardiac dysfunction with left ventricular dilatation as shown by significantly higher end systolic volume (Figure 4.3A, Ctrl 35.2 ± 11.4 µL, iCMp38KO 94.8 ± 16.7 µL) and end diastolic volumes (Figure 4.3B, Ctrl 72.9 ± 13.7 µL, iCMp38KO 119.1 ± 19.9 µL) compared to the Ctrl. The significantly lower fractional shortening (Figure 4.3C, Ctrl 15.6 ± 4.5%, iCMp38KO 7.1 ± 2.3%) indicated a reduction in contractility. In combination, these effects led to a significantly lower stroke volume (Figure 4.3D, Ctrl 37.3 ± 4.6 µL, iCMp38KO 24.3 ± 7.1 µL), cardiac output (Figure 4.3E, Ctrl 21.2 ± 3.1 mL/min, iCMp38KO 13.1 ± 4.4 mL/min), and ejection fraction (Figure 4.3F, Ctrl 52.8 ± 7.3%, iCMp38KO 20.5 ± 4.9%), and therefore a decline in the overall cardiac function. In contrast, the Ctrl hearts were able to maintain ejection fraction above 50% with increased workload due to AngII administration.

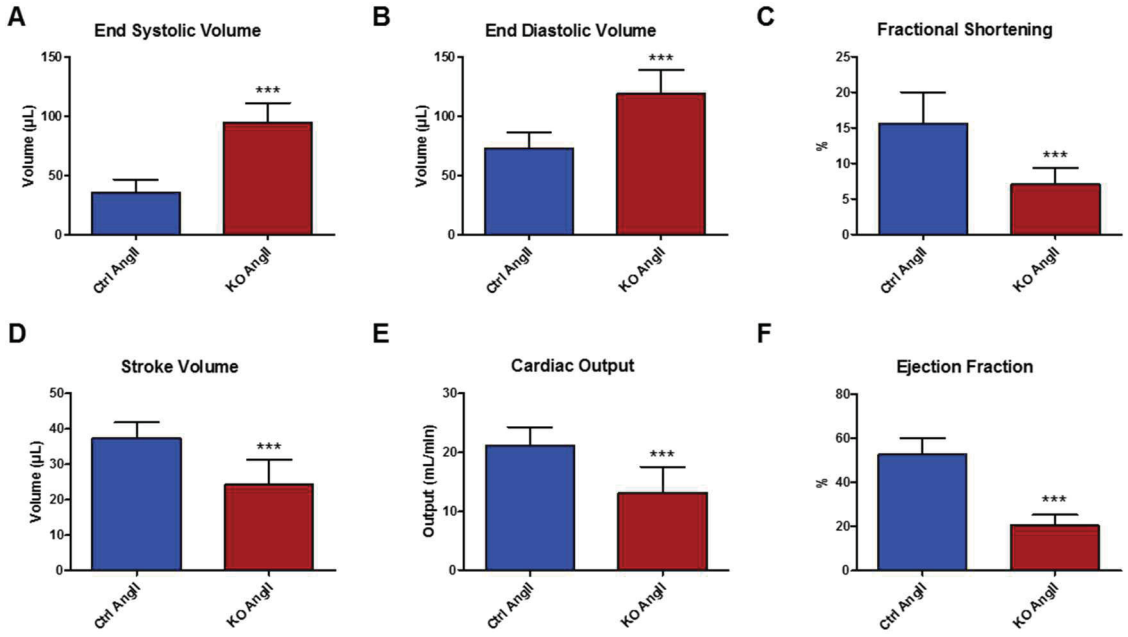

Figure 4.3: Echocardiography analyses of the Ctrl and iCMp38KO after 48 hours of continuous AngII administration. Functional parameters which were calculated include: end systolic volume (A), end diastolic volume (B), fractional shortening (C), stroke volume (D), cardiac output (E) and ejection fraction (F). Data are presented as mean ± SD, n = 12 - 14. Statistical significance between the two groups was calculated using unpaired, two-tailed Student's t-test; *** $p < 0.001$.

4.2. Cardiac lipid accumulation in the failing iCMp38KO hearts was positively correlated with the circulating lipolytic product, glycerol

After 48 hours of AngII administration, the hearts were collected and cryo-embedded for histological analyses. To confirm cardiac lipid accumulation in iCMp38KO after pressure overload induction, the hearts were stained for lipid using Sudan red staining. Figure 4.4A shows a cryosection of Ctrl heart, which shows no lipid accumulation. Figure 4.4B shows a cryosection of iCMp38KO heart, with substantial lipid accumulation stained in red. At a higher magnification, it was evident that the lipid accumulated within the cardiomyocytes (Figure 4.4C and D). Confirming the previous finding by Bottermann et al (Bottermann et al, in preparation), these results suggest that in this model, lipid accumulated within the cardiomyocytes concomitantly with failure to maintain normal cardiac function. Upon quantification, the lipid accumulation was significantly higher in the iCMp38KO hearts compared to the Ctrl hearts (Figure 4.4E).

Next, it was hypothesized that the elevated lipid droplets was due to an increased lipolysis occurring during pressure overload-induced cardiac stress. Therefore after 48h of AngII administration, plasma levels of lipolytic products, glycerol and free fatty acid (FFA), were measured as surrogate markers of lipolysis. Plasma FFA appeared to be unchanged (Figure 4.4F), which could be due to the short half-life of FFA in the circulation (Eaton et al 1969). In contrast, iCMp38KO mice had significantly higher plasma glycerol levels compared to the Ctrl (Figure 4.4G). Moreover, this increase in plasma glycerol level was positively correlated with the increase in cardiac lipid accumulation (Figure 4.4H). Thereafter, plasma level of glycerol was chosen as the indicator of lipolysis. Taken together, these results indicated that increased lipolysis and

lipid uptake, and/or reduced cardiac FA oxidation contributed to the observed lipid accumulation in the failing iCMp38KO hearts.

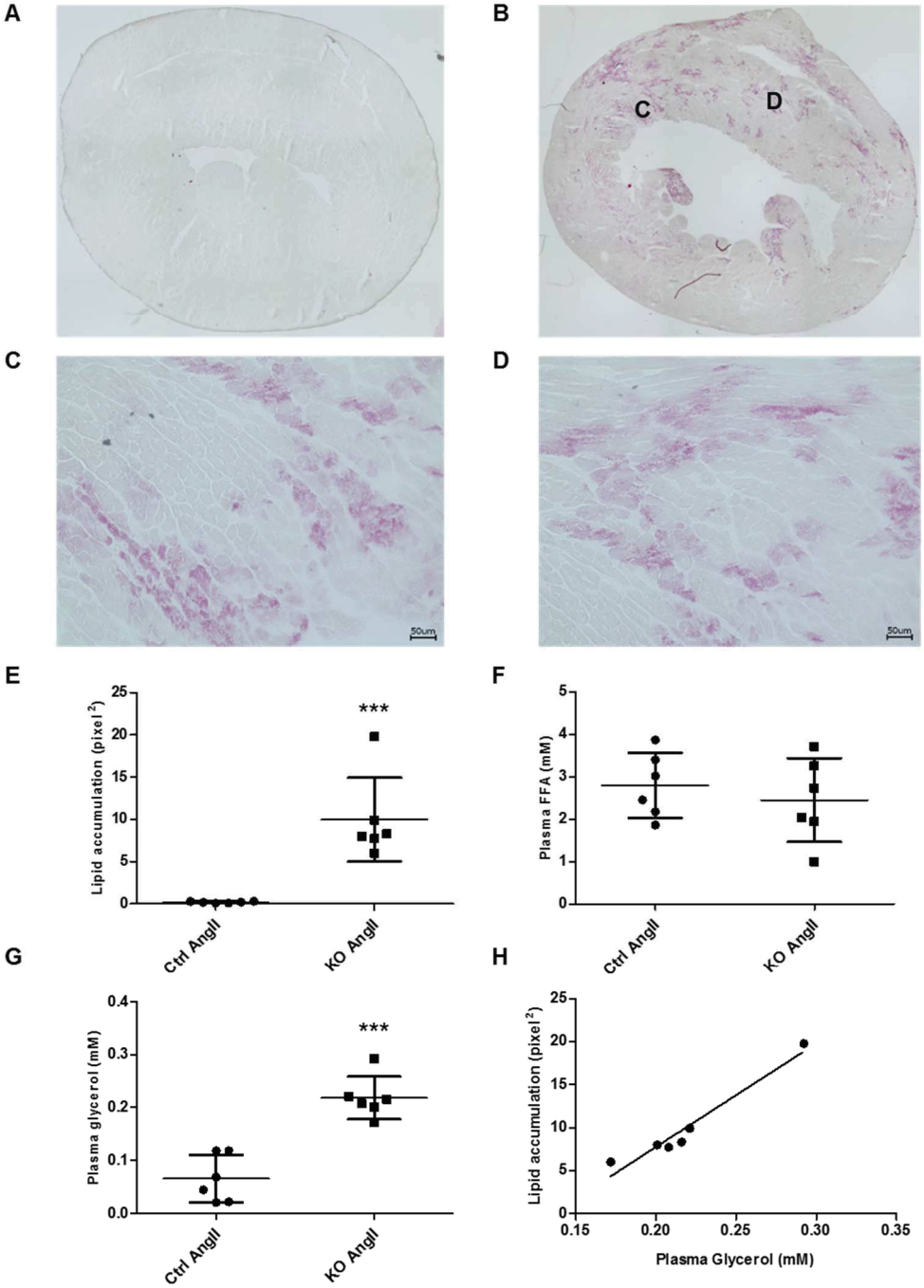

Figure 4.4: Cardiac lipid accumulation detected by histological staining of lipid (stained red) using Sudan red dye reagent and its correlation to lipolysis. After 48h of AngII infusion, cryosections of Ctrl hearts show no lipid accumulation (representative image A). In contrast, staining of cryosections of iCMp38KO hearts show lipid accumulation (representative image B) within the cardiomyocytes (C and D, magnified figures were captured using 20x objective). Cardiac lipid accumulation was quantified using ImageJ (E). Adipose tissue lipolysis was indicated by the measurement of circulating levels of FFA (F) and glycerol (G). Linear regression plot showing positive correlation (Pearson's r = 0.94, r^2 = 0.89) between plasma glycerol and lipid accumulation in iCMp38KO hearts (H). Data E, F and G are presented as mean ± SD, with n = 6 per group. Statistical significance between the two groups was calculated using unpaired, two-tailed Student's t-test; *** $p < 0.001$.

Microarray analysis on the hearts of the Ctrl and iCMp38KO after AngII infusion was performed to characterize the transcriptional expression profiles (Bottermann et al, in preparation). Several of the genes involved in the homeostasis of cardiac triacylglycerol (TAG) pools were differentially expressed in the Ctrl and iCMp38KO mice (Table 4.1). The genes involved in TAG synthetic pathway including *Agpat2, Dgat2, Lipin1* and *Lipin3* were expressed at lower levels, at least by two folds, in iCMp38KO hearts compared to the Ctrl hearts. Data analyzed by using Ingenuity Pathway Analysis (IPA) demonstrated that genes assembled under the terms "Mitochondrial dysfunction" and "Oxidative phosphorylation" were affected (p-value of overlap < 10^{-22}). This was marked by the downregulated expression of genes involved in the regulation of mitochondrial oxidation (*Ppara, Ppargc1a, Ppargc1b*), mitochondrial transport of fatty acyl-CoA (*Cpt1b, Cpt2*), and electron transport chain complexes (*Ndufb5, Nduf8s, Atpaf1*) by at least two folds in iCMp38KO hearts compared to the Ctrl. Additionally, the genes which encode the subunits of cytochrome c reductase and cytochrome c oxidase (electron transport chain complex III and IV respectively) were moderately (1.5 – 2-fold) downregulated in iCMp38KO hearts compared to Ctrl hearts. These results suggest a lower capacity of the heart for oxidative phosphorylation. Therefore, uptake of FA into the iCMp38KO cardiomyocytes combined with reduced FA oxidation possibly led to the accumulation of lipid intermediates and lipid droplet accumulation in the cytosol, which may contribute to the reduction in contractility and eventually the progression of HF.

Gene name	**Gene description**	**Function**	**Fold change in KO AngII (vs Ctrl AngII)**
Agpat2	Lysophosphatidic acid acyltransferase (isoform 2)	Second step of TAG synthesis	2 x ↓
Atpaf1	ATP synthase (electron transport chain complex V) alpha subunit	ATP synthesis	2.3 x ↓
Cpt1b	Carnitine palmitoyl transferase 1 beta	Mitochondrial transport of long-chain fatty acyl-CoA	2.2 x ↓
Cpt2	Carnitine palmitoyl transferase 2	Regenerates long-chain fatty acyl-CoA in the mitochondrial matrix	3.5 x ↓
Dgat2	Diacylglycerol acyltransferase (isoform 2)	Final step of TAG synthesis	3.2 x ↓
Fabp1	Fatty acid binding protein 1	Intracellular FA chaperon protein	13.5 x ↓
Lipa	Lysosomal acid lipase A	Lipophagy	2.5 x ↑
Lipin1	Phosphatidic acid phosphatase (isoform 1)	Third step of TAG synthesis	4.5 x ↓

Lipin3	Phosphatidic acid phosphatase (isoform 3)	Third step of TAG synthesis	2 x ↑
Lpl	Lipoprotein lipase	Intravascular hydrolysis of TAG	2 x ↓
Ndufb5	NADH dehydrogenase (electron transport chain complex I) supernumerary subunit	Electron transport chain	2.1 x ↓
Ndufs8	NADH dehydrogenase (electron transport chain complex I) core subunit	Electron transport chain	2.1 x ↓
Plin5	Perilipin-5	Lipid droplet protein coating	2.4 x ↓
Ppara	Peroxisome proliferator-activated receptor	Regulation of lipid catabolism and FA oxidation	2.1 x ↓
Ppargc1a	Peroxisome proliferator-activated receptor gamma coactivator 1 alpha	Regulation of mitochondrial biogenesis and oxidation	4.5 x ↓
Ppargc1b	Peroxisome proliferator-activated receptor gamma coactivator 1 beta	Regulation of mitochondrial biogenesis and oxidation	2.2 x ↓

Table 4.1: Differentially expressed genes involved in the intramyocardial TAG homeostasis. Overall downregulation of the key lipogenic genes and genes involved in mitochondrial FA oxidation in iCMp38KO hearts (n = 4) compared to Ctrl hearts (n = 4). Data were analyzed by Agilent Mouse Array technology.

4.3. Activation of the inflammatory response in the failing iCMp38KO hearts

In addition to the lipid staining, we performed immunohistochemical staining to scan for any alteration in cardiac immune cell population. Cryo-sections of the hearts were incubated with primary anti-Ly6G (Figure 4.5A) or anti-CD68 (Figure 4.5B) antibody as markers for neutrophils and macrophages, respectively. Fluorescence detection was performed by incubation with a secondary antibody conjugated with Rhodamine Red-X. Upon imaging of the antibody stained heart sections, it was evident that neutrophils and macrophages accumulated in iCMp38KO hearts, whereas less Ly6G-positive and CD68-positive cells were detected in Ctrl hearts, demonstrating the expansion of immune cell population in the pressure overloaded hearts.

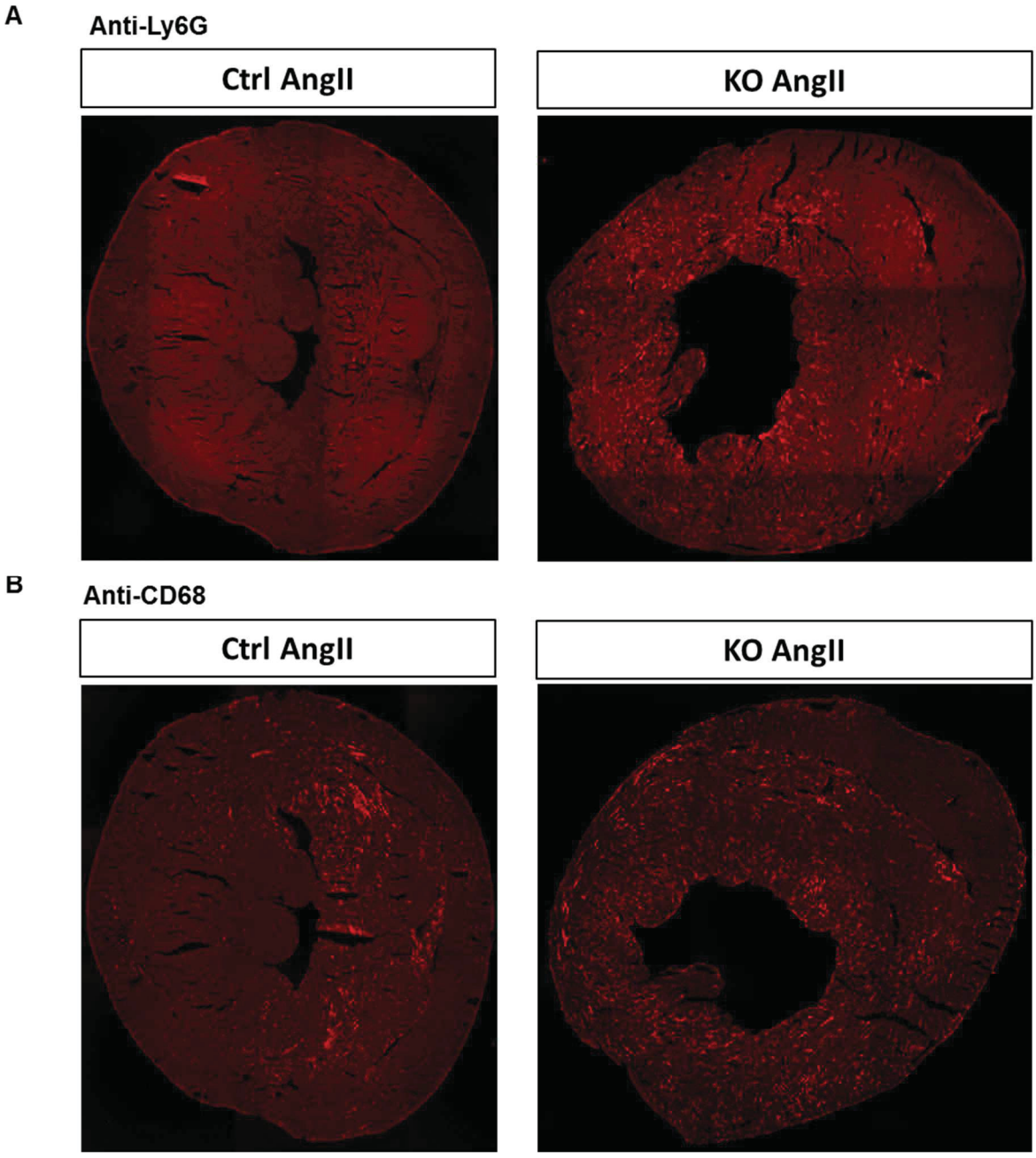

Figure 4.5: Representative images showing increased neutrophils and macrophages in iCMp38KO hearts following 48h of AngII infusion. Neutrophils were detected by staining with primary rat anti-Ly6G antibody (A). Macrophages were detected by staining with primary rat anti-CD68 antibody (B). Secondary anti-rat antibody conjugated with Rhodamine Red-X was used for the fluorescent detection of Ly6G-and CD68- positive staining (red dots).

Analysis of microarray data obtained from the heart tissues revealed upregulated expression of several genes involved in the proinflammatory pathways and the immune cell recruitment in the iCMp38KO, following 48 hours of AngII infusion (Table 4.2). Genes of the chemokine system which regulate the recruitment of monocytes, macrophages and neutrophils, including *Ccl3, Ccl7*, *Cxcl5* and *Cxcr2* were expressed at higher levels in iCMp38KO hearts compared to Ctrl hearts. The expression of the pattern recognition receptors C-type lectin (*Clec1b, Clec4d, Clec4e*) and toll-like receptors (*Tlr4, Tlr13*) which initiate the activation of the major proinflammatory

modulator NF-$_K$B were also upregulated. Moderate (1.5 – 2-fold) upregulation of the downstream genes of TLR including *Myd88*, *Tirap* and *Trak4* was detected in iCMp38KO hearts. Higher gene expression of the receptors of proinflammatory cytokines IL6 and IL17 (*Il6ra* (moderate) and *Il17ra*, respectively) as well as the superfamily members of TNF ligands and receptors were detected in iCMp38KO hearts, compared to Ctrl AngII. Taken together, these data show that cardiac pressure overload stress activates the chemokine system, leading to immune cell recruitment into heart. These cells induce an inflammatory state in the heart, potentially contributing to the progression of HF. In addition, the stimulation of the NF-$_K$B pathway could result in an increased release of proinflammatory cytokines which could further enhance cardiac inflammation and mediate cardiac stress-induced systemic inflammation.

Gene name	**Gene description**	**Function**	**Fold change in KO AngII (vs Ctrl AngII)**
Ccl3	Cysteine-cysteine chemokine ligand 3	Macrophages and natural killer cells trafficking, T-cells and dendritic cells interaction	4.5 x ↑
Ccl7	Cysteine-cysteine chemokine ligand 7	Monocyte recruitment	5.1 x ↑
Clec1b	C-type lectin domain family 1 member b	Innate immune response to pathogens and/or damage associated molecular patterns	2.2 x ↑
Clec4d	C-type lectin domain family 4 member d	Innate immune response to pathogens and/or damage associated molecular patterns	6.2 x ↑
Clec4e	C-type lectin domain family 4 member e	Innate immune response to pathogens and/or damage associated molecular patterns	14.9 x ↑
Cxcl5	Cysteine-X-cysteine chemokine ligand 5	Neutrophil recruitment	6.4 x ↑
Cxcr2	Cysteine-X-cysteine chemokine receptor 2	Neutrophil recruitment	12.9 x ↑
Hsp90aa1	Heat shock protein 90 class A member 1	Damage associated molecular pattern	2.2 x ↑
Hspb1	Heat shock protein 1	Damage associated molecular pattern	2.3 x ↑

Il17ra	Interleukin 17 receptor A	Receptor of the proinflammatory cytokine IL17	3.6 x ↑
Relt	Tumor necrosis factor receptor superfamily member 19L	TNF-mediated inflammation	3 x ↑
Tnfrsf12a	Tumor necrosis factor receptor superfamily member 12a	TNF-mediated inflammation	2.1 x ↑
Tnfrsf26	Tumor necrosis factor receptor superfamily member 26	TNF-mediated inflammation	2 x ↑
Tnfsf14	Tumor necrosis factor superfamily member 14	TNF-mediated inflammation	6.3 x ↑
Tnfsf9	Tumor necrosis factor superfamily member 9	TNF-mediated inflammation	2.1 x ↑
Tlr13	Toll-like receptor isoform 13	Regulation of the NF-$_K$B pathway	3.1 x ↑
Tlr4	Toll-like receptor isoform 4	Regulation of the NF-$_K$B pathway	2.7 x ↑

Table 4.2: Differentially expressed genes involved in the inflammatory pathways in the cardiac tissue. Overall upregulation of immune cell recruitment and cytokine-mediated proinflammatory pathways in iCMp38KO hearts (n = 4) compared to Ctrl hearts (n = 4). Data were analyzed by Agilent Mouse Array technology.

4.4. Pharmacological inhibition of lipolysis: testing the anti-lipolysis efficiency of atglistatin

The two major hallmarks of HF in iCMp38KO, namely lipid accumulation and inflammation, led to the hypothesis that lipid accumulation contributed to the functional depression and/or the recruitment of immune cells into the myocardium. Cardiac dysfunction typically induces sympathetic signaling to enhance heart rate and contractile force. Sympathetic signaling also enhances lipolysis, therefore β-adrenergic stimulation of adipose tissue lipolysis could be a potential source of pressure overload-induced cardiac lipid accumulation. To test this hypothesis, methods to inhibit adipose tissue lipolysis were explored.

GS-9667 is a partial agonist of A_1 adenosine receptor which was developed to inhibit adipose tissue lipolysis (Fatholahi et al 2006, Dhalla et al 2007). Due to the absence of adverse cardiovascular effects, GS-9667 was tested *in vitro* and *in vivo* for its potential

implementation to the iCMp38KO HF model. Following a starvation period (two hours), differentiated 3T3-L1 adipocytes were incubated with: epinephrine to induce lipolysis via β-adrenergic stimulation, adenosine as a positive control for A_1 adenosine receptor stimulation, GS-9667, or co-incubations of either one of the A_1 adenosine receptor agonists and epinephrine. The results show that GS-9667 was able to inhibit epinephrine-induced adipocyte lipolysis, to a similar level compared to adenosine (Figure 4.6A). Next, GS-9667 was tested *in vivo* using C57BL/6 mice. Briefly, mice were starved overnight. GS-9667 was administered via i.p. injection, and plasma samples were collected at baseline, 10, 30, 60, and 120 minutes following injection. GS-9667 was able to reduce plasma glycerol, however statistical significance was not achieved (Figure 4.6B). Due to this, as well as the short half-life of GS-9667 described in the literature (Dhalla et al 2007), GS-9667 may not be suitable to sufficiently inhibit lipolysis of HF induction in iCMp38KO. Therefore, another anti-lipolytic compound, atglistatin, was investigated.

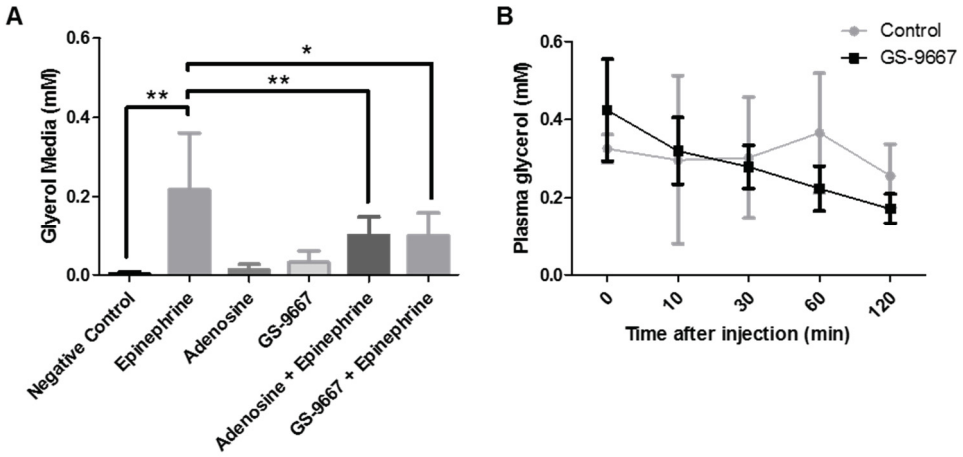

Figure 4.6: GS-9667 inhibition of stimulated lipolysis *in vitro* (3T3-L1) (A) and *in vivo* (C57BL/6) (B). (A) *In vitro* validation of GS-9667 efficiency in inhibiting lipolysis. Mature 3T3-L1 adipocytes were starved for two hours prior to the addition of the listed compounds, with the following protocol: epinephrine (1 µM, 45 minutes), adenosine (10 µM, 30 minutes), and GS-9667 (10 µM, 30 minutes). Negative control was incubated with vehicles for the same incubation periods. Samples from the media were collected for the measurement of glycerol concentration. Data = mean ± SD, n = 4 per group. Statistical significance was calculated using one-way ANOVA, *$p < 0.05$, and **$p < 0.01$. (B) *In vivo* validation of GS-9667 (i.p. 5 mg/kg) efficiency in lipolysis inhibition. Plasma samples were collected for the measurement of glycerol concentration. Data = mean ± SD, n = 4 – 5, no statistical significance detected.

Atglistatin is a small molecule inhibitor of adipose triglyceride lipase (ATGL), the rate limiting enzyme which catalyzes the first step of lipolysis. After its oral administration, atglistatin is preferentially taken up by lipid-storing tissues including the adipose tissues, possibly due to the lipophilic property of the compound (Mayer et al 2013). Importantly, it was reported that atglistatin treatment for as long as 140 days did not lead to any lipid accumulation in the heart, and cardiac function remained normal (ejection fraction: > 60%) (Schweiger et al 2017). Thus, atglistatin is highly specific for the inhibition of lipolysis in murine adipose tissue and was therefore selected for the application to our HF model.

To establish a protocol for inhibition of lipolysis, atglistatin was tested *in vitro* using 3T3-L1 preadipocyte cell line which was differentiated into mature adipocytes. After

complete differentiation, 3T3-L1 adipocytes were starved for two hours, and then incubated with either atglistatin, or epinephrine, or a co-incubated with both compounds. The level of lipolysis was measured by glycerol released into the media (Figure 4.7A). Compared to the negative control, atglistatin had no effect on the glycerol concentration in the media, indicating that under baseline conditions atglistatin did not affect lipolysis. Epinephrine stimulated lipolysis in 3T3-L1 adipocytes up to around two fold. Epinephrine-stimulated lipolysis was inhibited upon co-incubation with atglistatin down to the baseline level.

The *in vivo* testing of the anti-lipolytic efficiency of atglistatin was performed using weight-matched C57BL/6 male mice. Atglistatin was administered via food for three days. Mice were starved for 5 hours, then lipolysis was stimulated via i. p. injection of isoproterenol (ISO), a non-selective β-adrenergic receptor agonist. The level of lipolysis was determined by measurement of plasma glycerol levels at baseline and 15 minutes after ISO injection (Figure 4.7B). Similar to the *in vitro* results, atglistatin had no effect on baseline lipolysis (Control baseline 0.37 ± 0.09 mM, Atgli baseline 0.39 ± 0.07 mM). ISO significantly induced lipolysis by around three-fold as compared to baseline (Control ISO 1.13 ± 0.19 mM). Atglistatin treatment significantly reduced ISO-stimulated lipolysis (Atgli ISO 0.70 ± 0.22 mM), although a complete inhibition down to the baseline levels was not achieved.

In summary, atglistatin is able to attenuate stimulated lipolysis both *in vitro* as well as *in vivo*. The inhibition of ATGL by atglistatin did not result in a compensatory increase in lipolysis, which was described for other pharmacological inhibitors of lipolysis such as acipimox (Vaag & Beck-Nielsen 1992). Hence, due to its inhibitory activity, the absence of acute increase in lipolysis, long half-life and duration of action and the feasibility (Mayer et al 2013) of integration into the iCMp38KO heart failure model, atglistatin was chosen for further lipolysis experiments.

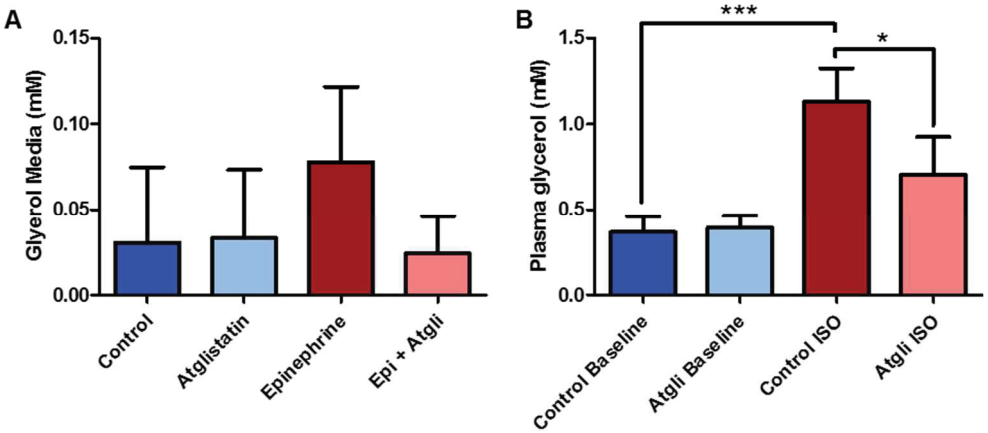

Figure 4.7: Protocol validation for the inhibition of lipolysis using altglistatin. (A) *In vitro* validation of atglistatin efficiency in inhibiting lipolysis. Mature 3T3-L1 adipocytes were starved for two hours prior to the addition of the listed compounds. After starvation, cells were incubated with atglistatin (10 µM) for 45 minutes. Lipolysis was induced by the addition of epinephrine (1 µM, 45 minutes). As a negative control, cells were incubated with vehicles for the same incubation times. n = 3 per group. (B) *In vivo* validation of atglistatin efficiency in lipolysis inhibition when administered via food (0.4mg/g chow food) for three days prior to ISO stimulation of lipolysis (i.p. 10 mg/kg, 15 minutes). n = 4 per group. Data are presented as mean ± SD. Statistical significance between two groups was calculated using unpaired, two-tailed Student's t-test; * $p < 0.05$ and *** $p < 0.001$.

4.5. Atglistatin-dependent inhibition of adipose tissue lipolysis in iCMp38KO – effects on cardiac function and lipid accumulation

To investigate whether the inhibition of adipose tissue lipolysis affected lipid accumulation in the heart of iCMp38KO, atglistatin was administered according to the following timeline:

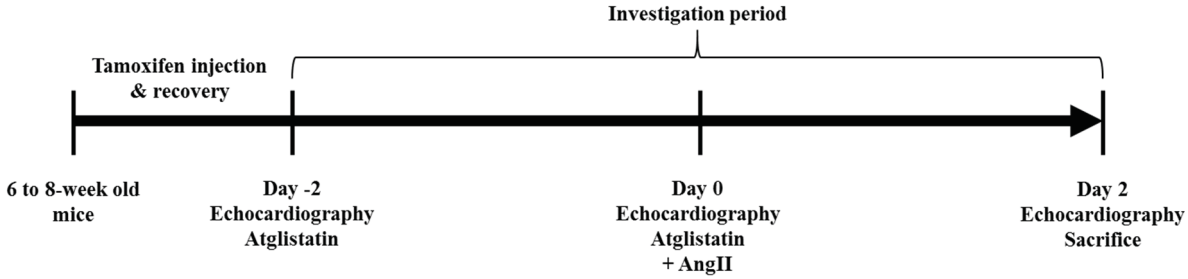

Figure 4.8: Timeline of investigation of atglistatin effect on the iCMp38KO model. On day -2 of the investigation period, mice were given food containing atglistatin (0.4 mg/g chow food). Cardiac stress was induced on day 0 of the investigation period by AngII infused via osmotic mini-pump. 48 hours later (day 2), the mice were starved for 4 to 5 hours and sacrificed. Echocardiography was performed on day -2 prior to atglistatin treatment, day 0 before AngII mini-osmotic pump implantation, and on day 2.

Echocardiography was performed before the start of atglistatin diet (i.e. baseline cardiac function, day -2) and on day 0 before AngII osmotic mini-pump implantation to monitor for any alteration in cardiac function due to atglistatin treatment. Figure 4.9A and Figure 4.9B shows the left ventricular wall movements of Ctrl and iCMp38KO respectively, with the top panels showing the parasternal long axis of the left ventricle and the bottom panels showing the M-mode of the long axis. The cardiac geometry was normal and unchanged by atglistatin treatment which revealed that atglistatin did not affect cardiac function in Ctrl and iCMp38KO mice.

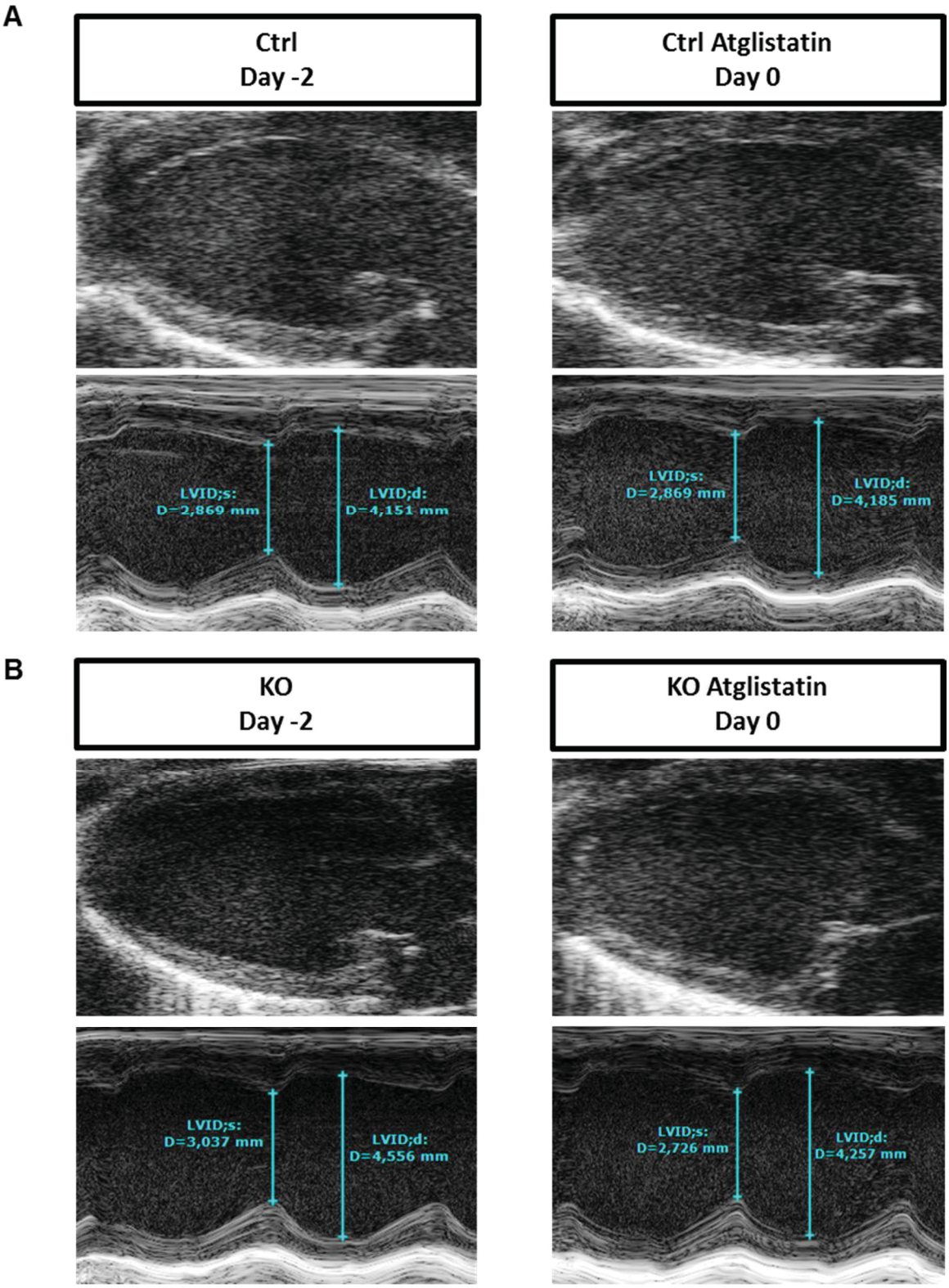

Figure 4.9: Echocardiography analyses of atglistatin-treated mice to investigate the effect of atglistatin on cardiac function. Images of the B-mode (top panels) and M-mode (bottom panels) taken from the parasternal long axis of the left ventricles of Ctrl (A) and iCMp38KO (B) hearts were acquired and analyzed. The left panels were captured at baseline (day -2) before the start of atglistatin treatment, and the right panels were captured on day 0 before AngII administration. Blue labeling on the M-mode images represents the left ventricular systolic diameter (LVID;s) and diastolic diameter (LVID;d).

Figure 4.10 summarizes the echocardiography analyses. No left ventricular dilatation was observed, as indicated by the normal end systolic volumes (Figure 4.10A, Ctrl 26.3 ± 7.4 µL, KO 27.5 ± 8.1 µL) and end diastolic volumes (Figure 4.10B, Ctrl 70.8 ± 12.3 µL, KO 72.8 ± 13.2 µL). Contractility measured by fractional shortening was maintained by day 0 for both the Ctrl (19.8 ± 4.7%) and the KO (19.2 ± 5.8%) (Figure 4.10C). Stroke volume was maintained at 44.5 ± 6.7 µL in the Ctrl and at 46.0 ± 6.6 µL in the KO (Figure 4.10D). Cardiac output remained similar to the baseline levels (Figure 4.10E, Ctrl 23.5 ± 2.9 mL/min, KO 24.3 ± 4.2 mL/min). The overall ejection fraction was unchanged from day -2 to day 0 both in Ctrl (63.3 ± 5.3 %) and KO (61.1 ± 6.2 %) (Figure 4.10F). Thus, atglistatin treatment had no effect on cardiac function.

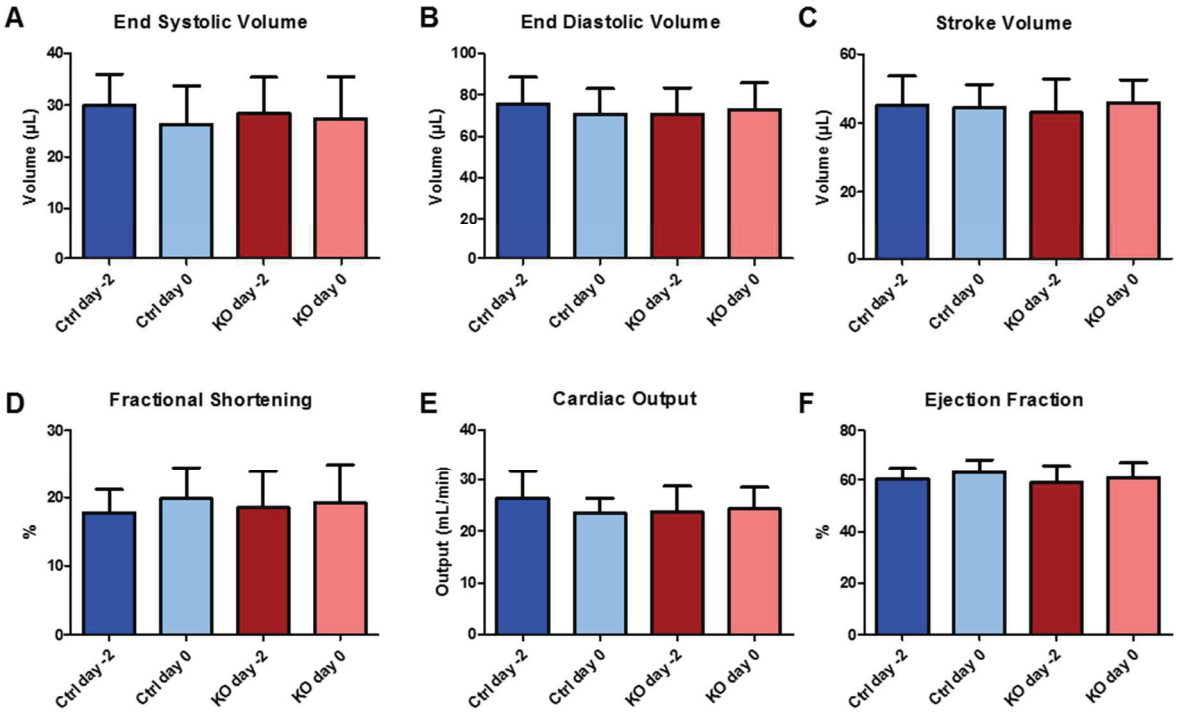

Figure 4.10: Echocardiographic quantification of atglistatin-treated mice to investigate the effect of atglistatin on cardiac function. Cardiac function parameters comparing the atglistatin-treated Ctrl (n = 12) and iCMp38KO (n = 12) on day -2 and day 0 are shown from (A) to (F). Functional parameters which were calculated include: end systolic volume (A), end diastolic volume (B), fractional shortening (C), stroke volume (D), cardiac output (E) and ejection fraction (F). Data are presented as mean ± SD.

Plasma samples of AngII-treated mice were collected on day 2, and FFA and glycerol levels were measured. Plasma FFA appeared to be unchanged across the groups (Figure 4.11A). However, measurement of glycerol levels as a marker for lipolysis revealed major differences between Ctrl and iCMp38KO mice (Figure 4.11B). Atglistatin did not affect lipolysis in Ctrl AngII mice, as indicated by the low plasma glycerol level (0.08 ± 0.02 mM). As previously mentioned, upon cardiac stress stimulation by AngII in the iCMp38KO, plasma glycerol level significantly increased up to around three folds higher than the Ctrl. This cardiac stress-stimulated plasma glycerol release was significantly reduced when iCMp38KO mice were treated with atglistatin to 0.13 ± 0.01 mM.

Heart tissues were cryoembedded and stained for the detection of lipid accumulation (representative images Figure 4.11D). A semi-quantitative analysis of lipid deposition

was performed using ImageJ (Figure 4.11C). Lipid accumulation was defined as the area occupied by the signal within the set threshold (pixel^2). As shown before, Ctrl hearts did not accumulate lipid after 48h of AngII infusion (0.20 ± 0.09 pixel^2), whereas in iCMp38KO hearts, a substantial lipid deposition was observed (9.96 ± 4.98 pixel^2). Atglistatin treatment did not affect lipid deposition in Ctrl hearts (0.12 ± 0.08 pixel^2). In contrast, atglistatin treatment resulted in significantly reduced lipid accumulation in the iCMp38KO AngII hearts (1.27 ± 1.37 pixel^2). Taken together, these results showed that a major cause of cardiac lipid accumulation in the AngII-infused iCMp38KO mice was due to adipose tissue lipolysis, since the suppression of adipose tissue lipolysis by atglistatin led to a significant reduction in cardiac lipid accumulation.

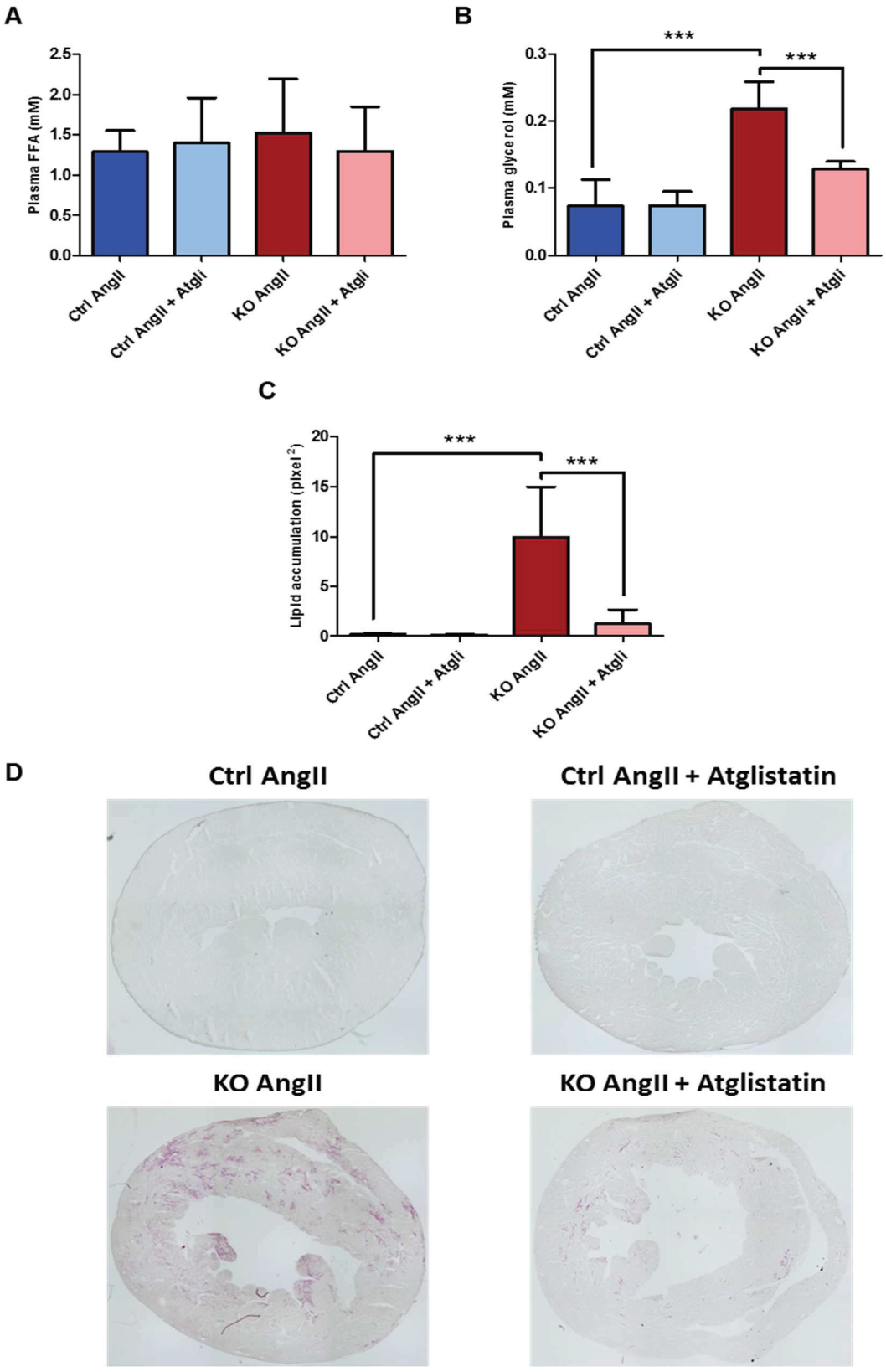

Figure 4.11: The effects of atglistatin on cardiac stress-induced adipose tissue lipolysis and cardiac lipid accumulation following AngII-induced pressure overload. Plasma FFA (A) and glycerol (B) were measured using colorimetric assays. Cardiac lipid accumulation was detected by Sudan red staining and the lipid accumulation was quantified by the stained area (quatification C and representative images D). Data are presented as mean ± SD. n = 6 per group. Statistical significance between two groups was calculated using unpaired, two-tailed Student's t-test; ** $p < 0.01$ and *** $p < 0.001$.

To investigate the effect of atglistatin on cardiac function, echocardiography was performed on the final day of investigation (i.e. day 2), 48 hours after the start of AngII administration. Left ventricular geometry was similar in the Ctrl groups, with and without atglistatin treatment (Figure 4.12A). However, a moderate improvement in the left-ventricular movement was observed in the atglistatin-treated iCMp38KO (Figure 4.12B), which was evident from the increased movement of the anterior wall (see arrows in M-mode picture).

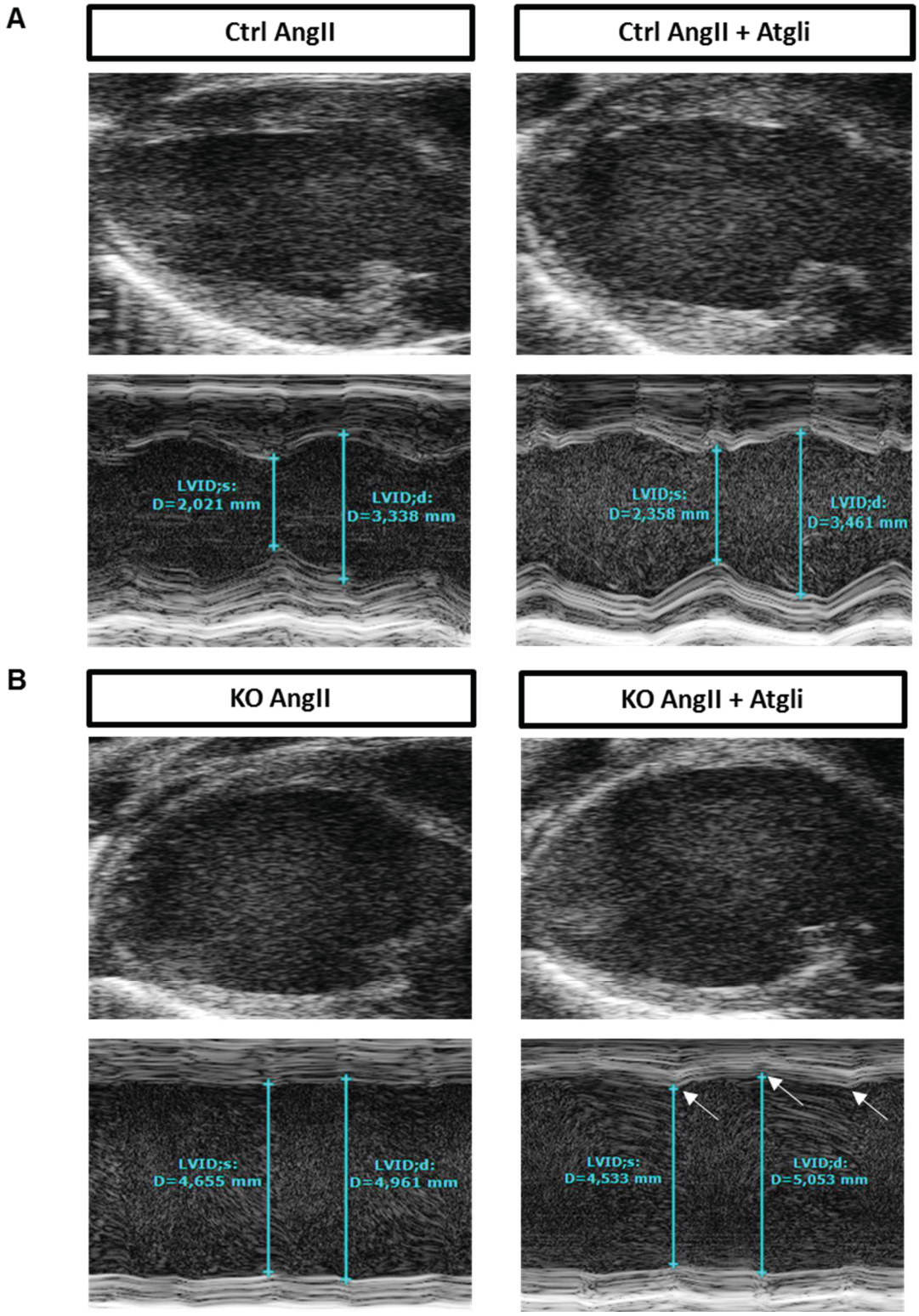

Figure 4.12: Echocardiography analyses of atglistatin-treated mice to investigate the effect of atglistatin on cardiac function following 48 hours of AngII-induced cardiac stress. Images of the B-mode (top panels) and M-mode (bottom panels) taken from the parasternal long axis of the left ventricles of Ctrl (A) and iCMp38KO (B) hearts were acquired on day 2 of the investigation period and analyzed. The left panels represent the AngII-treated Ctrl and iCMp38KO which did not receive atglistatin, whereas the right panels represent AngII-treated Ctrl and iCMp38KO which received atglistatin. Blue labeling on the M-mode images represents the left ventricular systolic diameter (LVID;s) and diastolic diameter (LVID;d).

The quantitative data (Figures 4.13A - F) demonstrated that atglistatin treatment did not affect cardiac function of the non-failing Ctrl hearts, as shown by the unaltered functional parameters including end systolic volume, end diastolic volume, fractional shortening, stroke volume, cardiac output and ejection fraction. In contrast, atglistatin treatment slightly but significantly improved several cardiac function parameters of the AngII-induced pressure overloaded iCMp38KO hearts. End systolic volume was 14.1% lower in atglistatin-treated iCMp38KO (Figure 4.13A, 81.4 ± 13.2 µL) compared to iCMp38KO AngII (94.8 ± 16.7 µL). End diastolic volume was moderately lower in the atglistatin-treated iCMp38KO (Figure 4.13B, 111.4 ± 17.5 µL) compared to iCMp38KO AngII (119.1 ± 19.9 µL). These data suggest that with atglistatin treatment, iCMp38KO heart developed less left ventricular dilatation. Cardiac contractility measured by fractional shortening was 38.5% higher in the atglistatin-treated iCMp38KO (Figure 4.13C, 9.9 ± 2.6%) compared to KO AngII (7.1 ± 2.3%). These factors contributed to a significantly higher stroke volume, which increased by 25.5% (Figure 4.13D, 30.5 ± 7.1 µL compared to 24.3 ± 7.1 µL), a higher trend in cardiac output (Figure 4.13E, 15.2 ± 3.3 mL/min compared to 13.1 ± 4.4 mL/min) and 31.4% improvement in ejection fraction (Figure 4.13F, 26.9 ± 5.1% compared to 20.5 ± 4.9%), relative to iCMp38KO + AngII group. Thus, inhibition of adipose tissue lipolysis using atglistatin partially improved cardiac function, particularly systolic function, of the pressure overloaded iCMp38KO hearts.

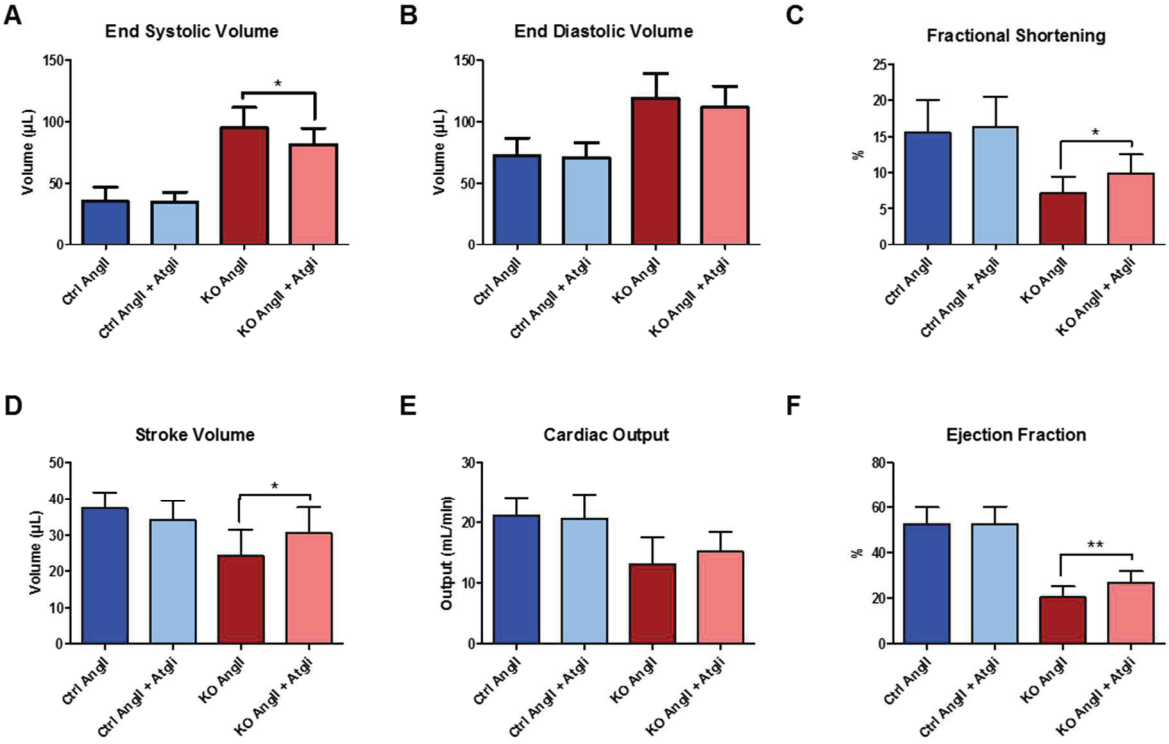

Figure 4.13: Echocardiography analyses to investigate the effect of atglistatin treatment on cardiac function after the induction of cardiac stress using AngII. Quantification of cardiac function parameters are shown from (A) to (F). Data are presented as mean ± SD. n = 12 - 14. Statistical significance between two groups was calculated using unpaired, two-tailed Student's t-test; * $p < 0.05$ and ** $p < 0.01$.

4.6. Atglistatin inhibition of lipolysis in iCMp38KO – effects on the inflammatory response

It was further investigated to what extent lipolysis inhibition affected inflammation due to pressure overload-induced cardiac stress in the iCMp38KO mice. It was hypothesized that the reduction in cardiac lipid accumulation protected the heart from lipotoxic damage, attenuating cardiac inflammation and the recruitment of immune cells.

Therefore, the immune cell populations in the heart, which indicate the local inflammatory state, were identified and measured via FACS analysis. Based on the histological data (Figure 4.5, page 38), it was evident that cardiac pressure overload stress may trigger immune cell infiltration to the heart, which leads to cardiac inflammation and possibly worsening of cardiac function. As expected, after 48 hours of AngII (day 2), the number of neutrophils (Figure 4.14A, page 52) was significantly higher in the iCMp38KO (1471 ± 140 cells/mg tissue) compared to the Ctrl (323 ± 189 cells/mg tissue) hearts, confirming the increase in neutrophil infiltration into the heart after pressure overload induction. Importantly, atglistatin treatment in the iCMp38KO significantly reduced the number of infiltrating neutrophils by 28% to 1059 ± 97 cells/mg tissue, whereas neutrophil number in the Ctrl hearts was not affected. Moreover, the number of cardiac neutrophils negatively correlated ($p < 0.0001$) with ejection fraction (Figure 4.14B), suggesting that neutrophil infiltration was a major factor modulating cardiac function. T lymphocyte infiltration (Figure 4.14C) was significantly higher in iCMp38KO (61 ± 22 cells/mg tissue) than Ctrl (28 ± 13 cells/mg tissue) hearts following AngII administration. Similarly, B lymphocyte populations (Figure 4.14D) were significantly higher in iCMp38KO (89 ± 23 cells/mg tissue) compared to Ctrl (41 ± 16 cells/mg tissue) hearts. Atglistatin treatment tended to reduce the numbers of infiltrating T and B lymphocytes, however, the alterations were not statistically significant.

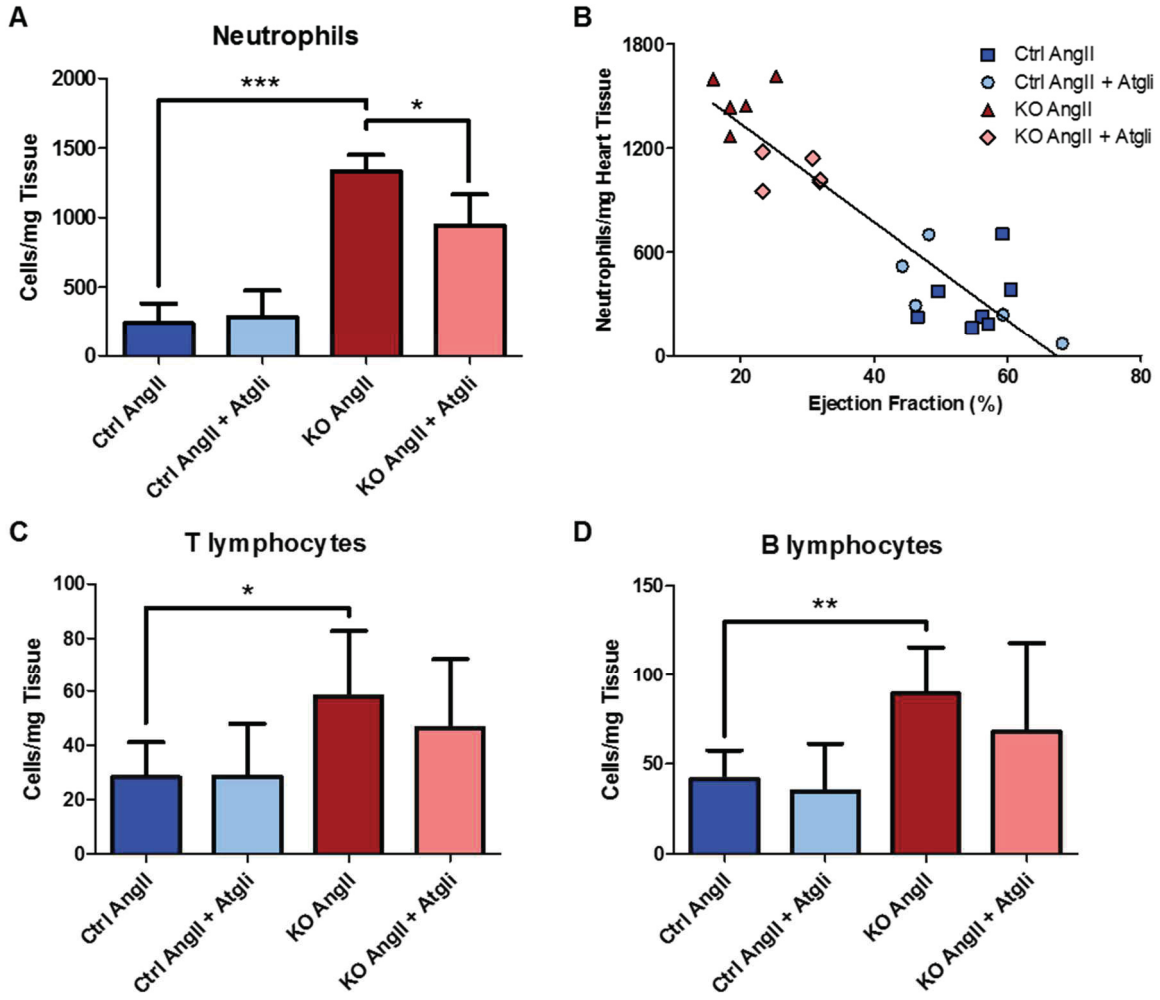

Figure 4.14: FACS analysis of the heart tissues. Heart tissues were collected on day 2, with all mice receiving 48h of AngII. The ventricles were minced and subjected to collagenase digestion. Cells were then isolated and cardiomyocytes were removed. The remaining cells were incubated with antibodies specific to: neutrophils (A), T lymphocytes (C) and B lymphocytes (D). The number of cells was normalized per mg tissue. (B) shows a correlation between the number of cardiac neutrophils and ejection fraction ($R^2 = 0.83$, $p < 0.0001$). Data are presented as mean ± SD with n = 4 – 8. Statistical significance between two groups was calculated using unpaired, two-tailed Student's t-test; * $p < 0.05$, ** $p < 0.01$ and *** $p < 0.001$.

As macrophages play an important role in mediating cardiac inflammation due pressure overload, the number of macrophages ($CD45^+CD11b^+CD64^+Ly6G^-$) and phagocyte subsets were measured. The number of total macrophages was significantly higher in the AngII-induced pressure overloaded iCMp38KO heart (2029 ± 478 cells/mg tissue) compared to the AngII-treated Ctrl (1250 ± 374 cells/mg tissue) (Figure 4.15A). This expansion of the macrophage population was likely due to an increase in recruited monocytes, since $CCR2^+$ macrophages and monocytes were significantly higher in iCMp38KO heart compared to the Ctrl (Figures 4.15C and D respectively), without any change in the resident $CCR2^-$ macrophage population (Figure 4.15B). Atglistatin-treated iCMp38KO tended to accumulate less $CCR2^+$ macrophages and monocytes in the heart, suggesting a lower monocyte recruitment. Monocytes and macrophages were further discriminated based on their Ly6C expression, which indicates to what extent a pro-inflammatory ($Ly6C^{hi}$) milieu developed. Inflammatory monocytes and macrophages

(Ly6C^{hi}) were significantly higher in the pressure overloaded iCMp38KO heart (Figure 4.15E and G respectively). In contrast, anti-inflammatory macrophages (Ly6C^{lo}) were significantly less in iCMp38KO heart compared to the Ctrl (Figure 4.15H). This suggests an overall increase in the inflammatory state mediated by macrophages in the AngII-induced pressure overloaded iCMp38KO heart compared to the AngII-treated Ctrl. Atglistatin treatment resulted in moderately less Ly6C^{hi} macrophages in the heart of AngII-treated iCMp38KO. This indicates that adipose tissue lipolysis and cardiac lipid accumulation may partially contribute to an overall less cardiac inflammation, mediated by immune cells including neutrophils, lymphocytes, monocytes and macrophages.

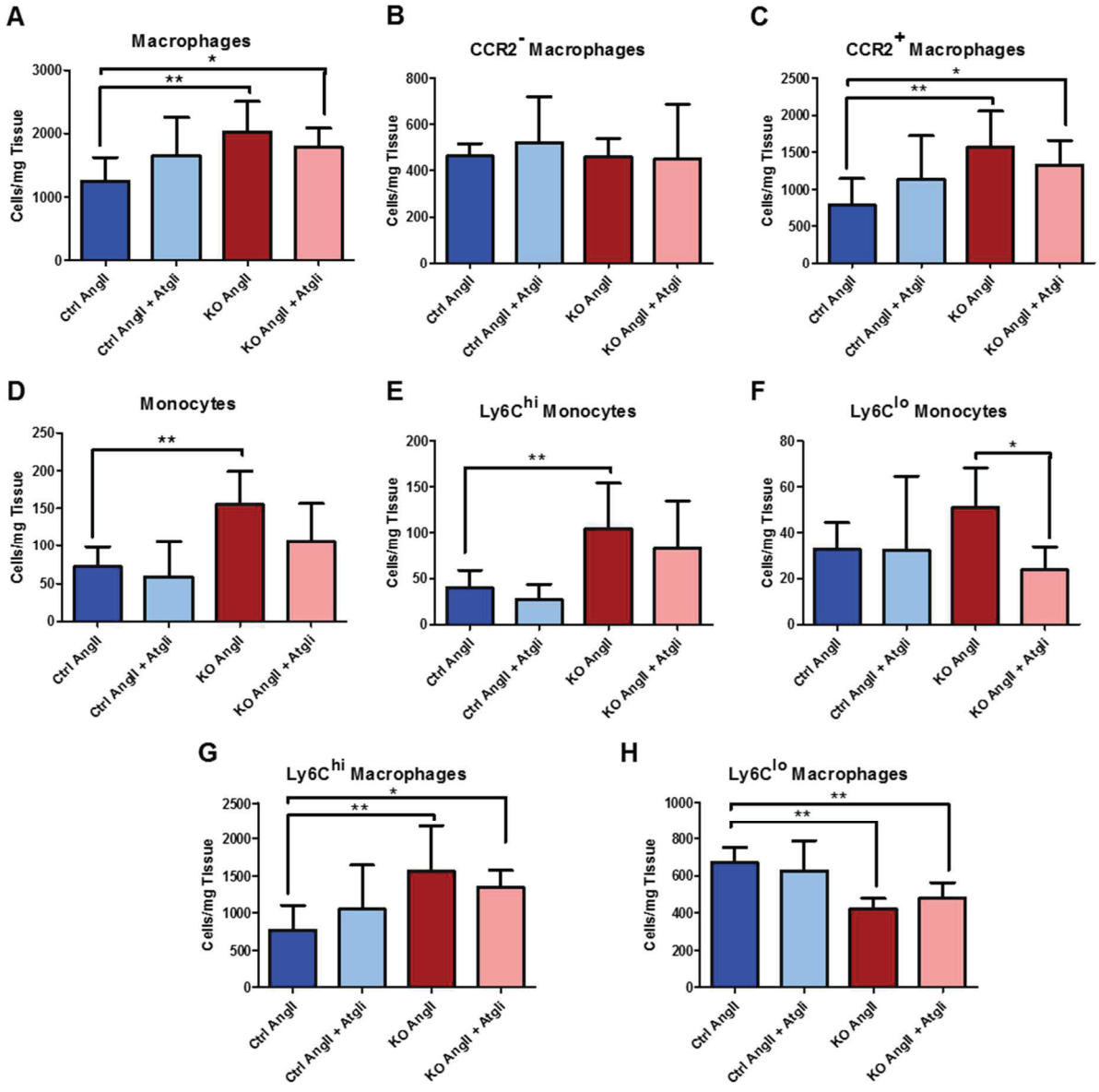

Figure 4.15: FACS analysis of cardiac macrophage and its subsets. All mice received 48h of AngII infusion. Total macrophages (A) were further characterized by origin (resident CCR2^{-} (B) vs monocyte-derived CCR2^{+} (C, and monocytes (D)). Monocytes were categorized by the inflammatory response (Ly6C^{hi} (E) and Ly6C^{lo} (F)). Similarly, macrophages were subcategorized by the inflammatory response (Ly6C^{hi} (G) and Ly6C^{lo} (H). The number of cells was normalized per mg tissue. Data are presented as mean ± SD with n = 4 – 7. Statistical significance between two groups was calculated using unpaired, two-tailed Student's t-test; * $p < 0.05$, ** $p < 0.01$ and *** $p < 0.001$.

Next, the transcriptional expression of proinflammatory cytokines TNFα, IL1β and IL6 in the heart was analyzed to detect any alteration due to atglistatin inhibition of lipolysis. The transcript expression of these cytokines were upregulated in the AngII-induced pressure overloaded iCMp38KO heart. *Tnfa* expression was five folds higher in iCMp38KO compared to the Ctrl hearts (Figure 4.16A). Similarly, *Il1b* and *Il6* expression was over five folds and 7 folds higher respectively in KO than Ctrl hearts (Figure 4.16B and 4.16C respectively). The increase in *Tnfa* expression in the KO heart was moderately, but not significantly, attenuated by atglistatin treatment.

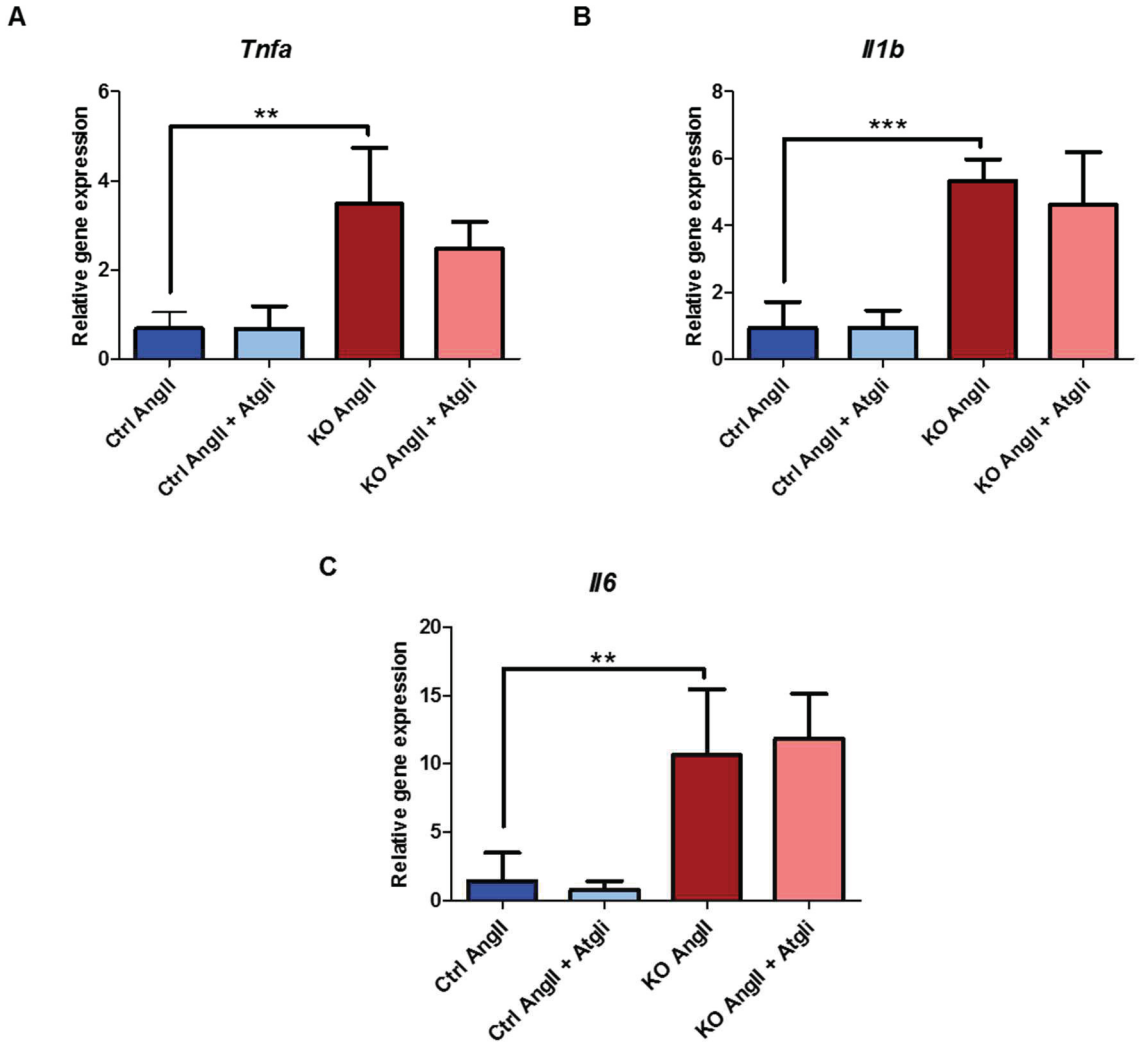

Figure 4.16: Relative transcriptional expression of proinflammatory cytokines TNFα (A), IL1β (B) and IL6 (C) in heart tissues. Data are presented as mean ± SD with n = 5 per group. Statistical significance between two groups was calculated using unpaired, two-tailed Student's t-test; ** $p < 0.01$ and *** $p < 0.001$.

The results presented above demonstrate that adipose tissue lipolysis affects the development of cardiac inflammation and function in line with an adipose-to-heart communication. Further analysis was performed to identify a possible communication in the opposite direction, i.e. from the failing heart to the adipose tissue.

4.7. Heart - adipose tissue communication

To study the potential heart-adipose tissue crosstalk during the development of heart failure and the effects of atglistatin mediated inhibition of lipolysis, adipose tissues were harvested on day 2 of the investigation period. White adipose tissues (WATs) were harvested from the perigonadal region (i.e. visceral WAT, Figure 4.17A) and inguinal region (i.e. subcutaneous WAT, Figure 4.17B). Brown adipose tissue (BAT) was harvested from the interscapular region (Figure 4.17C). After AngII administration, iCMp38KO mice had lower perigonadal WAT mass (4.8 ± 1.8 mg/g body weight) and inguinal WAT mass (5.2 ± 1.5 mg/g body weight) compared to the Ctrl (6.9 ± 3.6 mg/g body weight and 6.8 ± 2.0 mg/g body weight, respectively), which could be indicative of enhanced cardiac stress-mediated WAT lipolysis in the iCMp38KO. Surprisingly, atglistatin inhibition of lipolysis led to WAT loss in both Ctrl and iCMp38KO mice after AngII infusion. Atglistatin-treated Ctrl mice had significantly lower inguinal WAT mass (3.5 ± 0.9 mg/g body weight) and perigonadal WAT mass (3.3 ± 1.3 mg/g body weight) compared to the untreated Ctrl. Similarly, atglistatin-treated iCMp38KO had significantly lower inguinal WAT mass (2.3 ± 0.4 mg/g body weight) and perigonadal WAT mass (2.1 ± 0.7 mg/g body weight) compared to the untreated iCMp38KO. In contrast, BAT weight remained similar across all the experimental groups.

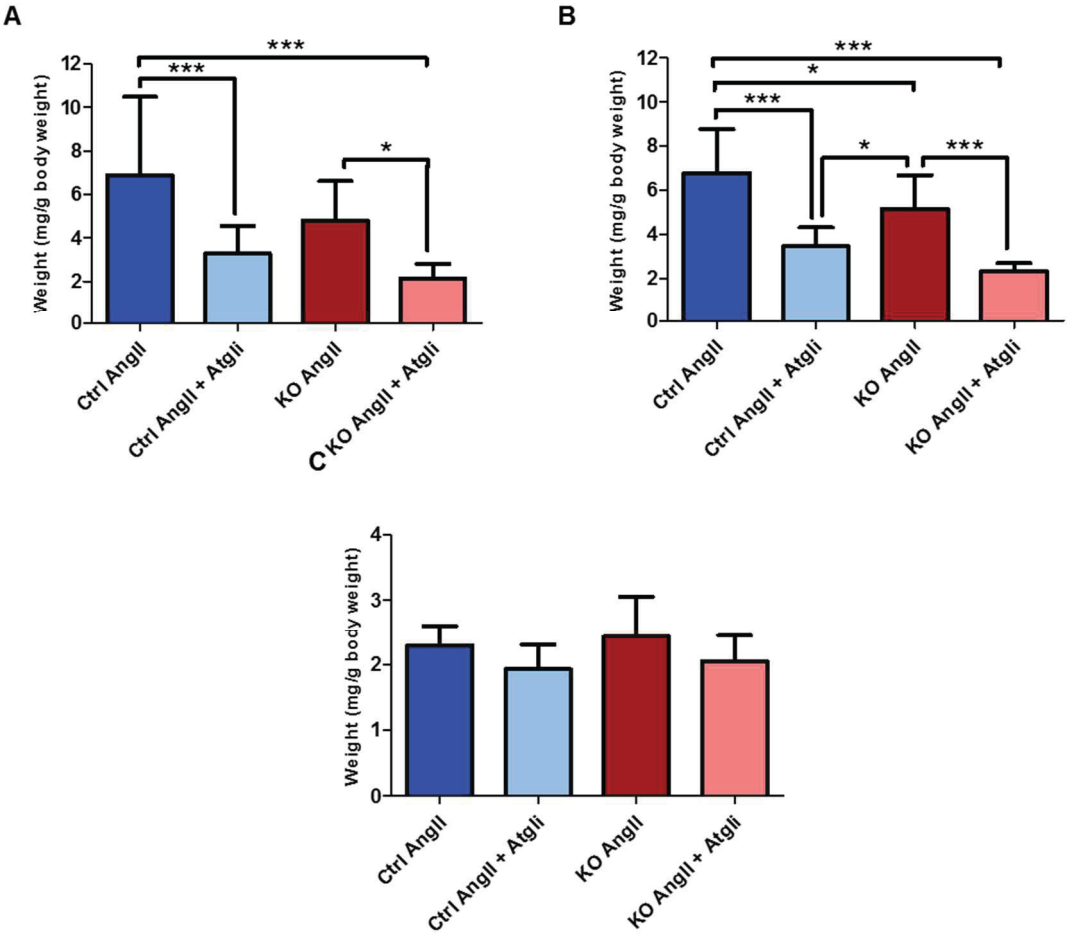

Figure 4.17: Weights of inguinal WAT (A), perigonadal WAT (B) and BAT (C) on day 2 following AngII infusion. Tissue weights were normalized per g of body weight. Data are presented as mean ± SD, and the statistical significance between two groups was calculated using one-way ANOVA with Tukey's multiple comparison post-test, * $p < 0.05$, ** $p < 0.01$, and *** $p < 0.001$. (A), (B) and (D) n = 12 - 14, (C) n = 5 – 8.

Body weight was recorded throughout the period of investigation (Figure 4.18). All mice lost weight by the end of the investigation period. Weight loss was more prominent in iCMp38KO compared to Ctrl following AngII treatment. Atglistatin treatment did not significantly alter the change in body weight, both in Ctrl as well as iCMp38KO mice.

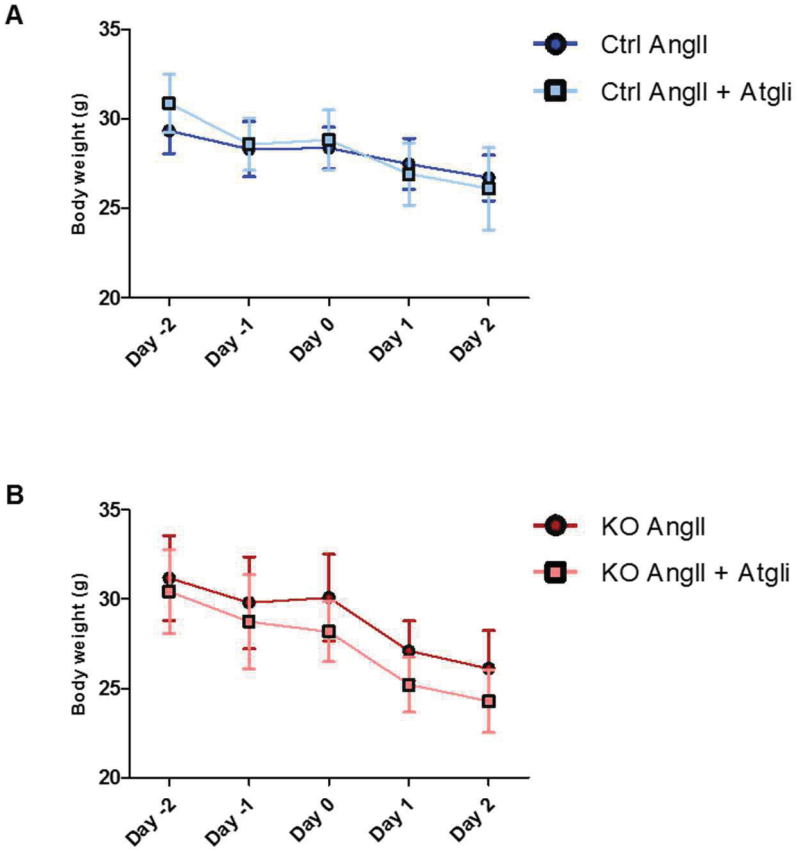

Figure 4.18: Body weight progression over the period of investigation. Daily body weight and food intake were monitored for each group; (A) represents Ctrl and (B) represents iCMp38KO following 48h of AngII administration. Data are presented as mean ± SD with n = 12 – 14.

4.8. Atglistatin inhibition of cardiac pressure overload-induced lipolysis in iCMp38KO – effects on WAT

A number of possible reasons observed by others could explain the loss of white adipose mass despite lipolysis inhibition, including: an incomplete inhibition of lipolysis by atglistatin (Figure 4.11B), suppressed adipogenesis, and increased energy expenditure (Schreiber et al 2015, Schoiswohl et al 2015, Schweiger et al 2016). These factors could result in a decrease in the stored lipid mass, and consequently overall tissue mass. For these reasons, the transcriptional expression of several markers were measured in inguinal and perigonadal WAT. These markers include: adipogenic markers *Pparg* and *Ppara,* and browning markers which include *Ucp1, Cidea, Cox8b,* and *Ppargc1a.* Additionally, alteration in adipokines adiponectin (*Adipoq*) and leptin (*Lep*) expression was investigated to further elucidate mechanisms of interorgan crosstalk.

4.8.1. Altered adipogenesis

After 48h of AngII administration, in perigonadal WAT (Figure 4.19A) of Ctrl mice, atglistatin moderately (<2-fold change) suppressed *pparg* expression, suggesting suppression of adipogenesis. However, *Pparg* expression in the atglistatin-treated iCMp38KO remained similar to the untreated iCMp38KO after AngII infusion. The expression of *Ppara* was similar across all the experimental groups. The expression of *Pparg* in the inguinal WAT was moderately increased due to cardiac pressure overload in the iCMp38KO (Figure 4.19B). Atglistatin suppressed *Pparg* expression, as indicated by the 2.8-fold reduction in the atglistatin-treated Ctrl and 3.2-fold decrease in the atglistatin-treated iCMp38KO. Atglistatin also suppressed the expression of *Ppara* in both groups, however more prominently in the iCMp38KO (4.6-fold lower than iCMp38KO AngII). In summary, atglistatin suppressed genes regulating adipogenesis more strongly in inguinal WAT, suggesting that WAT depots behave differently towards inhibition of ATGL and lipolysis.

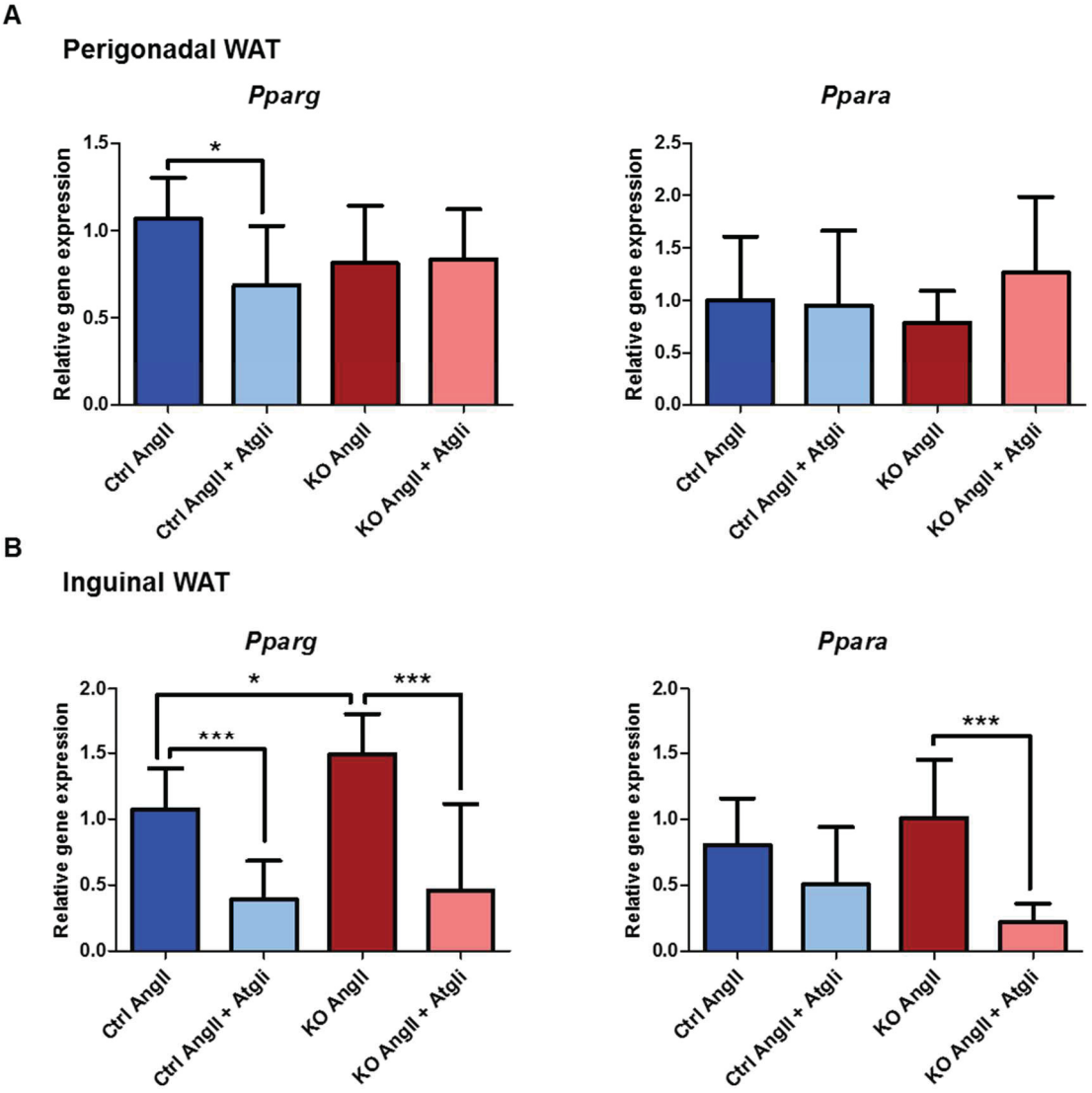

Figure 4.19: Relative transcriptional expression of the regulators of adipogenesis, *pparg* and *ppara,* following AngII infusion. RT-PCR was performed on perigonadal WAT (A) and inguinal WAT (B). Data are presented as mean ± SD with n = 8 – 9. Statistical significance between two groups was calculated using unpaired, two-tailed, Student's t-test; ** $p < 0.01$, and *** $p < 0.001$.

4.8.2. Browning – increased energy expenditure

After AngII administration, WAT was collected from all the experimental groups. Perigonadal WAT showed brownish coloring, which could indicate browning. To further investigate this, histological staining was performed on perigonadal WAT. Microscopic analysis revealed that perigonadal WAT of the atglistatin-treated iCMp38KO contained smaller cells with multilocular lipid droplets (Figure 4.20A and Figure 4.20B indicated by *). Moreover, immunofluorescence detected UCP1-expressing cells (Figure 4.21). Both findings are classic characteristics of brown-like adipocytes. Conversely, the other experimental groups maintained classical WAT morphology which include larger cells containing unilocular lipid droplet and lacking UCP1-positive staining.

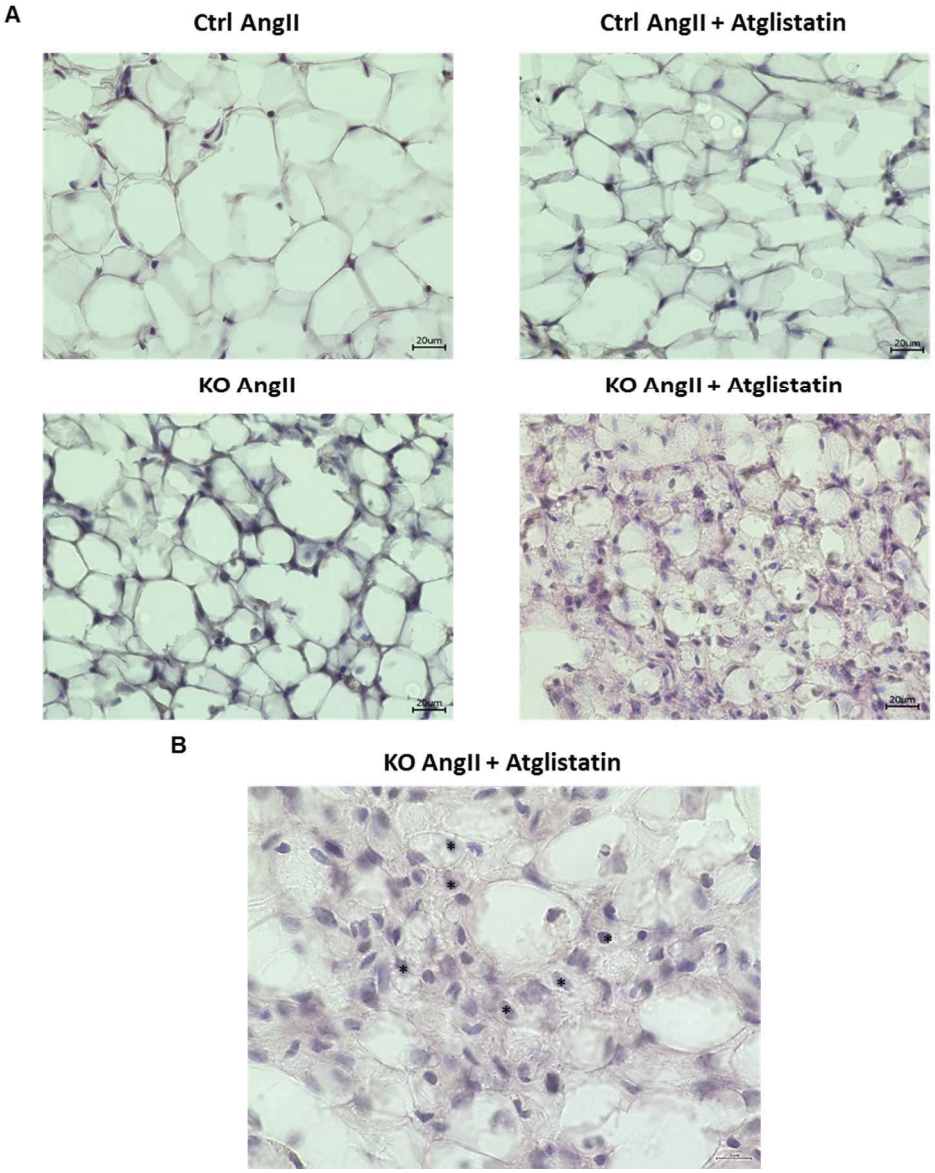

Figure 4.20: Histological staining of cryosections of perigonadal WAT to visualize tissue morphology. All tissues were collected following AngII administration. Hematoxylin & Eosin was performed and visualized using 60x objective. (A) Upper panel represent Ctrl AngII (left) and atglistatin-treated Ctrl AngII (right). Bottom panel represent iCMp38KO AngII (left) and atglistatin-treated iCMp38KO AngII (right). (B) Higher magnification of iCMp38KO AngII + Atglistatin (100x objective). * marks some of the multilocular cells.

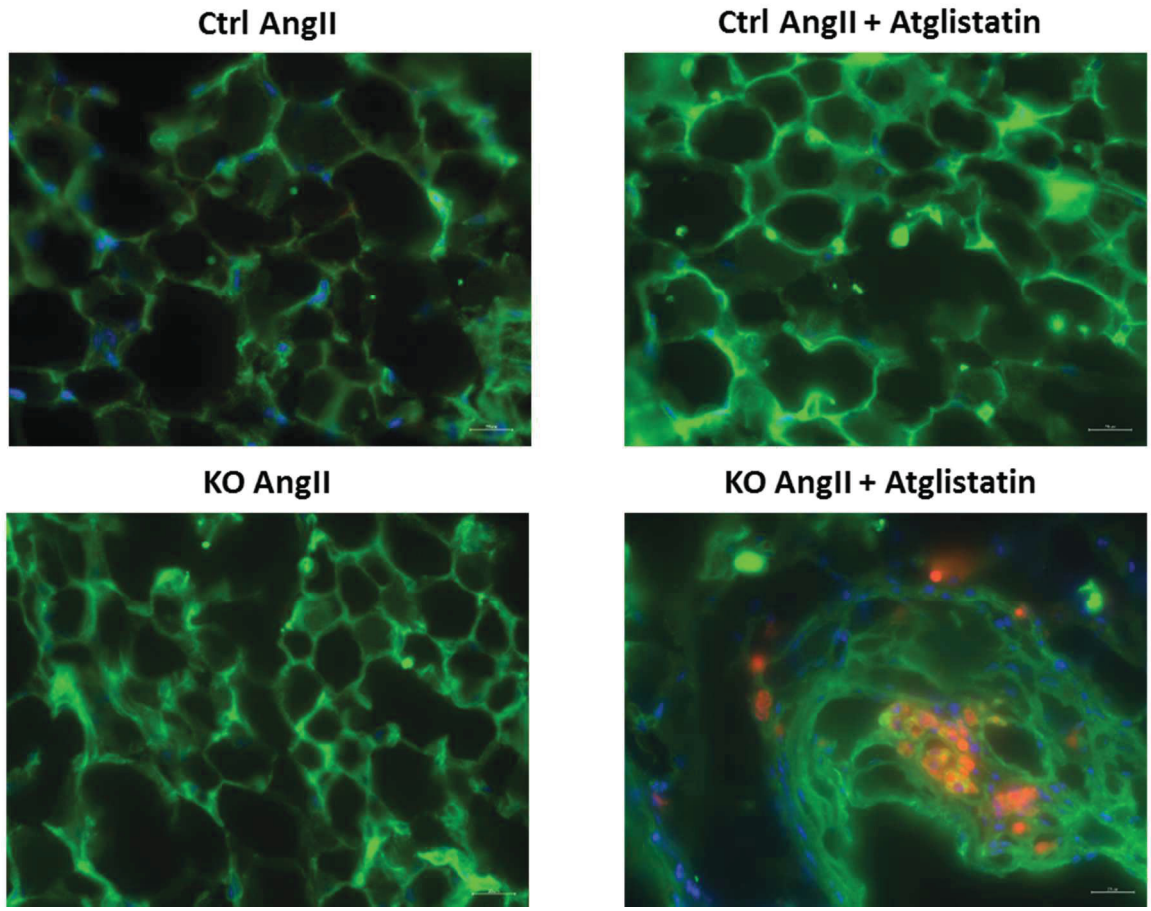

Figure 4.21: Histological staining of cryosections of perigonadal WAT to visualize UCP1 expression. All tissues were collected following AngII administration. Immunofluorescence staining of perigonadal WAT using FITC-labelled wheat germ agglutinin (green), DAPI (blue) and anti-UCP1 antibody detected with a secondary antibody conjugated with Rhodamine Red-X (red). The upper panel represent untreated Ctrl AngII (left) and atglistatin-treated Ctrl AngII (right). The bottom panel shows representative images from iCMp38KO AngII (left) and atglistatin-treated iCMp38KO AngII (right).

Due to the hint of browning detected via histology particularly in atglistatin-treated iCMp38KO after AngII administration, transcriptional expression of browning markers was measured in perigonadal and inguinal WAT by RT-PCR. These markers include: uncoupling protein 1 (*Ucp1*), cell death inducing DFFA like effector A (*Cidea*), and cytochrome oxidase 8b (*Cox8b*). In perigonadal WAT, these markers were all upregulated in atglistatin-treated iCMp38KO after AngII administration (Figure 4.22A). Atglistatin significantly upregulated *Ucp1* (5.1-fold), *Cidea* (6.9-fold), and *Cox8b* (10.1-fold) expression in iCMp38KO after AngII infusion. Noteworthy, browning markers were not upregulated to the same extent in all atglistatin-treated iCMp38KO, suggesting variability of response. In contrast, in inguinal WAT, the expression of those browning markers were not upregulated in atglistatin-treated iCMp38KO (Figure 4.22B), suggesting that browning was not a contributing factor in the loss of inguinal WAT mass.

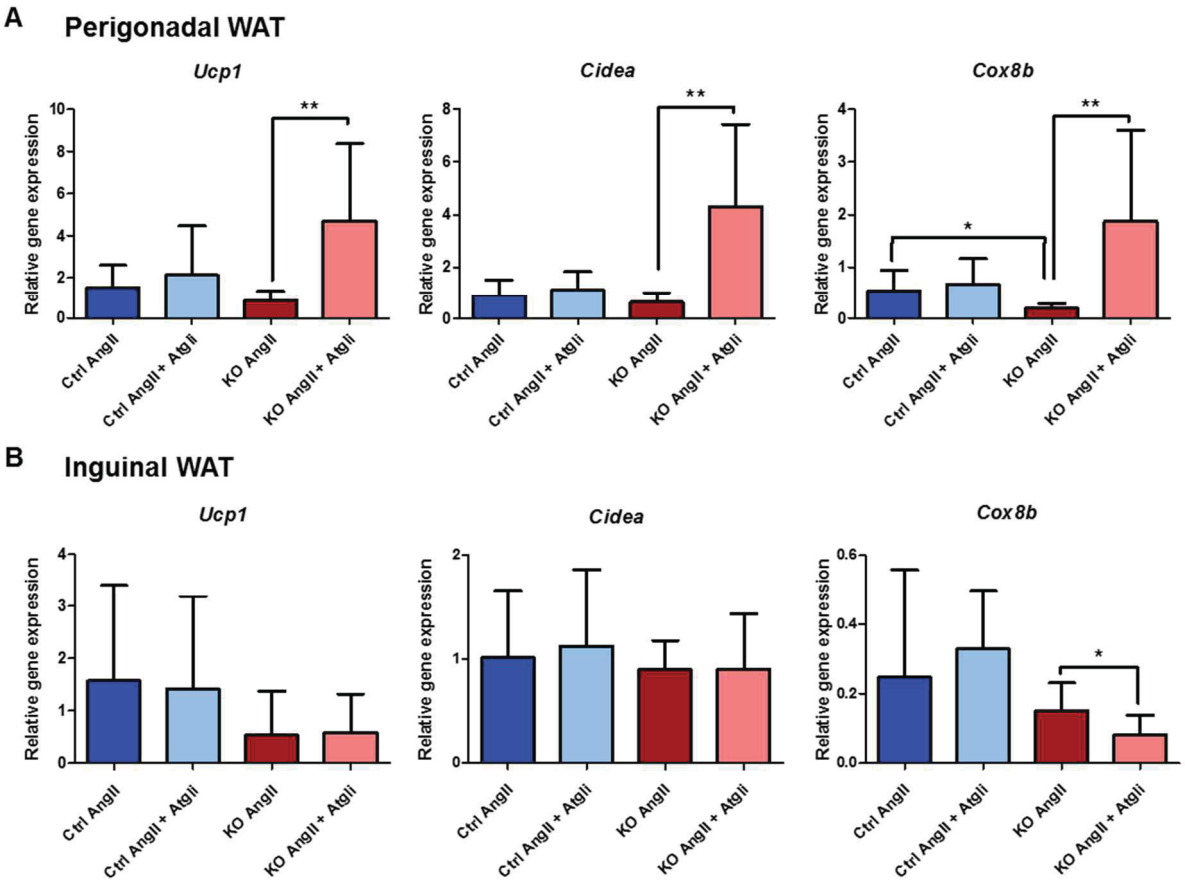

Figure 4.22: Relative transcriptional expression of browning markers in perigonadal (A) and inguinal (B) WAT, following AngII infusion. The transcript expression of *ucp1*, *cidea* and *cox8b* were measured via RT-PCR. Data are presented as mean ± SD with n = 8 – 9. Statistical significance between two groups was calculated using unpaired, two-tailed, Student's t-test; ** $p < 0.01$, and *** $p < 0.001$.

The surprising histological and initial transcript analyses of the perigonadal WAT prompted further analyses to investigate the potential mechanisms behind these initial findings. Total RNA was isolated from perigonadal WAT, and transcript expression were measured using Agilent 8x60K Mouse Array technology (Dr. Patrick Petzsch from the Biologisch Medizinishces Forschungszentrum (BFMZ), Heinrich-Heine University, Düsseldorf) allowing for the detection of up to 60,000 transcripts per chip.

After 48h of AngII administration, transcript expression of 163 genes (corrected p-value cut-off = 0.05, absolute fold change ≥1.5) were differentially regulated in KO compared to the Ctrl, suggesting a moderate effect of AngII-induced cardiac pressure overload on the transcriptional expression in perigonadal WAT. Since atglistatin preferentially targets adipose tissues, it was not surprising that atglistatin treatment resulted in over 4,000 deregulated genes (corrected p-value cut-off = 0.05, absolute fold change ≥1.5) both in Ctrl as well as KO WAT, compared to the respective untreated controls. The transcriptional profiles from each sample were separated by two varying components using the principal component analysis (PCA) (Figure 4.23). Components 1 and 2 account for most of the variables present in this set of data. Therefore, PCA was used to group and separate this large set of data based on the differences in the major variables. The PCA demonstrates that for all atglistatin-treated samples component 1 led to a

deviation from the untreated samples. In addition, for some atglistatin-treated samples, component 2 also led to a variability from untreated samples. This suggests that atglistatin treatment caused a shift based on the two major principal components which distinguish the transcriptional profiles of atglistatin-treated Ctrl and KO from the respective untreated controls.

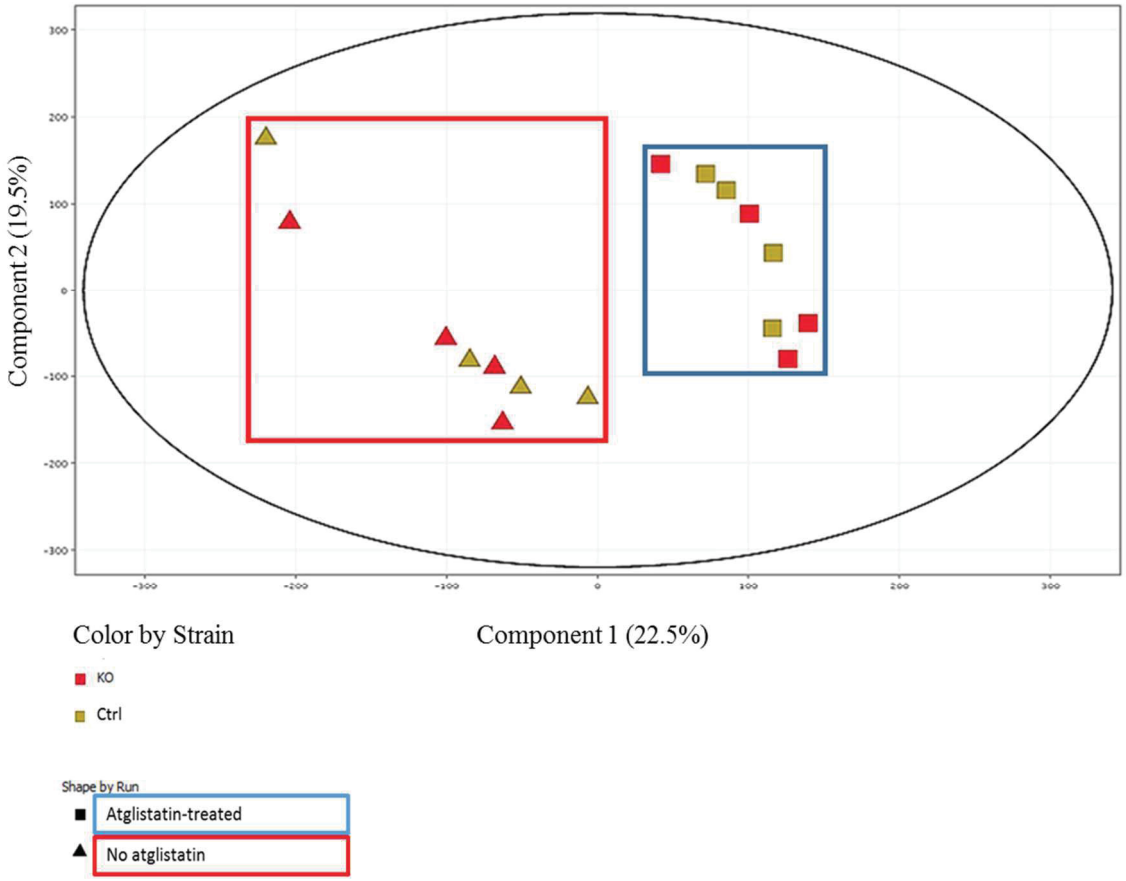

Figure 4.23: Principal component analysis (PCA) of perigonadal WAT total RNA microarray data. All mice received AngII. Red box indicates Ctrl AngII (green triangle) and iCMp38KO AngII (red triangle). Blue box indicates atglistatin-treated Ctrl AngII (green square) and iCMp38KO AngII (red square). n = 4 per group.

Analysis of the transcriptional profile of atglistatin-treated iCMp38KO WAT after administration of AngII revealed upregulation in the expression of transcriptional regulators and genes involved in signaling pathways implicated in the induction of browning of WAT (e.g. apoptosis, thyroid hormone signaling, autophagy, TNF signaling) (summarized in Table 4.3). These results suggest that browning of perigonadal WAT of iCMp38KO was possibly, at least in part at the transcriptional level, induced by atglistatin.

Gene name	**Gene description**	**Function**	**Fold change in atglistatin-treated iCMp38KO (vs KO AngII)**
Atf3	c-AMP-dependent transcription factor 3	Lipid metabolism and thermogenesis	4.6 x ↑

Atg16l2	Autophagy-related protein 16-2	Autophagy	2.2 x ↑
Cox8b	Cytochrome c oxidase 8b	Mitochondrial electron transport chain	2.7 x ↑
Fbxo32	F-box only protein 32	Protein ubiquitination	2.6 x ↑
Mtrnl	Meteorin-like	Adipokine involved in browning of WAT, adipocyte differentiation and metabolism	2.6 x ↑
Ppargc1a	Peroxisome proliferator-activated receptor gamma coactivator 1 alpha	Regulation of mitochondrial biogenesis and oxidation, and transcriptional expression of UCP1	2.7 x ↑
Thrsp	Thyroid hormone responsive	Regulation of lipid metabolism	2.3 x ↑
Vegfa	Vascular endothelial growth factor a	Angiogenesis and cellular migration	2.4 x ↑

Table 4.3: Differentially expressed genes involved in browning of WAT. Overall upregulation of genes involved in the regulation of *ucp1* transcription and/or were found to be upregulated in the case of browning, in the perigonadal WAT of atglistatin-treated KO (n = 4) compared to untreated KO (n = 4). *Selected genes were differentially regulated by at least two folds. Data were analyzed by Agilent Mouse Array technology.

Ingenuity Pathway Analysis (IPA) of microarray data was performed to identify altered pathways due to pressure overload (i.e. iCMp38KO AngII compared to Ctrl AngII) and atglistatin treatment. After AngII administration, over 170 genes were altered in perigonadal WAT of iCMp38KO compared to the Ctrl, but only a small percentage of these genes could be assigned to specific pathways. This suggests that AngII-induced pressure overload did not significantly alter perigonadal WAT at the transcriptional level.

Following 48h of AngII infusion, atglistatin-treated iCMp38KO WAT showed significant alterations at the transcriptional levels, with over 4000 differentially regulated genes compared to the control iCMp38KO AngII. Following IPA, several of the most highly altered canonical pathways, defined by -log (p-value) (>2) and absolute z-score (>2), were upregulated and summarized in Figure 4.24. Functional analysis summarized in Table 4.4 revealed that molecules involved in leukocyte adhesion and chemotaxis were activated (activation z-score >3) resulting in predicted increase in leukocyte infiltration and inflammatory processes. These pathways were not altered in atglistatin-treated Ctrl compared to Ctrl after AngII administration (Figure 4.25),

suggesting that the increased inflammatory response was a combined effect of AngII-induced pressure overload and atglistatin treatment.

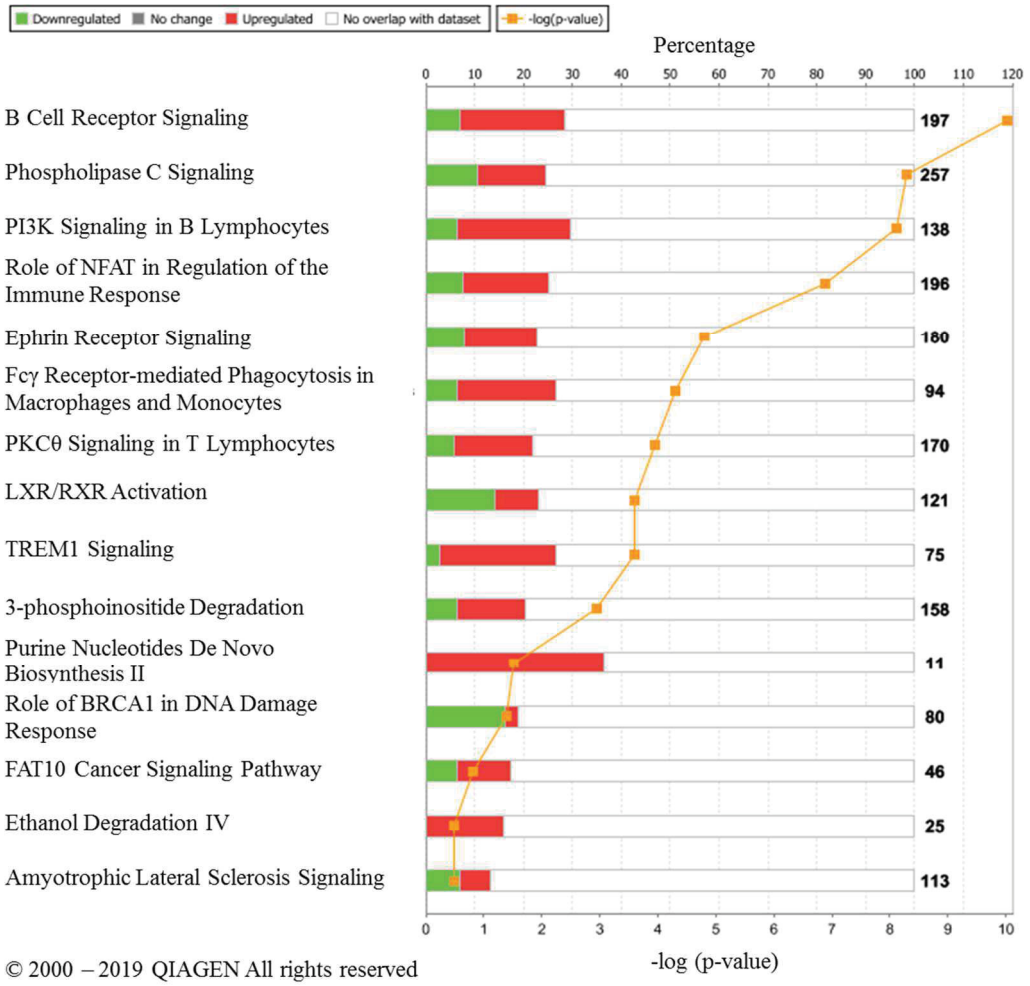

Figure 4.24: Ingenuity Pathway Analysis (IPA) of transcriptional expression of perigonadal WAT showing the effect of atglistatin in the iCMp38KO after AngII administration. The most highly altered canonical pathways were upregulated due to atglistatin treatment.

Diseases or Functions Annotation	p-value	Predicted Activation State	Activation z-score	# Molecules
Adhesion of immune cells	7.05E-14	Increased	3.985	123
Adhesion of lymphocytes	5.10E-06	Increased	3.347	42
Adhesion of mononuclear leukocytes	3.22E-06	Increased	3.189	49
Adhesion of T lymphocytes	5.24E-05	Increased	3.514	34
Binding of neutrophils	3.26E-11	Increased	3.065	47
Cell movement of granulocytes	1.65E-12	Increased	3.125	102
Cell movement of leukocytes	9.82E-18	Increased	3.175	230
Cell movement of neutrophils	2.62E-13	Increased	3.285	91
Cell movement of phagocytes	4.60E-15	Increased	3.4	167
Cell movement of T lymphocytes	1.99E-04	Increased	3.232	54
Chemotaxis of leukocytes	1.87E-08	Increased	3.206	112
Chemotaxis of phagocytes	1.09E-07	Increased	3.325	94
Homing of leukocytes	1.82E-10	Increased	3.559	125
Leukocyte migration	1.30E-15	Increased	3.097	263

Table 4.4: IPA functional analysis of WAT microarray. Overall activation of immune cell adhesion and migration in the perigonadal WAT of atglistatin-treated iCMp38KO AngII compared to control iCMp38KO AngII (n = 4 per group). Cut-off: absolute activation z-score >3, -log(p-value) >2.

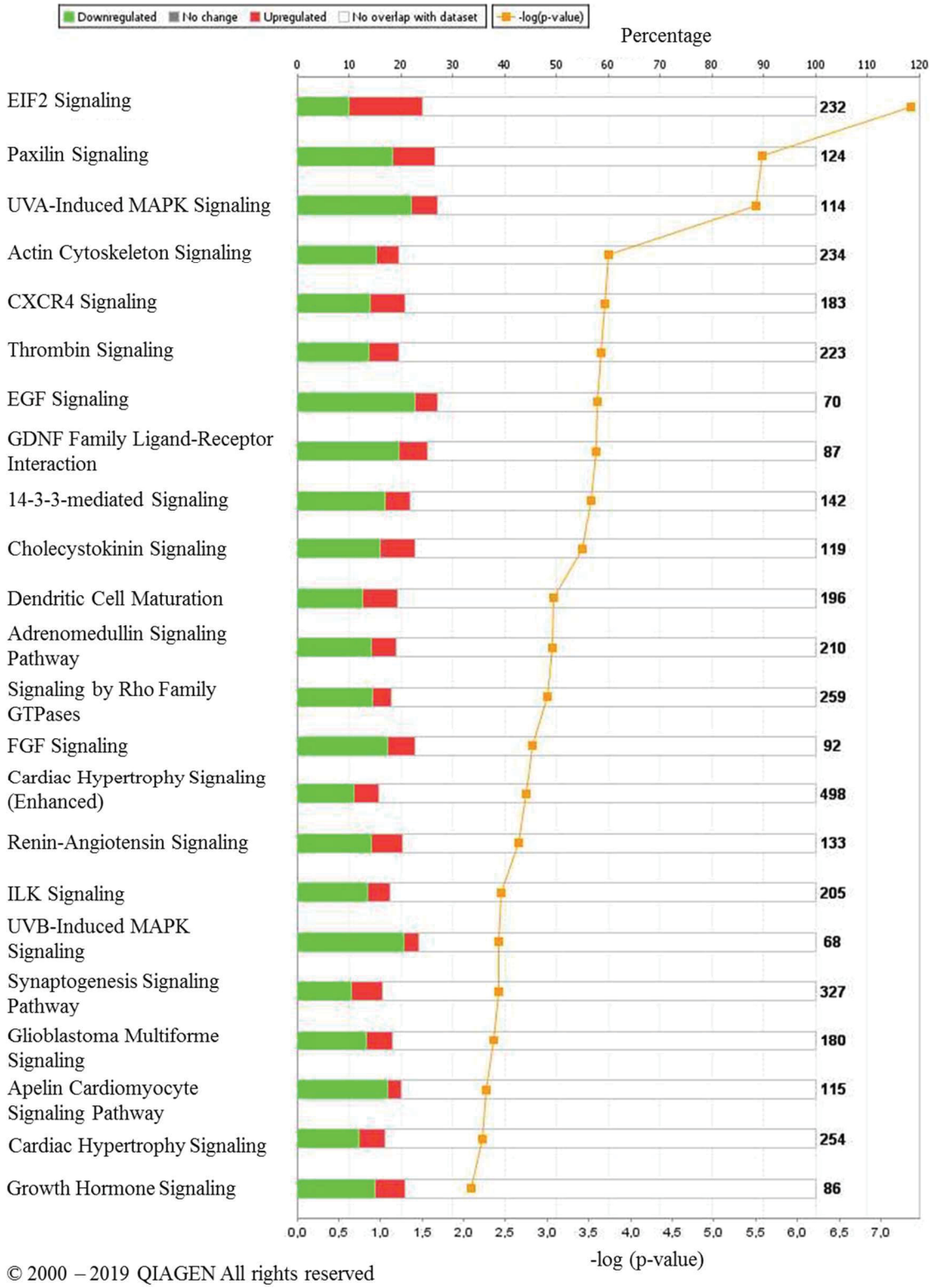

Figure 4.25: Ingenuity Pathway Analysis (IPA) of transcriptional expression of perigonadal WAT showing the effect of atglistatin in Ctrl mice after AngII administration. The most highly altered canonical pathways were downregulated due to atglistatin treatment.

To summarize the microarray analyses of perigonadal WAT, as a result of atglistatin treatment and AngII-induced cardiac pressure overload, several mechanisms implicated in the activation of browning were upregulated. Surprisingly, inflammatory response

was also activated through several signaling pathways and the recruitment of immune cells in the WAT of iCMp38KO treated with atglistatin, suggesting an interplay between lipolysis and WAT inflammation in our pressure overload model of HF.

4.8.3. Adipokines: adiponectin and leptin

A number of adipokines have been implicated in cardiovascular diseases (Akoumianakis & Antoniades 2017). Among these adipokines, the most highly investigated were adiponectin and leptin. Adiponectin has been shown to protect against pathological cardiac remodeling (Guo et al 2013), whereas evidence on leptin are controversial.

To investigate the possible contribution of adipokines in mediating interorgan communication, the expression of *Adipoq* and *Lep* were measured in WAT of Ctrl and iCMp38KO after AngII administration, with and without atglistatin treatment.

In perigonadal WAT (Figure 4.26A), *Adipoq* expression was two-fold lower in iCMp38KO compared to Ctrl, 48h after AngII administration. This expression level was restored in the atglistatin-treated iCMp38KO. Conversely, atglistatin treatment moderately lowered *Adipoq* expression in Ctrl AngII. Atglistatin treatment led a reduction in *Lep* expression both in the Ctrl and iCMp38KO following AngII administration. These results suggest that firstly, cardiac pressure overload stress in the iCMp38KO led to a change in the perigonadal WAT endocrine function mediated by adiponectin, which could be a result of and further mediate the interorgan crosstalk between the failing heart and WAT. Additionally, atglistatin treatment may restore adiponectin signaling in iCMp38KO, and suppress leptin signaling regardless of the presence of AngII-induced pressure overload.

In inguinal WAT (Figure 4.26B), the expression of *Adipoq* was decreased by atglistatin treatment in both the Ctrl (2.3-fold lower) and the iCMp38KO (3.5-fold lower), following 48h of AngII infusion. Similarly, the expression of another adipocyte marker *Lep* was reduced due to atglistatin treatment, indicated by 2.1-fold downregulation in the Ctrl and 4.9-fold downregulation in the iCMp38KO. Noteworthy, *Lep* expression was higher in AngII-treated iCMp38KO, compared to AngII-treated Ctrl. These results suggest a suppression of adiponectin and leptin –mediated signaling derived from inguinal WAT. In addition, pressure overload induced by AngII resulted in the upregulation of *Lep*, suggesting an increased leptin-mediated signaling initiated by inguinal WAT.

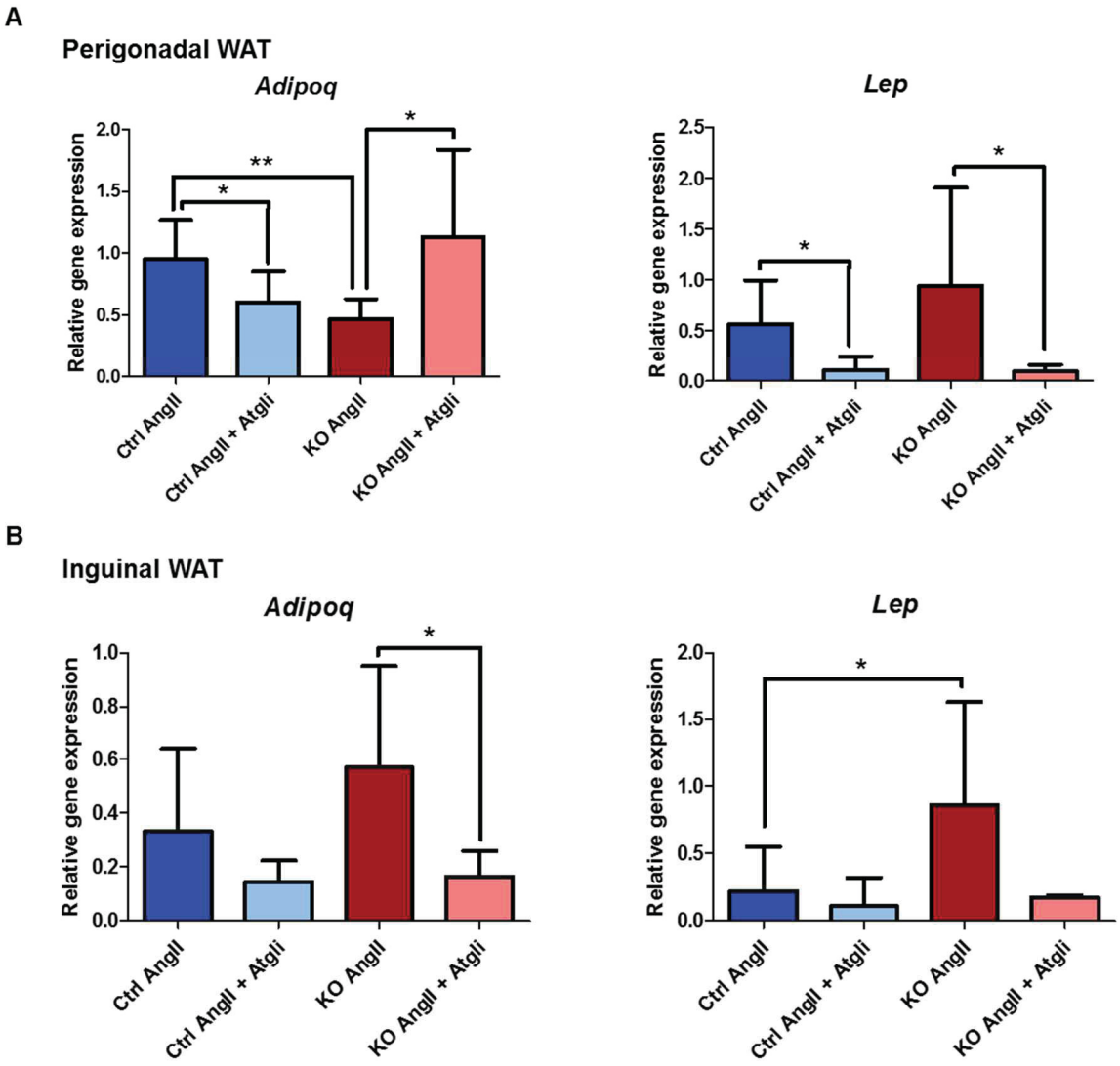

Figure 4.26: Relative transcriptional expression of adipokines in perigondal (A) and inguinal (B) WAT, following AngII infusion. The transcript expression of *adipoq* and *lep* were measured via RT-PCR. Data are presented as mean ± SD with n = 8 – 9. Statistical significance between two groups was calculated using unpaired, two-tailed, Student's t-test; ** $p < 0.01$, and *** $p < 0.001$.

To summarize the WAT effects, perigonadal and inguinal WAT responds differently towards pressure overload induction by AngII, and ATGL inhibition by atglistatin. Perigonadal WAT mass was lost possibly due to browning. The combination of AngII-induced pressure overload and atglistatin treatment resulted in altered inflammatory response in this tissue. Additionally, adiponectin signaling may be altered in perigonadal WAT due to AngII-induced pressure overload. In contrast, suppression of adipogenesis was found in inguinal WAT as a response to atglistatin treatment, which may contribute to the loss of inguinal WAT mass. No indication of browning was observed in this tissue, suggesting that energy expenditure was similar across all the experimental groups. The transcriptional expression of leptin seemed to be upregulated in this tissue due to AngII-induced pressure overload, suggesting alteration in leptin-mediated interorgan crosstalk.

5

Discussion

A dysregulated metabolism in cardiovascular diseases substantially increases the percentage of cardiovascular-related mortality (Mendis et al 2011). Cardiac lipotoxicity as a potential complication of metabolic dysfunction has been associated clinically with heart failure (HF) (Chokshi et al 2012, McGavock et al 2007, Nakanishi & Kato 2014, Sharma et al 2004, Szczepaniak et al 2003), marking the importance of understanding the mechanisms leading to lipid-induced cardiac dysfunction. The interaction between cardiac stress signaling and the regulation of whole body lipid metabolism by adipose tissue presents a potential mechanism of cardiac lipid accumulation. In this study, this possible mechanism of pathophysiology was investigated by pharmacologically inhibiting adipose tissue lipolysis in a pressure overload-induced HF mouse model.

There are several main findings from the present study: (1) Cardiomyocyte-specific deletion of p38 MAPK α (iCMp38KO) and AngII infusion lead to a cardiac lipid accumulation similar to several other previously described experimental models of HF, (2) adipose tissue is a major contributor of cardiac lipid accumulation in pressure overload-induced HF, (3) adipose tissue lipolysis and the resultant cardiac lipid deposit promotes cardiac inflammation with a substantial contribution by neutrophils thus resulting in cardiac dysfunction and the progression of HF, and lastly (4) in the HF model, inhibition of white adipose tissue (WAT) lipolysis leads to altered transcriptional profile of WAT. These results are discussed further in this chapter.

5.1. Intramyocardial lipid accumulation in pressure overloaded hearts

Cardiac lipid accumulation and toxicity in HF have been described clinically and experimentally, for instance by Sharma and colleagues (Sharma et al 2004). The authors showed that 74% of patients with pressure overload, non-ischemic HF accumulated lipids in the hearts at moderate to high levels. Reduced cardiomyocyte FA oxidation and

neutral lipid formation are often observed and associated with toxic lipid accumulation and insulin resistance in the hearts of patients with advanced HF, which increases the risk of mortality (Chokshi et al 2012, Doehner et al 2005, Kelly & Strauss 1994, Sharma et al 2004). It was later found that pressure overload-induced intramyocardial lipid accumulation in HF patients was reduced after mechanical unloading (Chokshi et al 2012). Mechanical unloading corrected not only intramyocardial lipid accumulation, but also FA oxidation and insulin sensitivity, further supporting the causative role of pressure overload in cardiac lipid accumulation. This leads to the question of the source of lipid accumulating in response to pressure overload stress in the heart, and a possible intervention as lipotoxicity and insulin resistance are independent risk factors of mortality in HF patients regardless of etiology (ischemic vs non-ischemic) (Doehner et al 2005). Therefore, iCMp38KO represent an interesting model to study the medically relevant questions.

Using AngII, a significant intramyocardial lipid accumulation was observed in iCMp38KO hearts (Figure 4.4, page 35). Consistently, the AngII-induced pressure overloaded iCMp38KO heart had downregulated expression of genes associated with mitochondrial FA oxidation and TAG synthesis (Table 4.1, page 36). In view of these findings, iCMp38KO is an interesting model to study clinically relevant mechanisms during HF progression.

There are several mechanisms which might cause lipid accumulation in the myocardium: either an excessive FA uptake from the circulation and/or impaired FA oxidation in the heart may cause lipid accumulation. Since adipose tissue lipolysis is the main source of circulating lipid (Roden 2006), the induction of lipolysis in the context of HF may contribute to lipid accumulation. A decline of cardiac function in HF generally leads to the activation of the sympathetic nervous system, aiming at restoring arterial blood pressure. Besides the stimulation of contractile and chronotropic function of the heart, β-adrenergic stimulation also induces lipolysis in adipose tissue (Himms-Hagen 1970). These combined processes may play an important role in normal cardiac physiology, since β-adrenergic stimulation usually occurs to elevate cardiac function, for example in the context of exercise. The heart prefers to oxidize FA to generate ATP. Therefore, an increase in workload combined with enhanced lipolysis would help to supply the heart with sufficient source of energy substrate. However in HF, metabolic dysfunction is frequently observed, which may attenuate the oxidation of FA leading to an imbalance of FA supply and oxidation. Therefore, adipose tissue lipolysis could be the source of accumulated lipids in the myocardium.

To test this hypothesis, adipose lipolysis was inhibited in iCMp38KO mice using atglistatin, a small molecule inhibitor of ATGL which preferentially acts on adipose tissues (Mayer et al 2013, Schweiger et al 2016). Atglistatin was chosen due to the absence of a compensatory increase in lipolysis, which often occurs with other pharmacological lipolysis inhibitors such as acipimox, which does not directly interfere with enzymes involved in lipolysis, but rather modulates the activity of cAMP-dependent mechanisms via niacin receptor 1. Moreover, the specificity of atglistatin towards adipose tissues alleviates off-target effects, particularly the inhibition of ATGL in the heart (Haemmerle et al 2006, Mayer et al 2013, Schweiger et al 2016).

Adipose tissue lipolysis was determined by plasma glycerol measurement. Plasma glycerol was chosen as a marker of lipolysis due to its longer half-life in the circulation (approximately 72 – 348 minutes in human male subjects) in comparison to FFA (approximately 3 minutes in human male subjects). In addition, plasma glycerol release has been shown to be proportional to FFA release into the circulation (Eaton et al 1969, Reaven et al 1965). In this study, pressure overload significantly induced plasma glycerol release in iCMp38KO mice, suggesting an increase in the available FA for uptake into the heart. Indeed, plasma glycerol positively correlated with ectopic lipid accumulation in the failing iCMp38MAPKα KO heart (Figure 4.4H, page 35). Atglistatin significantly reduced lipid accumulation in iCMp38MAPKα KO hearts (Figure 4.11, page 47), supporting the hypothesis that adipose tissue lipolysis is a major contributor of cardiac lipid accumulation in our model of a pressure-overloaded heart.

Genetic and pharmacological (atglistatin) inhibition of adipose tissue lipolysis had been shown to reduce ectopic lipid accumulation in the liver, attributed to the reduced circulating lipid (Schoiswohl et al 2015, Schweiger et al 2016). Moreover, our findings are consistent with other experimental models investigating lipid accumulation specifically in the heart, where high circulating lipids (Buchanan et al 2005, Kobayashi et al 2000, Zhou et al 2000) and excessive cardiac lipid uptake (Chiu et al 2005, Luiken et al 2003, Yagyu et al 2003) were linked to cardiac lipid overload consisting of long chain, and potentially toxic, lipids formed within cardiomyocytes.

In the past decade, imaging studies have been useful in the investigation of lipid-induced cardiac dysfunction (i.e. cardiac lipotoxicity) in humans. In one such study, McGavock and colleagues (McGavock et al 2007) used magnetic resonance spectroscopy and imaging, to investigate the connection between cardiac dysfunction and lipid accumulation. They found that cardiac lipid accumulation precedes the development of systolic dysfunction, suggesting a role of intramyocardial lipid accumulation in the disease progression to advanced HF, but the underlying mechanism remained unknown. Our findings suggest a number of mechanisms which could link cardiac lipid deposition to HF. Long chain lipid intermediates (e.g. ceramides), byproducts of incomplete FA oxidation, and an impaired electron transport chain (e.g. ROS) may contribute to the impaired cardiac function by inducing cardiomyocyte apoptosis (Chiu et al 2001, Galloway et al 1987, He et al 2012, Parra et al 2008) and inflammation (discussed in section 5.2).

By inhibiting adipose tissue lipolysis using atglistatin, cardiac lipid accumulation was attenuated and cardiac function was improved in iCMp38KO mice. Fractional shortening, stroke volume, end systolic volume and ejection fraction (Figure 4.13, page 50) were significantly improved. A recent study in mice with adipose tissue-specific KO of ATGL (AKO) also addressed the effect of adipose tissue lipolysis on a TAC-induced pressure overload mouse model (Salatzki et al 2018). HPLC-MS analysis of left ventricular tissue revealed a significant attenuation of TAC-induced cardiac lipid accumulation in AKO. Moreover, functional analysis performed 11 weeks after TAC surgery revealed a significantly higher ejection fraction and fractional shortening in AKO compared to the WT, indicating that adipose tissue lipolysis indeed played a significant role in pressure overload-induced cardiac lipid accumulation and the resulting decline in cardiac function.

5.2. Characterization of cardiac inflammatory profile in pressure overload-induced heart failure

HF of a dilative phenotype can be categorized based on etiology; ischemic HF involves loss of blood flow and therefore oxygen supply for instance occurring post-MI. In contrast, non-ischemic HF develops without a reduction in perfusion. In terms of hemodynamic changes, AngII was used in this study to induce pressure overload in the heart, as a model of non-ischemic HF. As described in section 1.5 (page 11), pressure overload-induced HF develops through four phases: acute decompensated phase, compensated phase, decompensated phase and establishment of HF, and finally congestive to end-stage HF. Based on the hemodynamic changes, AngII application to iCMp38KO mice can be categorized into the congestive to end-stage HF phase with increases in EDV and ESV and reduced ejection fraction (Figure 4.3, page 34). iCMp38KO hearts fail to adapt to pressure overload and develop left ventricular dilation, as early as 48h after the start of AngII infusion. In contrast, control mice functionally recover within 48h after the onset of AngII infusion and develop a concentric hypertrophy within the next two weeks, which is the normal response of the heart to AngII (Bottermann et al, manuscript in preparation). Thus, the loss of p38 MAPK α substantially reduces the adaptive potential of the heart to pressure overload and highly accelerates the development of a dilative phenotype.

The phases of HF are also marked by changes in immune cell profile and pro-inflammatory cytokine expression in the heart (Nevers et al 2015, Patel et al 2017, Patel et al 2018, Zouggari et al 2013). To characterize the inflammatory cell profile in iCMp38KO with and without atglistatin treatment, we analyzed cardiac tissues via FACS and mRNA expression via RT-PCR.

To investigate the effect of reduced cardiac lipid accumulation on the cardiac inflammatory cell profile, FACS analysis of cardiac tissue from atglistatin-treated iCMp38KO following 48h of AngII infusion was performed. The most prominent change was that following 48h of AngII, iCMp38KO accumulated a substantially higher number of neutrophils compared to the Ctrl (Figure 4.14A, page 52). Surprisingly, atglistatin treatment significantly lowered the number of cardiac neutrophils, indicating that adipose tissue lipolysis, and potentially cardiac lipid accumulation, at least partially, caused the recruitment of neutrophils to the heart. The reduction of neutrophil accumulation was accompanied by a significant improvement in systolic function, particularly fractional shortening (38.5% higher relative to iCMp38KO AngII), and ejection fraction (31.4% higher relative to iCMp38KO AngII) (Figure 4.13, page 50).

The finding that neutrophils play a major role in pressure overload-induced HF in iCMp38KO mice is particularly interesting, because these cells were considered to play a minor role in pressure overload-induced HF. Neutrophil infiltration has been more strongly associated with the inflammatory phase post-MI injury, where neutrophils are recruited very early following the insult (Elgebaly et al 1989, Yan et al 2013). In contrast, the role of neutrophils in pressure overload-induced HF has not been fully established. In an early study on TAC-induced HF (Weisheit et al 2014), only a slight increase in neutrophils was observed raising the question if this minor increase played a role in the inflammatory response at all. Major effects were attributed to monocytes and

macrophages. In a recent review, Brenes-Castro and colleagues (Brenes-Castro et al 2018) postulated that the inflammatory response in pressure overload-induced hypertrophy was mainly governed by monocyte-derived macrophages followed by the infiltration of T- and B- cells, whereas neutrophils were considered to play a minor role.

However, in a time-course study, following TAC-induced pressure overload in mouse heart, neutrophils reached a peak accumulation by day 3 and were persistently high (compared to sham) by day 21, suggesting a prolonged neutrophil-mediated inflammation (Weisheit et al 2014). The first functional proof that neutrophils can contribute to the pathology of pressure overload-induced HF was provided by a recent study (Wang et al 2019). It was demonstrated that neutrophils infiltrate the heart as early as three days following TAC, with a gradual increase up to day 7, and a decline thereafter. Neutrophil depletion resulted in preserved fractional shortening and the attenuation of left ventricular dilation. This study suggests a marked contribution of neutrophils to the progression of pressure overload-induced HF. These findings suggest that regardless of etiology (i.e. ischemic vs non-ischemic), neutrophils rapidly infiltrate the heart and mediate cardiac inflammation. Non-ischemic insult such as pressure overload may result in neutrophil accumulation for a longer period in the heart compared to ischemic insult. Based on histological analysis, our group demonstrated that also in the early adaptive phase, local neutrophil infiltration of Ctrl hearts occurred in AngII-induced hypertrophy. This response was only minor in Ctrl hearts but substantially elevated in iCMp38KO hearts.

Of note, earlier work performed in this context by our group (Bottermann et al, manuscript in preparation) using anti-Ly6G antibodies to deplete neutrophils in iCMp38KO revealed a substantial improvement of cardiac function 48h after AngII infusion. This finding shows that neutrophils invading the heart in the early phase of pressure overload are important trigger of left ventricular dilation. However, significant lipid accumulation was still found in iCMp38KO hearts even with global depletion of neutrophils, leading to our hypothesis that cardiac lipids may contribute to neutrophil recruitment into the heart of iCMp38KO mice.

The cytotoxic and pro-inflammatory properties of neutrophils are attributed to the released factors, such as ROS and hypochlorite generated by NADPH oxidase and myeloperoxidase, thereby causing oxidative injury and apoptosis in the infiltrated tissue (Chen et al 1995, Entman et al 1992). Another example of neutrophil-derived factor is S100a8/a9, a ligand of TLR4 (Wu et al 2014), which stimulates immune cell recruitment and proinflammatory cytokine expression. Neutrophils release chemotactic molecules such as CCL2, which promote the recruitment of other inflammatory immune cells such as monocytes and T cells (Codolo et al 2013), thereby amplifying the inflammatory responses mediated by these cells.

Additionally, the interaction between cardiac lipid and neutrophils was highlighted in a study conducted by Chen and colleagues (Chen et al 1995) using a canine model of MI. They found that lipid peroxidation as a result of lipid accumulation and oxidative stress following reperfusion was associated with increased infiltrating neutrophils and decreased cardiac function due to lower fractional shortening. The data provided in this

study demonstrate that lipid accumulation contributes to neutrophil recruitment and consequently impaired cardiac function.

Pressure overload induces oxidative stress (Sriramula & Francis 2015) and enhances mechanotransduction (Lindner et al 2014), which promote the release of proinflammatory cytokines and chemokines. This initiates the recruitment of monocytes to the cardiac tissue. Tissue macrophages clear the injured site of apoptotic cells and cellular debris. However, macrophages may also recruit inflammatory cells such as lymphocytes, which could induce adverse cardiac remodeling and impaired cardiac function, marking the transition of pressure overload-induced HF to a decompensated phase (Brenes-Castro et al 2018). The immune response in AngII-induced HF in iCMp38KO mice was not restricted to neutrophils. In the present study, the number of cardiac macrophages in the iCMp38KO following 48h of AngII infusion was found to be significantly higher compared to the Ctrl (Figure 4.15, page 53). These macrophages were likely to be monocyte-derived, since $CCR2^{+}$ macrophages were significantly more abundant compared to the Ctrl, whereas the $CCR2^{-}$ subset of resident macrophages remained unchanged. Therefore, the elevated macrophage population enhances the pro-inflammatory response in iCMp38KO hearts.

In a TAC-induced pressure overload model, the macrophage population in the heart increases, reaching its peak on day 6 (Weisheit et al 2014), before any significant impairment in cardiac function was observed. Cardiac macrophages significantly decline by approximately 50% by day 21. Similarly, Patel and colleagues (Patel et al 2017) found that prior to significant TAC-induced cardiac dysfunction, the heart recruits proinflammatory monocytes ($Ly6C^{hi}$) resulting in the expansion of the cardiac macrophage population. Once HF has been established and the number of circulating monocytes has normalized, cardiac macrophage populations decline and become dispensable in the inflammatory processes and the progressive decline in cardiac function. Monocyte-derived macrophages play a role in T cell expansion and the consequent inflammation at the late phase of HF progression (Patel et al 2018). However, based on the findings in the present study, macrophages may also play a role in cardiac inflammation when functional decompensation due to pressure overload can be detected. It can be speculated that 48h after the start of AngII infusion, the iCMp38KO heart starts to undergo a transition to the decompensated phase. During this phase, the number of macrophages in the heart is still high, leading to lymphocyte recruitment which mediate the development of adverse left ventricular remodeling.

The numbers of T cells and B cells in the heart tissue of iCMp38KO mice were significantly higher compared to the Ctrl following 48h of AngII-induced pressure overload (Figure 4.14C and D respectively, page 52). Surprisingly, atglistatin treatment resulted in a tendency to lower numbers of cardiac lymphocytes, suggesting a potential role of adipose tissue lipolysis and cardiac lipid, and perhaps neutrophils, in the recruitment of lymphocytes.

This finding is consistent with previous observation (Kalliourdis et al 2017, Laroumanie et al 2014, Nevers et al 2015, Patel et al 2018, Zouggari et al 2013), which demonstrated that T and B cells infiltrate the heart as it fails to compensate hemodynamic changes and cardiac function declines due to pressure overload. T cell

and B cell recruitment are found to be essential for the transition into decompensated HF, as mice lacking T cells and B cells are protected against cardiac dysfunction due to TAC-induced pressure overload 6 weeks post-surgery (Laroumanie et al 2014). Upon interaction, T cells and B cells mediate cardiac inflammation and cardiomyocyte apoptosis, therefore driving the progressive decline in cardiac contractility and ejection fraction during HF establishment in the TAC-induced pressure overload model (Kalliourdis et al 2017).

Since pro-inflammatory cytokines are important mediators and downstream effectors of inflammatory responses, pro-inflammatory cytokine expression was measured in the hearts of all the experimental groups. Following 48h of AngII infusion, iCMp38KO hearts expressed significantly higher *Tnfa, Il1b* and *Il6* mRNA, as compared to Ctrl (Figure 4.16, page 54). Atglistatin treatment in the iCMp38KO moderately (no statistical significance) suppressed *Tnfa* expression, without affecting *Il1b* and *Il6* expression.

The cytokine hypothesis of HF was first proposed due to the association between a higher plasma TNFα with the more advanced cardiac dysfunction in patients with HF (Levine et al 1990). Indeed, heart biopsies from patients with end-stage dilated cardiomyopathy contained higher transcript and protein levels of TNFα and its receptors compared to organ donors without cardiomyopathy (Torre-Amione et al 1996). In mice, blockage of TNFα either genetically or pharmacologically attenuates AngII-induced adverse cardiac remodeling (Sriramula & Francis 2015).

The detrimental effects of TNFα can be mediated through several mechanisms (Mann 2002). TNFα impairs mitochondrial function by directly disrupting mitochondrial structure, inhibiting of complex III and increasing ROS generation, thereby causing further damage to the mitochondria and cellular apoptosis (Goosen et al 1995, Schulze-Osthoff et al 1992). TNFα increases neutral sphingomyelinase activity and synthesis of sphingolipids such as ceramides in cardiomyocytes, which directly induce negative inotropy and apoptosis (Krown et al 1996, Oral et al 1997). Another mechanism of TNFα-mediated apoptosis is through direct activation of caspase-1 (Krown et al 1996). The adverse metabolic effect of TNFα can be attributed to its ability to promote serine phosphorylation of IRS-1, thereby inhibiting downstream insulin signaling (Hotamisligil et al 1994). The findings here suggest that cardiac lipids and immune cell infiltration partly account for TNFα expression in the failing heart, and that TNFα could be an important inflammatory mediator in our pressure overload-induced HF model due to its cytotoxicity and detrimental effect on cellular metabolism.

5.3. Effects of inhibition of lipolysis on WAT

Whereas the data discussed so far demonstrate a clear effect of adipose tissue-derived FA on cardiac function and inflammation, the effects on adipose tissue mediated by HF are less clear.

First, transcriptomic analysis of perigonadal WAT isolated from mice after 48h of AngII administration revealed only minimal changes in gene expression in iCMp38KO mice as compared to Ctrl mice. This was in contrast to skeletal muscle and liver which were analyzed in earlier studies (Leitner 2017, Nemmer in preparation). In the first case,

more than 3000 differentially expressed transcripts were detected, exhibiting the clear pattern of a wasting phenotype. Interestingly, the activation of a cachexia-related gene expression program was more pronounced in glycolytic than in oxidative skeletal muscle, which also reflects clinical findings (Leitner et al 2016). In the liver, over 1000 transcripts were modulated in the AngII-treated iCMp38KO mice. In view of these extensive alterations, the adipose tissue appears to be almost unchanged, with only 182 differentially expressed transcripts. IPA failed to assign the differentially expressed transcripts to specific pathways.

5.3.1. Loss of WAT mass

The surprising observation was that despite inhibition of lipolysis and expected retention of lipid within the adipose tissue compartments, a significant reduction due to atglistatin treatment in the inguinal and perigonadal WAT masses was observed (Figure 4.17A and B respectively, page 55). The apparently paradoxic loss of WAT mass due to the inhibition of lipolysis had been described in several studies involving inhibition of adipose ATGL or HSL, the rate limiting enzymes of lipolysis. These studies suggested that the disturbance in the balance between lipid catabolism and anabolism resulted in an adaptive response in order to restore the balance between the two metabolic pathways (Mottillo et al 2014, Schreiber et al 2015, Schweiger et al 2016). Based on this theory, a reduction or inhibition of adipose tissue lipolysis leads to an adaptive suppression of lipid-storing processes in adipocytes to prevent maladaptive adipocyte hypertrophy, resulting in the loss of adipose mass. Chronic activation of β_3-adrenergic signaling showed a coupling between lipolysis and *de novo* synthesis of FA (Mottillo et al 2014), suggesting an interdependent relationship between the catabolic and anabolic pathways based on the availability of circulating lipid.

The loss of WAT mass in our model may be explained by a reduction in adipogenesis. Indeed following 48h of AngII administration, inguinal WAT from atglistatin-treated Ctrl and iCMp38KO mice expressed significantly lower *Pparg* compared to the mice which did not receive atglistatin (Figure 4.19, page 57). This suggests that suppressed *Pparg*-mediated adipogenesis could be a cause of inguinal WAT mass loss due to inhibition of ATGL by atglistatin. In line with this finding, mice lacking HSL expressed lower levels of adipogenic genes and genes involved in lipid and FA *de novo* syntheses in WAT, resulting in the loss of fat mass (Zimmermann et al 2003). Similarly, global ATGL KO mice (Schreiber et al 2015) and adipose tissue-specific ATGL KO mice (Schoiswohl et al 2015) lost significant adipose tissue weight from subcutaneous and perigonadal regions. Transcriptional investigations revealed a significant downregulation of genes involved in lipid uptake and synthesis, as well as genes regulating adipocyte differentiation. Among these genes, the master regulator of adipogenesis *Pparg* and its downstream target genes were downregulated, suggesting its role in the adaptive suppression of adipogenesis.

Furthermore, our findings are similar to data by Schweiger and colleagues (Schweiger et al 2016) who treated a high fat diet-induced obese mice with atglistatin. They observed significant reductions in inguinal and perigonadal WAT mass during atglistatin treatment, which was associated with significant downregulation in PPARγ and its target genes. Although extensive studies need to be performed to further clarify

this relationship, FAs have been implicated as regulators in the maintenance of balance between lipid catabolic and anabolic pathways, due to their ability to bind and regulate PPARs (Itoh et al 2008). Therefore, it could be speculated that in our model of chronic stress, the reduction in FA availability as a result of inhibited lipolysis leads to decreased PPAR activation, and eventually transcription of its downstream targets.

In contrast, perigonadal WAT expression of *Pparg* was not altered in iCMp38KO mice due to atglistatin treatment, indicating that: (1) regional (subcutaneous vs visceral) differences exist despite the same tissue type (i.e. WAT), (2) other mechanisms of WAT loss could be at play, and (3) a complex crosstalk between cardiac stress and regulation of adipose tissue lipolysis may exist.

5.3.2. Browning-related genes

Another potential mechanism of WAT loss could be due to increased energy expenditure as a result of browning, which is discussed in this section. The first hint that browning occurred was the observation of a browner color of perigonadal WAT from atglistatin-treated iCMp38KO mice, following 48h of AngII application. This prompted the detection of browning markers in this tissue at the transcriptional level via RT-PCR, which revealed that atglistatin treatment, particularly in the iCMp38KO significantly upregulated browning markers which include *Ucp1, Cidea* and *Cox8b* (Figure 4.22, page 60). Accordingly, morphological changes and histological detection of UCP1 were observed in perigonadal WAT of atglistatin-treated iCMp38KO mice (Figure 4.20 and 4.21, pages 58 and 59 respectively). In contrast, these results were not observed in atglistatin-treated Ctrl after AngII treatment, suggesting that cardiac impairment as a mechanism of interorgan communication contributed to the induction of browning.

Transcriptional expression *Ucp1* is driven by FAs, which are released from lipid storage through lipolysis. Therefore the upregulation of *Ucp1* in atglistatin-treated KO may seem paradoxical, since ATGL and consequently lipolysis are inhibited by atglistatin. Of note, as evident by the plasma glycerol data (Figure 4.11B, page 47), adipose tissue lipolysis was significantly suppressed but not completely inhibited. Atglistatin is a transient inhibitor of ATGL (Mayer et al 2013), thus during the period when ATGL is not inhibited, low-grade lipolysis may still occur. Activities of other lipases such as HSL (although less potent compared to ATGL in the degradation of TAG) as well as the lysosomal degradation of lipid droplets to release FA (lipophagy) (Martinez-Lopez et al 2016) cannot be completely ruled out. However, recent studies using mice with adipose tissue-specific KO of ATGL (Schreiber et al 2017) or CGI-58, a co-activator of ATGL (Shin et al 2018) revealed that adipose tissue lipolysis is not necessary in cold-induced browning when β-adrenergic innervation is intact, and sufficient energy substrate is available (i.e. free access to food).

To further elucidate the mechanisms leading to browning in perigonadal WAT, microarray analysis was performed. Several browning-related genes (summarized in Table 4.3, page 61) were found to be upregulated. The transcriptional upregulation of the gene encoding for thyroid hormone responsive protein (*Thrsp*) in atglistatin-treated iCMp38KO WAT following AngII treatment suggests a potential involvement of the thyroid-signaling pathway in *Ucp1* expression. Thyroid hormone-mediated pathway enhances cAMP-mediated *Ucp1* expression by increasing β-adrenergic receptor

expression, thereby enhancing catecholaminergic, sympathetic innervation (Nedergaard & Cannon 1992, Nedergaard et al 1997). Accordingly, circulating T_4 correlates with the expression of browning-related genes encoding for UCP1 and CIDEA in human WAT (Martinez-Sanchez et al 2017). Upregulation of *Ppargc1a* and *Atf3* observed in atglistatin-treated iCMp38KO WAT may contribute to an increase in *Ucp1* transcription. The classical mechanism of browning of WAT is mediated by sympathetic activation of β_3-adrenergic receptor (Cannon & Nedergaard 2004). Through a cAMP/PKA-dependent manner, p38 MAPK activates ATF and PGC-1α proteins by phosphorylation, which are known to regulate the transcription of *Ucp1* (Cao et al 2004).

The transcriptional expression of adiponectin in iCMp38KO mice following AngII application was downregulated compared to the Ctrl, and this was alleviated by atglistatin treatment (Figure 4.26A, page 66). Adiponectin KO in mice subjected to chronic and acute cold exposure (4°C) significantly suppressed the adaptive expression of browning-related genes in WAT, which include *Ucp1, Cox8b* and *Cidea* (Hui et al 2015). Further investigation in this study revealed that adiponectin is an important facilitator of M2 macrophage accumulation in WAT due to cold exposure. M2 macrophages act as local source of catecholamines, thereby enhancing the catecholamine activation of browning.

To summarize, the data obtained from histological and transcripitional analyses in this study suggest a number of mechanisms leading to the induction of browning. Browning of WAT was observed in mice with AngII-induced HF and atglistatin inhibition of lipolysis. This suggests an interplay between these two mechanisms.

5.3.3. AT immune cell infiltration and inflammation

IPA of the microarray data of perigonadal WAT shows that surprisingly atglistatin treatment only in the iCMp38KO following 48h of AngII application caused upregulation of pathways involved in inflammation, and increased immune cell migration and proliferation.

The crosstalk between ATGL-driven lipolysis and adipose tissue inflammation was recently highlighted by Schoiswohl and colleagues (Schoiswohl et al 2015). In this study, inducible KO of ATGL in adipose tissue was used to investigate the effects of ATGL on chronic metabolic stress caused by high-fat feeding. High fat feeding induced metabolic impairment, ectopic lipid accumulation in the liver, and WAT and BAT immune cell infiltration and inflammation. ATGL KO resulted in reduced lipid accumulation and immune cell infiltration in the liver. However, adipose tissue (both WAT and BAT) immune cell infiltration, mostly monocyte-derived macrophages, and inflammation due to high-fat diet tended to be exacerbated. The authors postulated that adipocyte death due to the lack of FA supply results in an upregulation of proinflammatory adipokine expression, and the release of lipid species which are capable of recruiting immune cells. Additionally, the loss of ATGL results in the suppression of its downstream signaling, which includes the PPARs. As previously mentioned, *Ppara* and *Pparg* are important master regulators of adipocyte metabolism, proliferation and inflammation (Varga et al 2011).

Another study performed on aged mice and differentiated 3T3-L1 adipocytes revealed a significant age-related downregulation of ATGL mRNA expression. This was accompanied by a downregulation of *Ppara*, and upregulation of *Il6* and *Tnfa* gene expression (Lettieri Barbato et al 2014a). In addition, another study performed by the same group using ATGL KO mice revealed that apoptosis and inflammation were enhanced in visceral WAT, similar to the effects seen in aged mice (Lettieri Barbato et al 2014b). The authors postulated that the increase in inflammation was due to the reduction in FA mobilization. FA is a stimulatory ligand of PPARα protein. Therefore, reduced FA mobilization leads to a decrease in PPARα activity. This results in a decline in PPARα-mediated suppression of NF-$_{K}$B, a transcriptional regulator of pro-inflammatory cytokines, thereby causing inflammation (Varga et al 2011).

To summarize, WAT is a complex endocrine organ which regulates whole-body metabolism. The results obtained here suggest that WAT lipolysis may have a role in inflammatory responses, leading to altered WAT functions. Thus, further studies still need to be performed to establish the exact, and/or other mechanism of adipose tissue inflammation due to the lack of ATGL-driven lipolysis.

Conclusion & Future Direction

Our model of HF is an accelerated model of lipotoxic, end-stage HF, which was characterized in this study by the marked cardiac lipid accumulation, severe cardiac dysfunction and cardiac immune cell and inflammatory profiles, following the induction of pressure overload in the heart.

Adipose tissue lipolysis was identified as the main source of cardiac lipid accumulation, as indicated by the reduction in cardiac lipid accumulation and circulating marker of lipolysis when adipose tissue lipolysis was inhibited. Further investigation of the cardiac immune cell profile revealed substantial accumulation of neutrophils, macrophages, T cells and B cells due to pressure overload, highlighting the role of immune cell-mediated inflammation. Neutrophil infiltration was significantly attenuated by inhibition of lipolysis and cardiac lipid accumulation. Moreover, the reduction in neutrophils was correlated with improved ejection fraction. Additionally, the amounts of macrophages, T and B cells were lower in atglistatin-treated iCMp38KO following AngII administration. Based on this, we conclude that cardiac lipid, at least partially, recruit neutrophils, and to some extent macrophages, T cells and B cells, resulting in prolonged inflammation driven by these cells. This potentially contributed to the progressive decline in cardiac function seen in AngII-induced pressure overloaded heart. Future studies in this area should be directed towards defining the mechanism(s) involved in the interaction between cardiac lipid pool and immune cell recruitment.

The investigation of WAT revealed, the different response between inguinal and perigonadal WAT. The results here suggest an interplay between the inhibition of lipolysis, AngII-induced HF, and WAT inflammation driven by ATGL-mediated lipolysis. This suggests other potential mechanisms of interorgan communication between the failing heart (i.e. chronic stress conditions) and adipose tissue. Another interesting effect is the induction of browning in perigonadal WAT due to the combined effect of AngII-induced HF and inhibition of lipolysis. This area requires further investigation to establish the effects of pressure overload-induced HF on adipose tissue physiology and function.

In summary, lipolysis mediates heart-adipose tissue crosstalk in the development of HF, partly by facilitating cardiac neutrophil recruitment and inflammation. Pharmacological modulation of adipose tissue lipolysis may offer an interesting strategy for therapeutical intervention in HF.

References

Achari AE & Jain SK (2017). "Adiponectin, a Therapeutic Target for Obesity, Diabetes, and Endothelial Dysfunction". *International Journal of Molecular Sciences.* 18:1321, doi:10.3390/ijms18061321.

Adams SH et al (2009). "Plasma Acylcarnitine Profiles Suggest Incomplete Long-Chain Fatty Acid b-Oxidation and Altered Tricarboxylic Acid Cycle Activity in Type 2 Diabetic African-American Women". *The Journal of Nutrition, Genomics, Proteomics, and Metabolomics.* 8, 1073 – 1081.

Adams V et al (2007). "Myocardial Expression of Murf-1 and MAFbx after Induction of Chronic Heart Failure: Effect on Myocardial Contractility". *Cardiovascular Research.* 73, pp 120 – 129.

Akoumianakis I & Antoniades C (2017). "The Interplay between Adipose Tissue and the Cardiovascular System: Is Fat Always Bad?". *Cardiovascular Research.* 113, pp 999 – 1008.

Akpek M et al (2012). "Relation of Neutrophil/Lymphocyte Ratio to Coronary Flow to In-Hospital Major Adverse Cardiac Events in Patients with ST-Elevated Myocardial Infarction Undergoing Primary Coronary Intervention". *The American Journal of Cardiology.* http://dx.doi.org/10.1016/j.amjcard.2012.04.041.

Ali A et al (2019). "Cardiolipotoxicity, Inflammation, and Arrhythmias: Role for Interleukin-6 Molecular Mechanisms". *Frontiers in Physiology.* 9:1866, doi: 10.3389/fphys.2018.01866.

Ashrafian H et al (2007). "Metabolic Mechanisms in Heart Failure". *Circulation.* 116, pp 434 – 448.

Bao W et al (2007). "Effects of p38 MAPK Inhibitor on Angiotensin II-Dependent Hypertension, Organ Damage, and Superoxide Anion Production". *Journal of Cardiovascular Pharmacology.* 49, pp 362 – 368.

Bartelt A & Heeren J (2014). "Adipose Tissue Browning and Metabolic Health". *Nature Reviews Endocrinology.* 10, pp 24 – 36.

Benigni A et al (2010). "Angiotensin II Revisited: New Roles in Inflammation, Immunology and Aging". *EMBO Molecular Medicine.* 2, pp 247 – 257.

Berry DC et al (2013). "The Developmental Origins of Adipose Tissue". *Development.* 140, pp 3939 – 3949.

Bharadwaj KG et al (2010). "Chylomicron- and VLDL-derived Lipids Enter the Heart

Through Different Pathways *In Vivo* Evidence for Receptor- and Non-Receptor-Mediated Fatty Acid Uptake". *The Journal of Biological Chemistry.* 285:49, pp 37976 – 37986.

Blankesteijn WM et al (2001). "Dynamics of Cardiac Wound Healing Following Myocardial
Infarction: Observations in Genetically Altered Mice". *Acta Physiologica Scandinavica.* 173, pp 75 – 82.

Boden G et al (2001). "Effects of Acute Changes of Plasma Free Fatty Acids on Intramyocellular Fat Content and Insulin Resistance in Healthy Subjects". *Diabetes.* 50, pp 1612 – 1617.

Bottermann K, Oenarto V et al (manuscript in preparation). "p38 MAP Kinase α promotes adaptation to pressure overload by regulating cardiac metabolism".

Brenes-Castro D et al (2018). "Temporal Frame of Immune Cell Infiltration during Heart Failure Establishment: Lessons from Animal Models". *International Journal of Molecular Sciences.* 19:3719, doi:10.3390/ijms19123719.

Buchanan J et al (2005). "Reduced Cardiac Efficiency and Altered Substrate Metabolism Precedes the Onset of Hyperglycemia and Contractile Dysfunction in Two Mouse Models of Insulin Resistance and Obesity". *Endocrinology.* 146:12, pp 5341 – 5349.

Cannon B & Nedergaard J (2004). "Brown Adipose Tissue: Function and Physiological Significance". *Physiological Reviews.* 84, pp 277 – 359.

Cao W et al (2004). "p38 Mitogen-Activated Protein Kinase Is the Central Regulator of Cyclic AMP-Dependent Transcription of the Brown Fat Uncoupling Protein 1 Gene". *Molecular and Cellular Biology.* 24:7, pp 3057 – 3067.

Carley AN et al (2013). "Multiphasic Triacylglycerol Dynamics in the Intact Heart during Acute *In Vivo* Overexpression of CD36". *Journal of Lipid Research.* 54, pp 97 – 106.

Chen B & Fangogiannis NG (2016). "Immune Cells in Repair of the Infarcted Myocardium". *Microcirculation.* 24:e12305, https://doi.org/10.1111/micc.12305.

Chen GY & Nunez G (2010). "Sterile Inflammation: Sensing and Reacting to Damage". *Nature Reviews Immunology.* 10:12, pp 826 – 837.

Chen LY et al (1995). "Myocardial Neutrophil Infiltration, Lipid Peroxidation, and Antioxidant Activity after Coronary Artery Thrombosis and Thrombolysis". *American Heart Journal.* 129:2, pp 211 – 218.

Chen X et al (1999). "The Effects of Free Fatty Acids on Gluconeogenesis and Glycogenolysis in Normal Subjects". *The Journal of Clinical Investigation.* 103:3, pp 365 – 372.

Cheng KKY et al (2014). “Signaling Mechanisms Underlying the Insulin-Sensitizing Effects of Adiponectin”. *Clinical Endocrinology & Metabolism.* 28, pp 3 – 13.

Cheng L et al (2004). “Cardiomyocyte-Restricted Peroxisome Proliferator Activated Receptor-δ Deletion Perturbs Myocardial Fatty Acid Oxidation and Leads to Cardiomyopathy”. *Nature Medicine.* 10:11, pp 1245 – 1250.

Chiu H et al (2001). “A Novel Mouse Model of Lipotoxic Cardiomyopathy”. *The Journal of Clinical Investigation.* 107, pp 813 – 822.

Chiu H et al (2005). “Transgenic Expression of Fatty Acid Transport Protein 1 in the Heart Causes Lipotoxic Cardiomyopathy”. *Circulation Research.* 96, pp 225 – 233.

Cho KW et al (2014). “Flow Cytometry Analyses of Adipose Tissue Macrophages”. *Methods in Enzymology.* 537, pp 297 – 314.

Chokshi A et al (2012). “Ventricular Assist Device Implantation Corrects Myocardial Lipotoxicity, Reverses Insulin Resistance and Normalizes Cardiac Metabolism in Patients with Advanced Heart Failure”. *Circulation.* 125:23, pp 2844 – 2853.

Coleman RA & Mashek DG (2011). “Mammalian Triacylglycerol Metabolism: Synthesis, Lipolysis and Signaling”. *Chemical Reviews.* 111:10, pp 6359 – 6386.

Coppack SW (2001). “Pro-inflammatory Cytokines and Adipose Tissue”. *Proceedings of the Nutrition Society.* 60, pp 349 – 356.

Cousin B et al (1992). “Occurrence of Brown Adipocytes in Rat White Adipose Tissue: Molecular and Morphological Characterization”. *Journal of Cell Science.* 103, pp 931 – 942.

Demine S et al (2017). “Mild Mitochondrial Uncoupling Induces HSL/ATGL-independent Lipolysis Relying on a Form of Autophagy in 3T3-L1 Adipocytes”. *Journal of Cellular Physiology.* 9999, pp 1 – 19.

Dewald O et al (2005). “CCL2/Monocyte Chemoattractant Protein-1 Regulates Inflammatory Responses Critical to Healing Myocardial Infarcts”. *Circulation Research.* 96, pp 881 – 889.

Dreyer MG et al (2003). “Leptin Activates the Promoter of the Interleukin-1 Receptor Antagonist through p42/44 Mitogen-Activated Protein Kinase and a Composite Nuclear Factor $_{K}$B/PU.1 Binding Site”. *Biochemical Journal.* 370, pp 591 – 599.

Dick SA & Epelman S (2016). “Chronic Heart Failure and Inflammation What Do We Really Know?”. *Circulation Research.* 119, pp 159 – 176.

Disteldorf EM et al (2015). “CXCL5 Drives Neutrophil Recruitment in T_H 17-Mediated GN”. *Journal of the American Society of Nephrology.* 26:1, pp 55 – 66.

Doehner W et al (2005). “Impaired Insulin Sensitivity as an Independent Risk Factor for Mortality in Patients with Stable Chronic Heart Failure”. *Journal of the American College of Cardiology.* 46:6, pp 1019 – 1026.

Doenst T et al (2013). “Cardiac Metabolism in Heart Failure Implications beyond ATP Production”. *Circulation Research.* 113, pp 709 – 724.

Dong B et al (2012). “TLR4 Regulates Cardiac Lipid Accumulation and Diabetic Heart Disease in the Nonobese Diabetic Mouse Model of Type 1 Diabetes”. *American Journal of Physiology-Heart and Circulatory Physiology.* 303:6, pp 732 – 742.

Drosatos K & Schulze PC (2013). “Cardiac Lipotoxicity: Molecular Pathways and Therapeutic Implications”. *Current Heart Failure Reports.* 10:2, pp 109 – 121.

Duncan RE et al (2007). “Regulation of Lipolysis in Adipocytes”. *Annual Review of Nutrition.* 27, pp 79 – 101.

Eaton RP et al (1969). “Kinetic Studies of Plasma Free Fatty Acid and Triglyceride Metabolism in Man”. *The Journal of Clinical Investigation.* 48, pp 1560 – 1579.

Ehrentraut S et al (2011). “*In Vivo* Toll-Like Receptor 4 Antagonism Restores Cardiac Function during Endotoxemia”. *SHOCK.* 36:6, pp 613 – 620.

Elgebaly SA et al (1989). “Cardiac Derived Neutrophil Chemotactic Factors; Preliminary Biochemical Characterization”. *Journal of Molecular and Cellular Cardiology.* 21, pp 585 – 593.

Entman ML et al (1992). “Neutrophil Induced Oxidative Injury of Cardiac Myocytes a Compartmented System Requiring CD11b/CD18-ICAM-1 Adherence”. *The Journal of Clinical Investigation.* 90, pp 1335 – 1345.

Ertunc ME & Hotamisligil GS (2016). “Lipid Signaling and Lipotoxicity in Metabolic Inflammation: Indications for Metabolic Disease Pathogenesis and Treatment”. *Journal of Lipid Research.* 57:12, pp 2099 – 2114.

Fantuzzi G (2005). “Adipose Tissue, Adipokines, and Inflammation”. *Journal of Allergy and Clinical Immunology.* 115, pp 911 – 919.

Fernandez-Real JM & Ricart W (2003). “Insulin Resistance and Chronic Cardiovascular Inflammatory Syndrome”. *Endocrine Reviews.* 24:3, pp 278 – 301.

Fernandez-Sada E et al (2017). “Proinflammatory Cytokines Are Soluble Mediators Linked with Ventricular Arrhythmias and Contractile Dysfunction in a Rat Model of Metabolic Syndrome“. *Oxidative Medicine and Cellular Longevity.* 2017, https://doi.org/10.1155/2017/7682569.

Ferrara D et al (2019). “Impact of Different Ectopic Fat Depots on Cardiovascular and Metabolic Diseases”. *Journal of Cellular Physiology.* 2019, pp 1 – 12.

Finck BN et al (2002). “The Cardiac Phenotype Induced by PPARα Overexpression Mimics that Caused by Diabetes Mellitus”. *The Journal of Clinical Investigation.* 109, pp 121 – 130.

Frieler RA & Mortensen RM (2015). “Immune Cell and Other Non-Cardiomyocyte Regulation of Cardiac Hypertrophy and Remodeling”. *Circulation.* 131:11, pp 1019 – 1030.

Frühbeck G et al (2014). “Regulation of Adipocyte Lipolysis”. *Nutrition Research Reviews.* 27, pp 63 – 93.

Fujishiro M et al (2003). “Three Mitogen-Activated Protein Kinases Inhibit Insulin Signaling by Different Mechanisms in 3T3-L1 Adipocytes”. *Molecular Endocrinology.* 17, pp 487 – 489.

Fukushima A & Lopaschuk GD (2016). “Cardiac Fatty Acid Oxidation in Heart Failure Associated with Obesity and Diabetes”. *Molecular and Cell Biology of Lipids.* http://dx.doi.org/10.1016/j.bbalip.2016.03.020.

Galloway JH et al (1987). “Abnormal Myocardial Lipid Composition in an Infant with Type II Glutaric Aciduria”. *Journal of Lipid Research.* 28, pp 279 – 284.

Gasic S et al (1999). “Tumor Necrosis Factor a Stimulates Lipolysis in Adipocytes by Decreasing Gi Protein Concentrations”. *The Journal of Biological Chemistry.* 274:10, pp 6770 – 6775.

Goldberg IJ et al (2012). “Lipid Metabolism and Toxicity in the Heart”. *Cell Metabolism.* 15, pp 805 – 812.

Goosens V et al (1995). “Direct Evidence for Tumor Necrosis Factor-Induced Mitochondrial Reactive Oxygen Intermediates and Their Involvement in Cytotoxicity”. *Proceedings of the National Academy of Sciences.* 92, pp 8115 – 8119.

Gray GA et al (2018). “Resident Cells of the Myocardium: More than Spectators in Cardiac Injury, Repair and Regeneration”. *Current Opinion in Physiology.* 01, pp 46 – 51.

Griendling KK et al (2016). “Measurement of Reactive Oxygen Species, Reactive Nitrogen Species, and Redox-Dependent Signaling in the Cardiovascular System: A Scientific Statement from the American Heart Association”. *Circulation Research.* 119:5, pp 39 – 75.

Guan Z et al (1998). “Induction of cyclooxygenase-2 by the activated MEKK1 —> SEK1/MKK4 —> p38 mitogen-activated protein kinase Pathway”. *Journal of Biological Chemistry.* 273:22, pp 12901 – 12908.

Guo Y et al (2009). “Lipid Droplets at A Glance”. *Journal of Cell Science.* 122, pp 749 – 752.

Guo J et al (2013). “Globular adiponectin attenuates myocardial ischemia/reperfusion injury by upregulating endoplasmic reticulum Ca(2)(þ)-ATPase activity and inhibiting endoplasmic reticulum stress”. *Journal of Cardiovascular Pharmacology.* 62, pp 143 – 153.

Haemmerle G et al (2006). “Defective Lipolysis and Altered Energy Metabolism in Mice Lacking Adipose Triglyceride Lipase”. *Science.* 312, pp 734 – 737.

Haffner CA et al (1993). “The Lipolytic Effect of β_1- and β_2-adrenoceptor Activation in Healthy Human Volunteers”. *British Journal of Clinical Pharmacology.* 35, pp 35 – 39.

Hall ME et al (2014). “Rescue of Cardiac Leptin Receptors in db/db Mice Prevents Myocardial Triglyceride Accumulation”. *American Journal of Physiology-Endocrinology and Metabolism.* 307, pp 316 – 325.

Hall ME et al (2015). “Lean Heart: Role of Leptin in Cardiac Hypertrophy and Metabolism”. *World Journal of Cardiology.* 7:9, pp 511 – 524.

Hammerschmidt P et al (2019). “CerS6-Derived Sphingolipids Interact with Mff and Promote Mitochondrial Fragmentation in Obesity”. *Cell.* 177, pp 1536 – 1552.

Harms M & Seale P (2013). “Brown and Beige Fat: Development, Function and Therapeutic Potential”. *Nature Medicine.* 19:10, pp 1252 – 1263.

Havel RJ & Gordon RS (1960). “Idiopathic Hyperlipidemia: Metabolic Studies in an Affected Family”. *The Journal of Clinical Investigation.* 39:12, pp 1777 – 1790.

He L et al (2012). “Carnitine Palmitoyltransferase-1b (CPT1b) Deficiency Aggravates Pressure-Overload-Induced Cardiac Hypertrophy due to Lipotoxicity”. *Circulation.* 126:14, pp 1705 – 1716.

Hector J et al (2007). “TNF- α Alters Visfatin and Adiponectin Levels in Human Fat”. *Hormone and Metabolic Research.* 39, pp 250 – 255.

Heinen A et al (2018). “Echocardiographic Analysis of Cardiac Function after Infarction
In Mice: Validation of Single-Plane Long-Axis View Measurements and the Bi-Plane Simpson Method”. *Ultrasound in Medicine & Biology.* 44:7, pp 1544 – 1555.

Hilzendeger AM et al (2012). “A Brain Leptin-Renin Angiotensin System Interaction in the Regulation of Sympathetic Nerve Activity”. *American Journal of Physiology-Heart and Circulatory Physiology.* 303:2, pp 197 – 206.

Horckmans M et al (2017). “Neutrophils Orchestrate Post-Myocardial Infarction Healing by Polarizing Macrophages towards a Reparative Phenotype”. *European Heart Journal.* 38, pp 187 – 197.

Holland WL et al (2011). “Lipid-Induced Insulin Resistance Mediated by the Proinflammatory Receptor TLR4 Requires Saturated Fatty Acid–Induced Ceramide Biosynthesis in Mice”. *The Journal of Clinical Investigation.* 121:5, pp 1858 – 1870.

Hollenbach E et al (2004). "Inhibition of p38 MAP Kinase- and RICK/NF-κB-Signaling Suppresses Inflammatory Bowel Disease". *The FASEB Journal.* 10.1096/fj.04-1642fje.

Holness CL & Simmons DL (1993). "Molecular Cloning of CD68, a Human Macrophage Marker Related to Lysosomal Glycoproteins". *Blood.* 81:6, pp 1607 – 1613.

Hubler MJ et al (2016). "Role of Lipids in the Metabolism and Activation of Immune Cells". *Journal of Nutritional Biochemistry.* 34, pp 1 – 7.

Hue L & Taegtmeyer H (2009). "The Randle Cycle Revisited: a New Head for an Old Hat". *American Journal of Physiology-Endocrinology and Metabolism.* 297:3, pp 578 – 591.

Hui X et al (2015). "Adiponectin Enhances Cold-Induced Browning of Subcutaneous Adipose Tissue via Promoting M2 Macrophage Proliferation". *Cell Metabolism.* 22, pp 279 – 290.

Itani SI et al (2002). "Lipid-Induced Insulin Resistance in Human Muscle Is Associated With Changes in Diacylglycerol, Protein Kinase C, and I_KB-α". *Diabetes.* 51, pp 2005 – 2011.

Itoh H et al (2008). "Structural Basis for the Activation of PPARγ by Oxidized Fatty Acids". *Nature Structural & Molecular Biology.* 15:9, pp 924 – 931.

Iwasa H et al (2003). "Mitogen-Activated Protein Kinase p38 defines the Common Senescence-Signalling Pathway". *Genes to Cells,* 8, pp 131 – 144.

Jaishy B & Abel DE (2016). "Lipids, Lysosomes, and Autophagy". *Journal of Lipid Research.* 57, pp 1619 – 1635.

Joseph JP et al (2017). "CXCR2 Inhibition – A Novel Approach to Treating Coronary Heart Disease (CICADA): Study Protocol for a Randomised Controlled Trial". *Trials.* 18:473, DOI 10.1186/s13063-017-2210-2.

Kallikourdis M et al (2017). "T cell Costimulation Blockade Blunts Pressure Overload-Induced Heart Failure". *Nature Communications.* 8:14680, DOI: 10.1038/ncomms14680.

Kaur J (2014). "A Comprehensive Review on Metabolic Syndrome". *Cardiology Research and Practice.* 2014, http://dx.doi.org/10.1155/2014/943162.

Kawakami M et al (1986). "Human Recombinant TNF Suppresses Lipoprotein Lipase Activity and Stimulates Lipolysis in 3T3-L1 Cells". *Journal of Biochemistry.* 101, pp 331 – 338.

Kelly DP & Strauss AW (1994). "Inherited Cardiomyopathies". *The New England Journal of Medicine.* 330:13, pp 913 – 919.

Kennedy EP & Weiss SB (1956). "The Function of Cytidine Coenzymes in the Biosynthesis of Phospholipids". *Journal of Biological Chemistry.* 222:1, pp 193 – 214.

Kershaw EE & Flier JS (2004). "Adipose Tissue as an Endocrine Organ". *The Journal of Clinical Endocrinology & Metabolism.* 89:6, pp 2548 – 2556.

Kienesberger PC et al (2011). "Myocardial ATGL Overexpression Decreases the Reliance on Fatty Acid Oxidation and Protects against Pressure Overload-Induced Cardiac Dysfunction". *Molecular and Cellular Biology.* 32:4, pp 740 – 750.

Kim TT & Dyck JRB (2016). "The Role of CD36 in the Regulation of Myocardial Lipid Metabolism". *Molecular and Cell Biology of Lipids.*1861, pp 1450 – 1460.

Klaus S et al (1995). "Functional Assessment of White and Brown Adipocyte Development and Energy Metabolism in Cell Culture Dissociation of Terminal Differentiation and Thermogenesis in Brown Adipocytes". *Journal of Cell Science.* 108, pp 3171 – 3180.

Kobayashi K et al (2000). "The db/db Mouse, a Model for Diabetic Dyslipidemia: Molecular Characterization and Effects of Western Diet Feeding". *Metabolism.* 49:1, pp 22 – 31.

Korn ED (1955)a. "Clearing Factor, A Heparin-Activated Lipoprotein Lipase I. Isolation and Characterization of the Enzyme from Normal Rat Heart". *Journal of Biological Chemistry.* 215:1, pp 1 – 14.

Korn ED (1955)b. "Clearing Factor, A Heparin-Activated Lipoprotein Lipase II. Substrate Specificity and Activation of Coconut Oil". *Journal of Biological Chemistry.* 215:1, pp 15 – 26.

Krown KA et al (1996). "Tumor Necrosis Factor Alpha-Induced Apoptosis in Cardiac Myocytes. Involvement of the Sphingolipid Signaling Cascade in Cardiac Cell Death". *The Journal of Clinical Investigation.* 98:12, pp 2854 – 2865.

Kubota T et al (1997). "Dilated Cardiomyopathy in Transgenic Mice with Cardiac-Specific Overexpression of Tumor Necrosis Factor-α". *Circulation Research.* 81:4, https://doi.org/10.1161/01.RES.81.4.627.

Lai S et al (2019). "Immune Responses in Cardiac Repair and Regeneration: A Comparative Point of View". *Cellular and Molecular Life Sciences.* 76, pp 1365 – 1380.

LaRocca TJ et al (2012). "CXCR4 Gene Transfer Prevents Pressure Overload Induced Heart Failure". *Journal of Molecular and Cellular Cardiology.* 53:2, pp 223 – 232.

Laroumanie F et al (2014). "$CD4^+$ T Cells Promote the Transition from Hypertrophy to Heart Failure during Chronic Pressure Overload". *Circulation.* 129, pp 2111 – 2124.

Lee Y et al (2012). "*In vivo* Identification of Bipotential Adipocyte Progenitors Recruited by β3-adrenoceptor Activation and High Fat Feeding". *Cellular Metabolism.* 15:4, pp 480 – 491.

Leitner LM et al (2017). "Reactive Oxygen Species/Nitric Oxide Mediated Inter-Organ Communication in Skeletal Muscle Wasting Diseases". *Antiox. Redox Signal.*

Lettieri BD et al (2014a). "Inhibition of Age-Related Cytokines Production by ATGL: A Mechanism Linked to the Anti-Inflammatory Effect of Resveratrol". *Mediators of inflammation.* http://dx.doi.org/10.1155/2014/917698.

Lettieri BD et al (2014b). "Proline Oxidase–Adipose Triglyceride Lipase Pathway Restrains Adipose Cell Death and Tissue Inflammation". *Cell Death and Differentiation.* 21, pp 113 – 123.

Levine B et al (1990). "Elevated Circulating Levels of Tumor Necrosis Factor in Severe Chronic Heart Failure". *The New England Journal of Medicine.* 323:4, pp 236 – 241.

Ley K et al (2018). "Neutrophils: New Insights and Open Questions". *Science Immunology.* 3, eaat4579.

Lindner D et al (2014). "Cardiac Fibroblasts Support Cardiac Inflammation in Heart Failure". *Basic Research in Cardiology,* 109:428 doi:10.1007/s00395-014-0428-7.

Listenberger LL et al (2001). "Palmitate-Induced Apoptosis can Occur through a Ceramide-Independent Pathway". *The Journal of Biological Chemistry.* 276:18, pp 14890 – 14895.

Listenberger LL et al (2003). "Triglyceride Accumulation Protects Against Fatty Acid-Induced Lipotoxicity". *Proceedings of the National Academy of Sciences of the United States of America.* 100:6, pp 3077 – 3082.

Liu S et al (2019). "Neutrophil-Initiated Myocardial Inflammation and Its Modulation by B-Type Natriuretic Peptide: A Potential Therapeutic Target". *International Journal of Molecular Sciences.* 20:129, doi:10.3390/ijms20010129.

Livak KJ & Schmittgen TD (2001). "Analysis of Relative Gene Expression Data Using Real-
Time Quantitative PCR and the 2^{-DDCT} Method". *Methods.* 25, pp 402 – 408.

Lodhi IJ et al (2015). "Peroxisomal Lipid Synthesis Regulates Inflammation by Sustaining Neutrophil Membrane Phospholipid Composition and Viability". *Cellular Metabolism.* 21:1, pp 51 – 64.

Lopaschuk GD et al (2010). "Myocardial Fatty Acid Metabolism in Health and Disease". *Physiology Review.* 90, pp 207 – 258.

Mann DL (2002). "Tumor Necrosis Factor–Induced Signal Transduction and Left Ventricular Remodeling". *Journal of Cardiac Failure.* 8:6, pp 379 – 386.

Mann DL (2015). “Innate Immunity and the Failing Heart: The Cytokine Hypothesis Revisited”. *Circulation Research.* 116:7, pp 1254 – 1268.

Marfella R et al (2009). “Myocardial Lipid Accumulation in Patients with Pressure-Overloaded Heart and Metabolic Syndrome”. *Journal of Lipid Research.* 50, pp 2314 – 2323.

Mark AL et al (1999). “Contrasting Blood Pressure Effects of Obesity in Leptin Deficient ob/ob Mice and Agouti Yellow Obese Mice”. *Journal of Hypertension.* 17, pp 1949 – 1953.

Martinez-Lopez N et al (2016). “Autophagy in the CNS and Periphery Coordinate Lipophagy and Lipolysis in the Brown Adipose Tissue and Liver”. *Cellular Metabolism.* 23:1, pp 113 – 127.

Martinez-Sanchez N et al (2017). “Thyroid Hormones Induce Browning of White Fat”. *Journal of Endocrinology.* 232, pp 351 – 362.

Mayer N et al (2013). “Development of Small-Molecule Inhibitors Targeting Adipose Triglyceride Lipase”. *Nature Chemical Biology.* 9, pp 785 – 787.

McGaffin KR et al (2011). “Cardiac-Specific Leptin Receptor Deletion Exacerbates Ischaemic Heart Failure in Mice”. *Cardiovascular Research.* 89, pp 60 – 71.

McGavock JM et al (2007). “Cardiac Steatosis in Diabetes Mellitus A 1H-Magnetic Resonance Spectroscopy Study”. *Circulation.* 116, pp 1170 – 1175.

Mendis S et al (2011). “Global Atlas on Cardiovascular Disease Prevention and Control 2011”. *World Health Organization, Geneva.*

Misharin AV et al (2013). “Flow Cytometric Analysis of Macrophages and Dendritic Cell Subsets in the Mouse Lung”. *American Journal of Respiratory Cell and Molecular Biology.* 49:4, pp 503 – 510.

Mocatta TJ et al (2007). “Plasma Concentrations of Myeloperoxidase Predict Mortality After Myocardial Infarction”. *Journal of the American College of Cardiology.* 49:20, pp 1993 – 2000.

Morak M et al (2012). “Adipose Triglyceride Lipase (ATGL) and Hormone-Sensitive Lipase (HSL) Deficiencies Affect Expression of Lipolytic Activities in Mouse Adipose Tissues”. *Molecular & Cellular Proteomics.* 11, pp 1777 – 1789.

Morigny P et al (2016). “Adipocyte Lipolysis and Insulin Resistance”. *Biochimie.* 125, pp 259 – 266.

Mortensen RM (2012). “Immune Cell Modulation of Cardiac Remodeling”. *Circulation.* 125, pp 1597 – 1600.

Mottillo EP et al (2014). “Coupling of Lipolysis and *de novo* Lipogenesis in Brown, Beige, and White Adipose Tissues during Chronic β3-adrenergic Receptor Activation”. *Journal of Lipid Research.* 55, pp 2276 – 2286.

Muller DN et al (2000). “NF-kappaB Inhibition Ameliorates Angiotensin II-Induced Inflammatory Damage in Rats”. *Hypertension.* 35, pp 193 – 201.

Nahrendorf M et al (2007). “The Healing Myocardium Sequentially Mobilizes Two Monocyte Subsets with Divergent and Complementary Functions”. *The Journal of Experimental Medicine.* 204:12, pp 3037 – 3047.

Nakanishi T & Kato S (2014). “Impact of Diabetes Mellitus on Myocardial Lipid Deposition: An Autopsy Study”. *Pathology Research and Practice.* http://dx.doi.org/10.1016/j.prp.2014.04.008.

Nedergaard J & Cannon B (1992). “The Uncoupling Protein Thermogenin and Mitochondrial Thermogenesis”. *New Comprehensive Biochemistry.* 23, pp 385 – 420.

Nedergaard J et al (1997). “The Interaction between Thyroid and Brown-Fat Thermogenesis
Central or Peripheral Effects?”. *Annals of the New York Academy of Sciences.* 813, pp 712 – 717.

Nevers T et al (2015). “Left Ventricular T Cell Recruitment Contributes to the Pathogenesis of Heart Failure”. *Circulation: Heart Failure.* 8:4, pp 776 – 787.

Nishida K et al (2004). “p38 Mitogen-Activated Protein Kinase Plays a Critical Role in Cardiomyocyte Survival but Not in Cardiac Hypertrophic Growth in Response to Pressure Overload”. *Molecular and Cellular Biology.* 24:24, pp 10611 – 10620.

Obama T et al (2014). “Targeting Neutrophil: A New Approach against Hypertensive Cardiac Remodeling?”. *Hypertension.* 63:6, pp 1171 – 1172.

Opie LH (2008). “Metabolic Management of Acute Myocardial Infarction Comes to the Fore and Extends Beyond Control of Hyperglycemia”. *Circulation.* 117, pp 1610 – 1619.

Oral H et al (1997). “Sphingosine Mediates the Immediate Negative Inotropic Effects of Tumor Necrosis Factor-a in the Adult Mammalian Cardiac Myocyte”. *The Journal of Biological Chemistry.* 272:8, pp 4836 – 4842.

Osborn O & Olefsky JM (2012). “The Cellular and Signaling Networks Linking the Immune System and Metabolism in Disease”. *Nature Medicine.* 18:3, pp 363 – 374.

Otsu K et al (2003). “Disruption of a single copy of the p38alpha MAP kinase gene leads to cardioprotection against ischemia-reperfusion”. *Biochemical and Biophysical Research Communications.* 302:1, pp 56 – 60.

Parra V et al (2008). “Changes in Mitochondrial Dynamics during Ceramide-Induced Cardiomyocyte Early Apoptosis”. *Cardiovascular Research.* 77, pp 387 – 397.

Patel B et al (2017). “Mononuclear Phagocytes Are Dispensable for Cardiac Remodeling in Established Pressure-Overload Heart Failure”. *PLOS One.* DOI:10.1371/journal.pone.0170781.

Petrovic N et al (2010). “Chronic Peroxisome Proliferator-activated Receptor γ (PPARγ) Activation of Epididymally Derived White Adipocyte Cultures Reveals a Population of Thermogenically Competent, UCP1-containing Adipocytes Molecularly Distinct from Classic Brown Adipocytes”. *Journal of Biological Chemistry.* 285:10, pp 7153 – 7164.

Pinto AR et al (2016). “Revisiting Cardiac Cellular Composition”. *Circulation Research.* 118:3, pp 400 – 409.

Potashnik R et al (2003). “IRS1 Degradation and Increased Serine Phosphorylation cannot Predict the Degree of Metabolic Insulin Resistance Induced by Oxidative Stress”. *Diabetologia.* 46, pp 639 – 648.

Randle PJ et al (1963). “The Glucose Fatty-Acid Cycle Its Role in Insulin Sensitivity and the
Metabolic Disturbances of Diabetes Mellitus”. *The Lancet.* pp 785 – 789.

Rao RR et al (2014). “Meteorin-Like is a Hormone that Regulates Immune-Adipose Interactions to Increase Beige Fat Thermogenesis”. *Cell.* 157:6, pp 1279 – 1291.

Reaven GM et al (1965). “Kinetics of Triglyceride Turnover of Very Low Density Lipoproteins of Human Plasma”. *The Journal of Clinical Investigation.* 44:11, pp 1926 – 1833.

Riehle C et al (2016). “Insulin Signaling and Heart Failure”. *Circulation Research.* 118:7, pp 1151 – 1169.

Roden M (2006). “Mechanisms of Disease: Hepatic Steatosis in Type 2 Diabetes – Pathogenesis and Clinical Relevance”. *Nature Clinical Practice Endocrinology & Metabolism.* 2:6, pp 335 – 346.

Rodriguez-Cuenca S et al (2012)a. “Ablation of Pparg2 Impairs Lipolysis and Reveals Murine Strain Differences in Lipolytic Responses”. *The FASEB Journal.* 26, pp 1835 – 1844.

Rodriguez-Cuenca S et al (2012)b. “Peroxisome Proliferator-Activated Receptor γ-Dependent Regulation of Lipolytic Nodes and Metabolic Flexibility”. *Molecular and Cellular Biology.* pp 1555–1565.

Rosen ED & Spiegelman BM (2006). “Adipocytes as Regulators of Energy Balance and Glucose Homeostasis”. *Nature.* 444: 7121, pp 847 – 853.

Rosen ED & Spiegelman BM (2014). “What We Talk About When We Talk About Fat”. *Cell.* 156, pp 20 – 44.

Rudolph V et al (2010). “Myeloperoxidase Acts as a Profibrotic Mediator of Atrial Fibrillation”. *Nature Medicine.* 16:4, pp 470 – 474.

Salatzki J et al (2018). “Adipose Tissue ATGL Modifies the Cardiac Lipidome in Pressure-Overload-Induced Left Ventricular Failure”. *PLOS One.* e1007171, https://doi.org/
10.1371/journal.pgen.1007171.

Salvador AM et al (2016). “Intercellular Adhesion Molecule 1 Regulates Left Ventricular
Leukocyte Infiltration, Cardiac Remodeling, and Function in Pressure Overload–Induced Heart Failure”. *Journal of the American Heart Association.* 5:e003126, doi: 10.1161/JAHA.115.003126.

Samuel VT et al (2010). “Lipid-Induced Insulin Resistance: Unravelling the Mechanism”. *The Lancet.* 375:9733, pp 2267 – 2277.

Savary S et al (2012). “Fatty Acids - Induced Lipotoxicity and Inflammation”. *Current Drug Metabolism.* 13, pp 1358 – 1370.

Schäffler A et al (2005). “Genomic Structure of Human Omentin, a New Adipocytokine Expressed in Omental Adipose Tissue”. *Biochimica et Biophysica Acta.* 1732, pp 96 – 102.

Scherer PE et al (1995). “A Novel Serum Protein Similar to C1q, Produced Exclusively in
Adipocytes”. *The Journal of Biological Chemistry.* 270:45, pp 26746 – 26749.

Schilling JD et al (2012). “Macrophages Modulate Cardiac Function in Lipotoxic Cardiomyopathy”. *American Journal of Physiology-Heart and Circulatory Physiology.* 303:11, pp 1366 – 1373.

Schiwon M et al (2014). “Crosstalk between Sentinel and Helper Macrophages Permits Neutrophil Migration into Infected Uroepithelium”. *Cell.* 156:3, pp 456 – 468.

Schoiswohl G et al (2015). “Impact of Reduced ATGL-Mediated Adipocyte Lipolysis on Obesity-Associated Insulin Resistance and Inflammation in Male Mice”. *Endocrinology.* 156:10, pp 3610 – 3624.

Schreiber R et al (2015). “Hypophagia and Metabolic Adaptations in Mice with Defective ATGL-Mediated Lipolysis Cause Resistance to HFD-Induced Obesity”. *Proceedings of the National Academy of Sciences of the United States of America.* 112:45, pp 13850 – 13855.

Schreiber R et al (2017). “Cold-Induced Thermogenesis Depends on ATGL-Mediated Lipolysis in Cardiac Muscle, but Not Brown Adipose Tissue”. *Cell Metabolism.* 26, pp 753 – 763.

Schreiber R et al (2019). “Of mice and men: The physiological role of adipose triglyceride lipase (ATGL)”. *Molecular and Cell Biology of Lipids.* 1864, pp 880 – 899.

Schulze PC et al (2016). “Lipid Use and Misuse by the Heart”. *Circulation Research.* 118, pp 1736 – 1751.

Schulze-Osthoff K et al (1992). “Cytotoxic Activity of Tumor Necrosis Factor Is Mediated by Early Damage of Mitochondrial Functions“. *The Journal of Biological Chemistry.* 267:8, pp 5317 – 5323.

Schweiger M et al (2016). “Pharmacological Inhibition of Adipose Triglyceride Lipase Corrects High-Fat Diet-Induced Insulin Resistance and Hepatosteatosis in Mice”. *Nature Communications*. 8:14859, DOI: 10.1038/ncomms14859.

Sears B & Perry M (2015). “The Role of Fatty Acids in Insulin Resistance”. *Lipids in Health and Disease.* 14:121, DOI 10.1186/s12944-015-0123-1.

Sebo ZL & Rodeheffer MS (2019). “Assembling the Adipose Organ: Adipocyte Lineage Segregation and Adipogenesis *In vivo*”. *Development.* 146:dev172098, doi:10.1242/dev.172098.

Sharma S et al (2004). “Intramyocardial Lipid Accumulation in the Failing Human Heart Resembles the Lipotoxic Rat Heart”. *The FASEB Journal.* 18, pp 1692 – 1700.

Shin H et al (2017). “Lipolysis in Brown Adipocytes Is Not Essential for Cold-Induced Thermogenesis in Mice”. *Cell Metabolism.* 26:5, pp 764 – 777.

Singh R et al (2009). “Autophagy Regulates Lipid Metabolism”. *Nature.* 458:7242, pp 1131 – 1135.

Sivasubramanian N et al (2001). “Left Ventricular Remodeling in Transgenic Mice with Cardiac Restricted Overexpression of Tumor Necrosis Factor”. *Circulation.* 104, pp 826 – 831.

Sokol CL & Luster AD (2015). “The Chemokine System in Innate Immunity”. *Cold Spring Harbor Perspectives in Biology.* 7:a016303, doi: 10.1101/cshperspect.a016303.

Sriramula S & Francis J (2015). “Tumor Necrosis Factor - Alpha Is Essential forAngiotensin II-Induced VentricularRemodeling: Role for Oxidative Stress”. *PLoS ONE,* 10(9): e0138372. doi:10.1371/journal.pone.0138372.

Stanley WC & Chandler MP (2002). “Energy Metabolism in the Normal and Failing Heart:
Potential for Therapeutic Interventions”. *Heart Failure Reviews.* 7, pp 115 – 130.

Stanley WC et al (2005). “Myocardial Substrate Metabolism in the Normal and Failing Heart”. *Physiological Reviews.* 85, pp 1093 – 1129.

Swirski FK & Nahrendorf M (2018). “Cardioimmunology: the Immune System in Cardiac Homeostasis and Disease”. *Nature Reviews Immunology.* 18, pp 733 – 744.

Szczepaniak LS et al (2003). “Myocardial Triglycerides and Systolic Function in Humans: In Vivo Evaluation by Localized Proton Spectroscopy and Cardiac Imaging”. *Magnetic Resonance in Medicine.* 49, pp 417 – 423.

Szendroedi J & Roden M (2009). “Ectopic Lipids and Organ Function”. *Current Opinion in Lipidology.* 20, pp 50 – 56.

Szendroedi J et al (2014). “Role of Diacylglycerol Activation of PKCθ in Lipid-Induced Muscle Insulin Resistance in Humans”. ”. *Proceedings of the National Academy of Sciences of the United States of America.* 111:26, pp 9597 – 9602.

Taegtmeyer H & Dilsizian V (2008). “Imaging Myocardial Metabolism and Ischemic Memory”. *Nature Clinical Practice Cardiovascular Medicine.* 5, doi:10.1038/ncpcardio1186.

Takenaka K et al (1998). “Activation of the protein kinase p38 in the spindle assembly checkpoint and mitotic arrest”. *Science.* 280, pp 599 – 602.

Tamoutounour S et al (2012). “CD64 Distinguishes Macrophages from Dendritic Cells in the Gut and Reveals the Th1-inducing Role of Mesenteric Lymph Node Macrophages during Colitis”. *European Journal of Immunology.* 42, pp 3150 – 3166.

Tanaka T et al (2004). “Interleukin-6-induced Reciprocal Expression of SERCA and Natriuretic Peptides mRNA in Cultured Rat Ventricular Myocytes”. *The Journal of International Medical Research.* 32, pp 57 – 61.

Taylor M et al (2001). “An Evaluation of Myocardial Fatty Acid and Glucose Uptake Using PET with [18F]Fluoro-6-Thia-Heptadecanoic Acid and [18F]FDG in Patients with Congestive Heart Failure”. *Journal of Nuclear Medicine.* 42, pp 55 – 62.

Tchkonia T et al (2013). “Mechanisms and Metabolic Implications of Regional Differences among Fat Depots”. *Cell Metabolism.* 17, pp 644 – 656.

Tham YK et al (2015). “Pathophysiology of Cardiac Hypertrophy and Heart Failure: Signaling Pathways and Novel Therapeutic Targets”. *Archives of Toxicology.* 89, pp 1401 – 1438.

Thompson BR et al (2010). “Fatty Acid Flux in Adipocytes; The in’s and out’s of Fat Cell Lipid Trafficking”. *Molecular and Cellular Endocrinology.* 318:1-2, pp 24 – 33.

Torre-Amione G et al (1996). “Tumor Necrosis Factor-α and Tumor Necrosis Factor Receptors in the Failing Human Heart“. *Circulation.* 93, pp 704 – 711.

Vaag AA & Beck-Nielsen H (1992). “Effects of Prolonged Acipimox Treatment on Glucose and Lipid Metabolism and on In Vivo Insulin Sensitivity in Patients with Non-insulin Dependent Diabetes Mellitus“. *Clinical & Translational Endocrinology.* 127:4, pp 344 – 350.

Van der Vusse GJ et al (2000). “ Cardiac fatty acid uptake and transport in health and disease“. *Cardiovascular Research.* 45, pp 279 – 293.

Varga T et al (2011). “PPARs are a Unique Set of Fatty Acid Regulated Transcription Factors Controlling Both Lipid Metabolism and Inflammation”. *Biochimica et Biophysica Acta.* 1812, pp 1007 – 1022.

Ventura A et al (2004). “Cre-lox-regulated Conditional RNA Interference from Transgenes”. *Proceedings of the National Academy of Sciences of the United States of America.* 10380 – 10385.

Villegas S et al (2000). “Leukemia Inhibitory Factor and Interleukin-6 Downregulate Sarcoplasmic Reticulum Ca2+ ATPase (SERCA2) in Cardiac Myocytes”. *Basic Research in Cardiology.* 95, pp 47 – 54.

Wang Y et al (2017). “Cardiovascular Adiponectin Resistance: The Critical Role of Adiponectin Receptor Modification”. *Trends in Endocrinology and Metabolism.* 28:7, pp 519 – 530.

Wang Y et al (2019). “Wnt5a-Mediated Neutrophil Recruitment has an Obligatory Role in Pressure Overload-Induced Cardiac Dysfunction”. *Circulation.* 140, pp 487 – 499.

Weisheit C et al (2014). “Ly6Clow and Not Ly6Chigh Macrophages Accumulate First in the Heart in a Model of Murine Pressure-Overload”. *PLOS One.* 9(11): e112710, doi:10.1371/journal.pone.0112710.

Wende AR & Abel DE (2010). “Lipotoxicity in the Heart”. *Biochimica et Biophysica Acta.* 1801:3, pp 311 – 319.

Wilkins E et al (2017). “European Cardiovascular Disease Statistics 2017”. *European Heart Network.*

Williamson JR et al (1966). “Mechanism for the Stimulation of Gluconeogenesis by Fatty Acids in Perfused Rat Liver”. *Proceedings of the National Academy of Sciences of the United States of America.* 56:1, pp 247 – 254.

Woo C et al (2019). “Mitochondrial Dysfunction in Adipocytes as a Primary Cause of Adipose Tissue Inflammation”. *Diabetes & Metabolism Journal.* pISSN 2233-6079 · eISSN 2233-6087, https://doi.org/10.4093/dmj.2018.0221.

Wu Y et al (2014). “S100a8/a9 Released by CD11b+Gr1+ Neutrophils Activates Cardiac Fibroblasts to Initiate Angiotensin II–Induced Cardiac Inflammation and Injury”. *Hypertension.* 63, pp 1241 – 1250.

Yagyu H et al (2003). “Lipoprotein lipase (LpL) on the Surface of Cardiomyocytes Increases Lipid Uptake and Produces a Cardiomyopathy”. *The Journal of Clinical Investigation.* 111, pp 419 – 426.

Yamaguchi T et al (2006). “MLDP, a Novel PAT Family Protein Localized to Lipid Droplets and Enriched in the Heart, Is Regulated by Peroxisome Proliferator-activated Receptor α”. *The Journal of Biological Chemistry.* 281:20, pp 14232 – 14240.

Yan J et al (2009). “Increased Glucose Uptake and Oxidation in Mouse Hearts Prevents High Fatty Acid Oxidation but Causes Cardiac Dysfunction in Diet Induced Obesity”. *Circulation.* 119:21, pp 2818 – 2828.

Yan X et al (2013). “Temporal Dynamics of Cardiac Immune Cell Accumulation Following Acute Myocardial Infarction”. *Journal of Molecular and Cellular Biology.* 62, pp 24 – 35.

Yang H & Li X (2012). “The Role of Fatty Acid Metabolism and Lipotoxicity in Pancreatic b-cell Injury: Identification of Potential Therapeutic Targets”. *Acta Pharmaceutica Sinica B.* 2:4, pp 396 – 402.

Yang L et al (2005). “ICAM-1 Regulates Neutrophil Adhesion and Transcellular Migration of TNF-α–activated Vascular Endothelium under Flow”. *Blood.* 106, pp 584 – 592.

Yang R & Barouch LA (2007). “Leptin Signaling and Obesity Cardiovascular Consequences”. *Circulation Research.* 101, pp 545 – 559.

Young ME et al (2002). “Impaired Long-Chain Fatty Acid Oxidation and Contractile Dysfunction in the Obese Zucker Rat Heart”. *Diabetes.* 51, pp 2587 – 2595.

Young P et al (1984). “Brown Adipose Tissue in the Parametrial Fat Pad of the Mouse”. *Federation of European Biochemical Societies.* 167:1, pp 10 – 14.

Young SG & Zechner R (2013). “Biochemistry and Pathophysiology of Intravascular and Intracellular Lipolysis”. *Genes & Development.* 27, pp 459 – 484.

Yu C et al (2002). “Mechanism by Which Fatty Acids Inhibit Insulin Activation of Insulin Receptor Substrate-1 (IRS-1)-associated Phosphatidylinositol 3-Kinase Activity in Muscle”. *The Journal of Biological Chemistry.* 277:52, pp 50230 – 50236.

Yu L & Feng Z (2018). “The Role of Toll-Like Receptor Signaling in the Progression of
Heart Failure”. *Mediators of Inflammation.* 2018,
https://doi.org/10.1155/2018/9874109.

Yu X et al (2005). “Inhibition of Sarcoplasmic Reticular Function by Chronic Interleukin-6 Exposure via iNOS in Adult Ventricular Myocytes”. *Journal of Physiology.* 566:2, pp 327 – 340.

Zandbergen HR et al (2009). “Macrophage Depletion in Hypertensive Rats Accelerates Development of Cardiomyopathy”. *Journal of Cardiovascular Pharmacology and Therapeutics.* 14:1, pp 68 – 75.

Zechner R et al (2012). “FAT SIGNALS - Lipases and Lipolysis in Lipid Metabolism and Signaling”. *Cell Metabolism.* 15:3, pp 279 – 291.

Zhang B et al (1996). “Negative Regulation of Peroxisome Proliferator-Activated Receptor-y

Gene Expression Contributes to the Antiadipogenic Effects of Tumor Necrosis Factor-a". *Molecular Endocrinology.* 10:11, pp 1457 – 1466.

Zhang HH et al (2002). "Tumor Necrosis Factor-α Stimulates Lipolysis in Differentiated Human Adipocytes through Activation of Extracellular Signal–Related Kinase and Elevation of Intracellular cAMP". *Diabetes.* 51, pp 2929 – 2935.

Zhang J et al (2006). "Generation of an Adult Smooth Muscle Cell-targeted Cre Recombinase Mouse Model". *Arteriosclerosis, Thrombosis, and Vascular Biology.* 26, e23 – e24.

Zhang L et al (2012). "Activating Cardiac E2F1 Induces Up-regulation of Pyruvate Dehydrogenase Kinase 4 in Mice on a Short Term of High Fat Feeding". *FEBS Letters.* 586, pp 996 – 1003.

Zhang W et al (2015). "Necrotic Myocardial Cells Release Damage-Associated Molecular
Patterns That Provoke Fibroblast Activation *In Vitro* and Trigger Myocardial Inflammation and Fibrosis *In Vivo*". *Journal of the American Heart Association.* 4:e001993, doi: 10.1161/JAHA.115.001993.

Zhang Y et al (2017). "Immune Mechanisms in Heart Failure". *European Journal of Heart Failure.* 19, pp 1379 – 3789.

Zhou Y et al (2000). "Lipotoxic Heart Disease in Obese Rats: Implications for Human Obesity". *Proceedings of the National Academy of Sciences of the United States of America.* 97:4, pp 1784 – 1789.

Ziegler-Heitbrock HW et al (1992). "*In vitro* desensitization to lipopolysaccharide suppresses tumour necrosis factor, interleukin-1 and interleukin-6 gene expression in a similar fashion". *Immunology.* 75, pp 264 – 268.

Statutory Declaration

I declare under oath that I have produced my thesis independently and without any undue assistance by third parties under consideration of the 'Principles for the Safeguarding of Good Scientific Practice' at Heinrich Heine University Düsseldorf.

Düsseldorf,

_____

Vici Oenarto

Acknowledgement

Axel

Thank you for the opportunity to work on my PhD thesis here, your kind mentorship and your time. I really hope that my work can be at least of use for the future projects

Prof. Dr. Jens Fischer

Thank you for agreeing to become my second supervisor and your time to review and mark my thesis

Katharina & Lucia

Thank you for establishing the model and the neutrophil depletion study which was the base of my project and helped my work to go smoothly

Rianne

Thank you for working with me on the FACS data

Jacqueline, Lisa & Christoph

Thank you for the professional and emotional support

Everyone at the Institute of Cardiovascular Physiology

Thank you all for being there and for helping me along the way with lab work

Thurl, Katelyn, Vidisha & Mitch from Harris Lab, Department of Pharmacology, UVA

Thank you for welcoming me in your lab, I really feel accepted when I was there

IRTG 1902 – especially Sandra

Thank you for the helping me with all administrative things. Sandra, thank you for organizing pretty much everything for us

Last but not least, **my lovely family: mama, Jessie, koko sekeluarga.**